ABSTRACT

VEDULA, JYOTSNA. REORGANIZATION OF STRUCTURE TO ALTER THE PROPERTIES OF PET. (Under the direction of Prof. Alan E. Tonelli)

This research focuses on the study of the unique behavior and properties exhibited by as-received Polyethylene Terephthalate (PET) subsequently processed by a simple precipitation method, and mainly involves the comparison of the properties of as-received and precipitated PET's at the microscopic and macroscopic levels. As-received PET is dissolved in Trifluoro Acetic acid (TFA) at 50°C and then precipitated by adding the solution drop wise to acetone stirred at a very high rate. The ar-PET is by nature a slowly crystallizing polymer. Bulk PET has been observed to reorganize both morphologically and conformationally by the precipitation method used.

Differential Scanning Calorimetry (DSC), Fourier Transform Infrared (FTIR), and X-ray studies of precipitated (ppt) PET show structures and morphologies that are different from those of the samples obtained by ordinary solution and melt processing techniques. Unlike as-received PET, the ppt PET is apparently repeatedly and rapidly crystallizable from the melt, with non-crystalline portions of the sample that do not evidence a glass transition nor a crystallization peak during the heating DSC scan. DSC results suggest that the precipitation method has transformed PET into a repeatedly, rapidly crystallizable polymer that is found to achieve very high levels of crystallinity even when crystallized from the melt at a very high cooling rate. The fact that the precipitated PET has high levels of crystallinity is also supported by FTIR analysis, which shows a higher amount of trans conformer. The reorganization induced in the ppt PET is different from ordinary solvent induced crystallization.

Shrinkage of films made from both PET's is observed with an increase in temperature. Heating the as-received film, prepared by melt pressing and rapid quenching in water, results in the abrupt shrinking of the material at around the glass transition temperature of the polymer, whereas the ppt PET film continues to contract at a controlled rate with rising temperature. This suggests that the amorphous regions in the ppt PET film are organized differently than that of the as-received material. Density measurements also support the fact that the non-crystalline regions in ppt-PET are different from the amorphous portions of ar-PET. Atomic Force Microscopy suggests a molecular-level difference between the precipitated and the as-received PET's even in their melts. Melting of the ppt PET has not erased the structural organization. Preliminary observations of the stress-strain behavior of their films indicate that as-received PET exhibits tough plastic behavior characteristic of glassy amorphous polymers, whereas ppt PET shows more rigid behavior similar to semi-crystalline polymers like isotactic polypropylene. Characterization of macroscopic properties, such as rheology using the Minimelter, indicates that the melt viscosity of ppt PET is less than that of the as-received sample, which will make processing easier. Blending of the as-received and the precipitated PET's has also been done.

Overall it is observed that ppt-PET is different from ar-PET in terms of both its microscopic (organization and conformation) and macroscopic behaviors.

Keywords: morphology; thermal behavior; reorganized poly(ethylene terephthalates); crystallinity; density; FTIR; X-ray

REORGANIZATION OF STRUCTURE TO ALTER THE PROPERTIES OF PET

by

JYOTSNA VEDULA

A thesis submitted to the Graduate Faculty of
North Carolina State University
in partial fulfillment of the
requirements for the Degree of
Master of Science

TEXTILE ENGINEERING

Raleigh

2005

APPROVED BY:

Dr. Juan P. Hinestroza Co-chair of the Advisory Committee	Dr. Saad Khan Member of the Advisory Committee Member

Dr. Alan E. Tonelli
Chair of the Advisory
Committee

DEDICATION

I dedicate this work to my parents, my sisters and my husband whose support and confidence in my capability has been unflinching throughout this academic sojourn.

BIOGRAPHY

Jyotsna Vedula was born on December 4^{h}, 1979 in Jeypore, Orissa, India. She spent her childhood in Korba where she completed both her primary and secondary school education. She got her Bachelors Degree in Chemical Engineering from National Institute of Technology, formally Regional Engineering College, Rourkela, Orissa, India in 2002.

She joined the research group of Prof. Alan E. Tonelli when she came to North Carolina State University for her Master's Degree in Textile Engineering in August 2003. She has since been a member of this group investigating the changes in the behavior of PET observed by precipitating the polymer.

ACKNOWLEDGEMENTS

I would like to express my sincere thanks and gratitude to the chair of my advisory committee Prof. Alan E. Tonelli for his support and encouragement in the course of my studies. My gratitude to the other members of the advisory committee: Prof. Juan Hinestroza and Prof. Saad Khan for giving their consent to be on my committee.

I am deeply indebted to Dr. Cristian Rusa, for his untiring effort in helping me understand things and for his generous help with my experiments. He has been an invaluable asset who has made this work possible.

I would like to thank Birget Anderson for her training in DSC, TGA and FTIR, and X-Ray, and Terezie Zapletova for help in viscosity measurements. Many thanks to Dr. Mariana Rusa, Marcus A. Hunt, Tamer Uyar, and Hyungchol Yang for helping me with my experiments and their analyses.

Finally, I would like to express my deep gratitude to my parents and especially my elder sister Rashmi Maruvada for their limitless blessings and support during my work. Without their support this thesis would not have been completed.

This work was financially supported by the Nonwoven Cooperative Research Centre. It was also greatly supported by North Carolina State University and the College of Textiles.

TABLE OF CONTENTS

Pages

LIST OF FIGURES

Pages

LIST OF TABLES

Pages

1. Background

1.1. Polyethylene Terephthalate

Polyesters were first investigated by Carothers of E. I. du pont de Nemours and Co (USA) during a program of fundamental research into polymerization which began in 1929. The aliphatic polyesters that were formed had low melting points, had poor resistance to hydrolysis, and were sparingly soluble in organic liquids. Later in 1941, Whinfield and Dickson of the Calico Printers Association Ltd. (UK) prepared the aromatic polyester polyethylene terephthalate (PET), which was found to have promising applications as fiber and film forming material. E. I. du pont de Nemours and Co (USA) and Imperial Chemical Industries Ltd. (UK) undertook large scale manufacturing in 1953 and since then, PET has become a major textile fiber [1].

PET is a long chain polymer that belongs to the family of polyesters [2]. PET is mainly formed from terephthalic acid (HOOC-C_6H_4-COOH) and ethylene glycol (HO-C_2H_4-OH), both of which are derivatives of oil feed stocks.

The reaction between ethylene glycol and terephthalic acid to form PET [3] can be shown as:

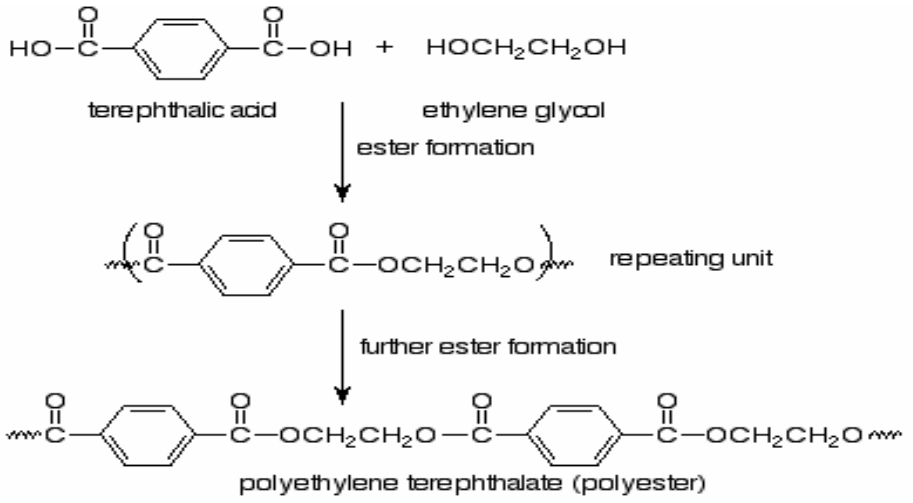

Figure 1.1. Reaction showing the formation of Polyethylene Terephthalate

The weight average molecular weight of the commercial polymer is 20,000 to 30,000. The amorphous polymer in film form is almost clear, but is deficient in some other outstanding physical properties. Thin films, crystallized by heat or by a reagent, such as acetone, become white, opaque, and brittle. However, a properly oriented, crystalline film of this polymer not only retains its clarity, but also exhibits excellent physical properties, being tough and flexible, to temperature over 200°C, and is commercially available as Mylar polyester film [4].

PET is a semi-crystalline polymer composed of crystalline and amorphous regions, and is a versatile engineering plastic material with excellent thermal and chemical resistance and mechanical performance. PET has been studied extensively due to its commercial importance and chemically flexible nature [5]. PET is extensively used as fiber for apparel, as film for packaging, in bottles for beverages, and is molded also into engineering components. Because of the high melting temperature (around 250°C) and glass transition temperature (around 80°C), PET retains its good mechanical properties at temperatures up to 175-180°C. Being a semicrystalline polymer, its crystallinity varies from amorphous to fairly high crystalline. It can be highly transparent and colorless, but thicker samples are usually opaque and off white. PET is a hard, stiff, strong, dimensionally stable material that absorbs very little water. It has good gas barrier properties and has good chemical resistance except to alkalis, which hydrolyze it [6]. All these properties of PET are described in detail in the next section.

1.2. Physical properties of PET

Physical properties of PET are described in [3] "Report on Packaging Materials: 1.Polyethylene Terephthalate (PET for Food Packaging Applications)". PET has been found to exhibit many interesting properties (morphologies). PET as described above has been characterized as a semicrystalline polymer, and, on heating above the range of 70 – 80°C, exhibits a transition from a rigid glass like state to a rubbery elastic form where the polymer chains can be stretched and aligned in either one direction to form fibers or in two directions to form films and bottles. The material melts in a temperature range of 250–260°C. After melting, if the melt is rapidly cooled while held in a stretched state, the material turns out to be very tough and can be formed into bottles that are used for storage purposes.

Also if PET is held in the stretched form at a temperature above the glass transition (70 - 80°C) it slowly crystallizes and the material starts to appear opaque, more rigid, and less flexible. It is then termed crystalline PET. At this stage PET can withstand high temperature and can be used to make containers that can cope with moderate oven temperatures. Careful manipulation between each of these forms helps in generating a wide range of different products, which are all processing variants of the same basic PET.

In the past few years PET is becoming the package of choice for many food products, particularly beverages and mineral waters. The main reasons for the popularity of PET are the properties of glass-like transparency, coupled with adequate gas barrier properties for retention of carbonation. Also, it exhibits a high toughness/weight property ratio which allows light weight, large capacity, and safe unbreakable containers.

In general, some of the properties of PET that make it a commercially important polymer can be listed as:

- PET has an excellent friction coefficient (almost as good as nylon)
- Moisture absorption is much lower than nylons
- Has superior dimensional stability (low creep) and has very good impact strength
- Wear resistance is also as good as the nylons
- FDA approved for use as packaging for food stuff
- Has good electrical properties
- PET is oxidized by mineral acids and hydrolyzed by hot water
- Has good optical clarity
- PET has excellent thermal properties that allows processing and use over a wide temperature range

All these key-properties of PET are listed in Tables 1.1.-1.3.

Table 1.1. Chemical Resistance of Polyethylene Terephthalate Film

Acids - Concentrated	Good
Acids – Dilute	Good
Alcohols	Good
Alkali	Poor
Aromatic Hydrocarbons	Fair
Greases and Oil	Good
Halogens	Good
Ketones	Good

Table 1.2. Electrical Properties of Polyester Film (1-mil thickness, 25 °C)

Dielectric constant, 60 c. p. s.	3.2
Dielectric strength, volts/mil	4500
Dissipation factor, 60 c. p .s.	0.003
Surface resistivity (ohm-100% R. H.)	4.8×10^{11}
Volume resistivity (ohm-cm)	1×10^{19}

Table 1.3. Mechanical properties of Polyethylene Terephthalate film (25°C, 35%R. H.)

Property	Mylar
Thickness, mils	1.0
Tensile strength, lb/sq. inch	23,500
Elongation, %	70
Tensile Modulus, lb./sq. inch	500,000
Tear, gram	18
Impact, kg-cm	90
Flex, cycles	20,000

All the above properties have been taken from the "Physical properties of Polyethylene Terephthalate films" [7].

1.3. Literature Review

1.3.1. Studies of Crystallinity in PET

As described by Kong *et. al.* [8], the crystallinity of a semi-crystalline polymer like PET is one of the most important physical parameters that reflects the morphology and determines mechanical properties, such as Young's Modulus, yield stress, fatigue response and impact strength, all of which increase with increased crystallinity. Another result of increased crystallinity is the increase in brittleness and the change in the fracture mechanism from ductile yielding to craze initiation of cracks. As stated previously, because PET is a semi-crystalline polymer it can de obtained in a wholly amorphous form or with various levels of crystallinity.

Different methods have been employed in order to study the behavior of PET at both the microscopic and the macroscopic levels. Various studies using Differential Scanning Calorimetry (DSC), spectroscopic analyses, such as Raman and Fourier Transform Infrared spectroscopy (FTIR), ^{13}C-NMR observations, Atomic Force Microscopy, Wide Angle X-ray Diffraction (WAXD) etc., have been employed, and are discussed in the following.

1.3.1.1. Differential Scanning Calorimetry studies on PET

The DSC method relies on measuring the heats of fusion and melting temperatures of semi-crystalline samples and comparing them directly with previously well characterized standard samples [9]. The melting temperature ranges observed depend on the thermal stability of the lamellae present in the sample and on their thickness distribution.

According to Kong *et. al.* [8], DSC is a widely used method for characterizing semi-crystalline polymers by determining melting characteristics and crystallization mechanisms,

because crystallization is a phase transition that plays an important role in determining the structures and morphologies of polymers produced in a wide range of technological processes. Because the crystal structure and the morphology (crystal habit and organization of crystals into aggregates of higher order) are responsible for the properties of the final product, knowledge and understanding of crystallization mechanisms is crucial for designing the material or product to have the required properties, and for this reason DSC study of the polymer is important.

The conventional DSC analysis of an amorphous polymer is illustrated in Figure 1.2.

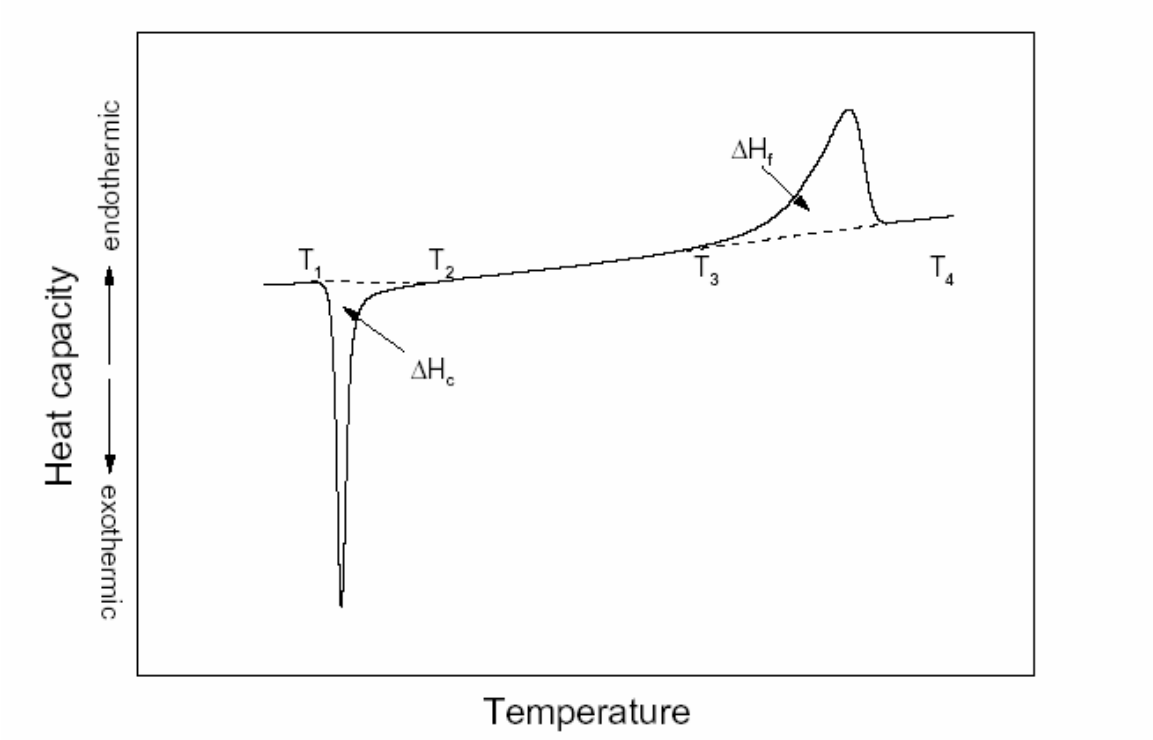

Figure 1.2. Schematic representation of the enthalpy changes on heating an amorphous cyrstallizable polymer [8]

According to Kong et al [8], the weight fraction crystallinity $X_c(T)$ of the as-received sample is measured by dividing the observed enthalpy of fusion $?H_f(T)$ by the enthalpy of fusion of a totally crystalline sample $?H_f^0(T)$, often obtained by extrapolation. $X_c(T) = ?H_f(T) / ?H_f^0(T)$, where $?H_f(T) = ?H_f - ?H_c$ = Enthalpy of fusion of the as-received sample (prior to heating) calculated by the difference of the areas under the endothermic melting peak and the exothermic crystallization peak, the latter produced during heating.

In almost all DSC analyses the crystallinity is calculated using this conventional method. The percent crystallinity in the PET sample is obtained by analyzing the areas under the endothermic melting peak and the exothermic crystallization peak. A review by Gerard Denis [10] also deals with the DSC method of analyzing the ability of PET to crystallize. It shows that crystallization of PET can be obtained by cooling from the melt, as well as by heating or by stretching from the amorphous glassy state. According to this paper the temperature at which the crystallization occurs should be between the glass transition temperature ($T_g \sim 75^\circ C$) and the cold crystallization temperature ($T_c \sim 135^\circ C$). The material is examined during the heating scan, followed by a cooling scan, and then again heating the sample, which is considered as the second heating scan. Thus the crystalline fraction can be determined from the cooling scan when the polymer is in the liquid state and/or in the heating scan when the polymer exhibits a glassy nature (exothermic crystallization peak at $\sim 135^\circ C$). An important conclusion made in this work is that the phase changes taking place in PET depend mainly on the thermal history of the sample. This fact has also been supported by Wasiak *et. al.* [11], who claims that memory of a previous structure, interpreted as the memory of the history of external conditions experienced by polymers, is of paramount importance for the DSC behavior exhibited by the polymer. The paper claims that

temperature has an effect on the crystallinity. The memory effect is due to the difference in the number of nuclei that are formed during crystallization, which is in turn affected by the thermal history of the sample [12]. Thus it has been concluded that memory effects play an important role in the formation of structure in real cases of industrial processing, where crystallization occurs during fast cooling of the molten polymer.

To date, most of the studies done on the isothermal crystallization of PET involve the melting of the polymer sample at temperatures well above the equilibrium melting point, followed by rapid quenching to the temperature, T_c, chosen for crystallization. Isothermal crystallization studies have revealed several fundamental aspects of the crystallization mechanism, but this has been criticized as being over simplified. Similarly, Tan *et. al.* [12] states that crystallization studies of PET are important and interesting, because the crystallization behavior is sensitive to both the thermal history and orientation of the PET sample. This article mainly analyses the double melting behavior and the corresponding morphological features of PET observed in the DSC scan of isothermally crystallized or annealed PET. Figure 1.3. shows the DSC thermogram of PET with two melting peaks, which are associated with two distinct crystal populations. These are also assumed to be melting and recrystallization phenomena of one initial crystal morphology, which is characteristic of the prior crystallization history.

All the above DSC analyses of the crystallization of PET were either performed by cooling PET from the melt to the crystallization temperature or by heating from the amorphous glassy state.

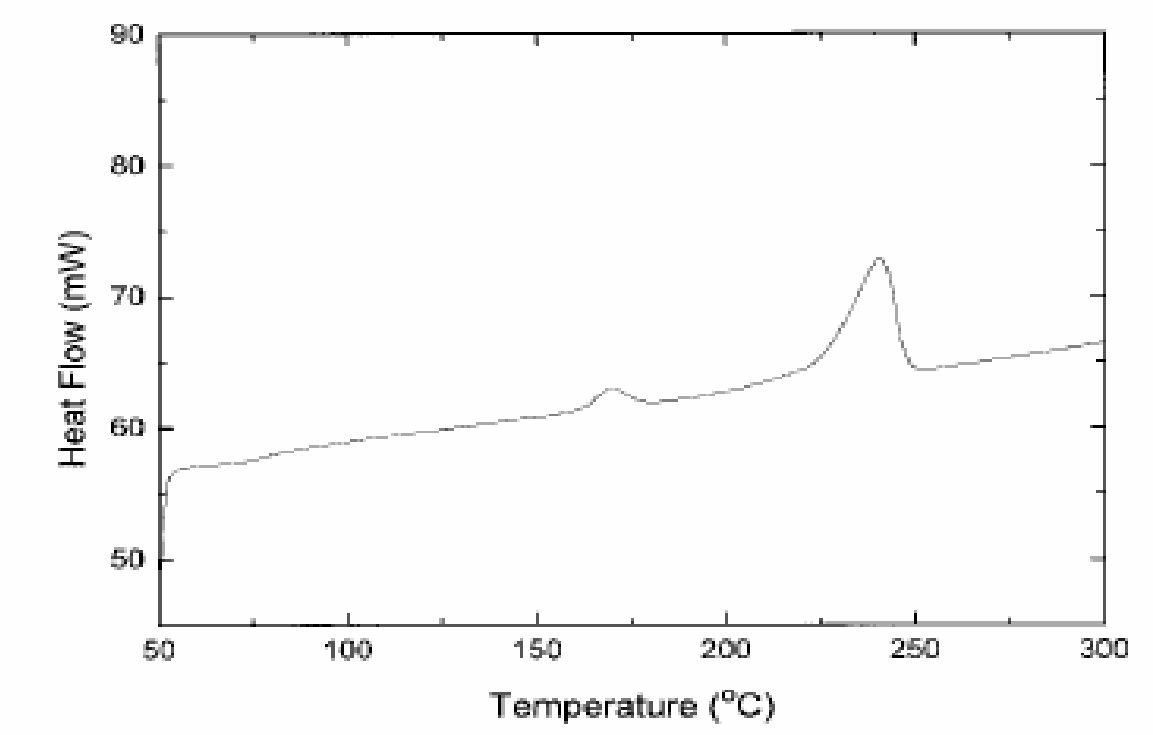

Figure 1.3. DSC thermogram of PET showing two melting peaks [12]

Crystallization of PET [11 and 13] under non-isothermal conditions, where fast heat exchange takes place because the crystallizing system is forced to change its temperature, has also been studied. Thus, the rate of crystallization is not only controlled by the momentary temperature of the material, but also may depend on the cooling rate.

1.3.1.2. Fourier Transform Infrared Studies of PET

Polymer chains undergo changes in their segmental motions and conformations when subjected to a change in temperature. FTIR is an important tool used to study their intermolecular interactions and intramolecular conformations. Changes in the absorption intensities and frequencies of conformationally sensitive bands occur as the polymer reaches

a transition temperature. As a consequence, changes in some FTIR bands occur in the vicinity of the T_g of a polymer.

Also, the infrared spectra of PET have several bands which show a change in their intensity with the increase in the crystallinity of the sample. An extensive study has been done by Cobbs and Burton [14], who followed the 972cm^{-1} crystallization band upon heating PET. Similar work was done by Miller and Willis [15] to study the amorphous content of the polymer by measuring the intensity of the band at 898cm^{-1}.

The most complete infrared study of PET has been done by Miyake [16], where the spectra of PET have been studied by varying both the temperature and the draw ratio. The conclusions that have been made in this paper are tabulated below:

Table 1.4. Variation in intensity of PET IR bands with temperature

Wave number (cm^{-1})	**Variation in Intensity** **'?'= increase with temperature**
973, 895 and 845	Increases with ?
794, 1410, 1018 and 874	Constant even with change in temperature
1172	Does not change appreciably
1475, 1387, 988 and 1022	Not found initially, but appears with the ?
1109	Initially hidden but appears later with ?
1277 and 1119	Become stronger with ?
1099	Become weaker with ?
874	Becomes a little stronger and moves to 873 cm^{-1} with ?

FTIR spectroscopy has also been used in the determination of the glass transition temperature of thin PET films. The changes that takes place in the absorbance ratios of the bands at 1340 cm^{-1} (characterized as having a trans conformation) and 1370 cm^{-1} (gauche conformation) during heating has been studied by Zhang *et. al*. [17]. Their main aim was to determine the T_g of thin PET films. The T_g for the thin films is found to be somewhat below that of the bulk sample. The influence of annealing on the glass transition temperature of the polymer was also examined. In PET, the –O-CH_2-CH_2-O- moiety adopts a trans conformation in the crystalline regions of the sample, whereas in the amorphous regions it predominantly adopts the gauche conformation. Results from the above mentioned articles indicate that as the temperature of PET is raised near to T_g a transition in the conformation of PET from gauche (1370 cm^{-1}) to trans (1340 cm^{-1}) takes place. Abrupt changes in the absorbance ratio of the 1340 and 1370 cm^{-1} bands are observed near the glass transition temperature of PET (~ 70–80°C). With an increase in the annealing time, the absorbance of the 1340 cm^{-1} band grows, while that of the 1370 cm^{-1} band can hardly be observed. Absorbance changes of the two bands indicate the occurrence of deorientation of the PET chains (i.e. the chains relax from what in the glassy state). Similar work on the FTIR determination of the T_g of PET has been done by O'Reilly *et al*. [18]. They determined the T_g of the polymer from a conformational energy calculation using FTIR spectroscopy.

Work in a similar direction has been done by Atkinson *et. al.* [19]. FTIR spectroscopy was used to observe the changes in the chain conformations of PET that occur during the glass transition and physical ageing. Cooling the liquid PET increases the population of gauche ethylene glycol conformations and decreases the trans content. The main outcome of this study is that 898 and 973 cm^{-1} absorption band intensities change with

temperature as the sample reaches its glass transition temperature. These bands correspond to the wagging of the oxy-ethylene group and to their gauche and trans conformations, respectively. Absorption bands at 1340 and 1370 cm^{-1} correspond to the wagging of the ethylene unit in trans and gauche conformations. These bands are found to show a greater change in intensity on crystallization and with the change in temperature than those at 973 and 898 cm^{-1}. The 1340 cm^{-1} band absorbance changes to a greater extent on crystallization and hence its assignment to the trans conformer is confirmed. Figure 1.4. taken from the above mentioned article [19], describes the absorbances of the 1340 and the 1370 cm^{-1} bands in quenched and crystalline PET.

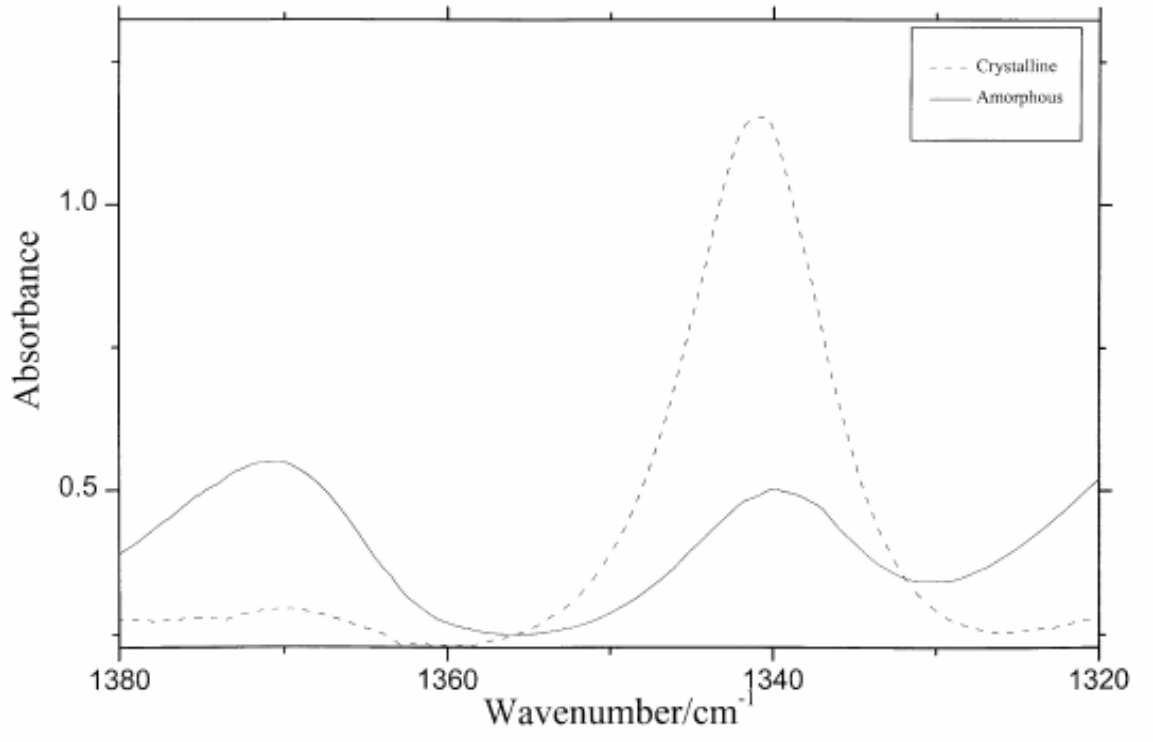

Figure 1.4. Absorbance of the 1340 and 1370 cm^{-1} bands in quenched and crystalline PET [19]

The FTIR spectrum of the PET film, which was allowed to cool down from 95 to 45°C at 5°C/min, was observed. The amount of trans conformation (1340 cm^{-1}) decreased with decreasing temperature and the gauche conformation (1370 cm^{-1}) increased. The onset of the glass transition temperature is determined from the change in the temperature dependence of the trans absorbance.

A further study on the crystallization of amorphous PET film using FTIR was done by Radhakrishnan *et. al.* [20] who observed the isothermal crystallization from the glassy state. They concluded that the structural organization during isothermal crystallization of PET consisted of three stages:

- In the initial stage thermodynamic relaxation occurs, which involves the conformational transition from gauche to trans, when the samples are heated above T_g.
- In the next stage, self-organization process occurs in the oriented amorphous structure in which the degree of orientation is found to increase with time from a nearly isotropic state and the gauche conformation is transformed to the trans conformation.
- The crystallization is finally found to occur in the third stage, and the crystalline order increases with time. The degree of orientation and the trans content are constant after this stage.

FTIR has been used to study the crystal structure. The 971cm^{-1} band that corresponds to the C-O stretching vibration of the trans unit in the ethylene glycol linkage and 1370 cm^{-1} which correspond to the $–CH_2–$ wagging mode of the gauche conformer have been studied to understand structure formation. The observations that were made on these bands show the absorption intensity of the 971 cm^{-1} band decreases and that of the 1340 cm^{-1} band increases

on heating the film from room temperature to the crystallization temperature as found in most of the papers that are described above.

At the start of the isothermal crystallization process the area of the trans band starts to increase and that of the gauche band starts to decrease (first stage of crystallization as described above). Afterwards the conformational transition proceeds from gauche to trans gradually (which is the second stage) and then the absorption intensity levels off and stays at a constant value. So far the variation in intensity and absorbance with temperature for the trans and gauche bands in PET's have been studied for films.

1.3.1.3. WAXD Crystallinity Measurements

WAXD is also used as a tool to study the crystallization behavior of polymers. Different studies have been carried out in order to determine the crystal structure of PET. Crystallization of polymer under fast cooling has emerged as a new method of technological interest which is also an objective of our research. Also, the crystallization of PET under fast cooling rate from the melt has been examined using WAXD. In a study that has been carried out by Calleja et. al. [21] the structure development in thin amorphous PET film quenched at high cooling rate from the melt was observed. Their X-ray diffraction results are seen in Figure 1.5. and indicate that with the decrease in cooling rate the diffraction curve shows a gradual transformation from amorphous to a crystalline nature.

Observed sharpening of the X-ray scattering peak that is associated with the triclinic crystal phase indicate that there is an increase in the perfection of crystals. At high cooling rates the PET behaves as a glassy material that was melt-quenched into an amorphous material.

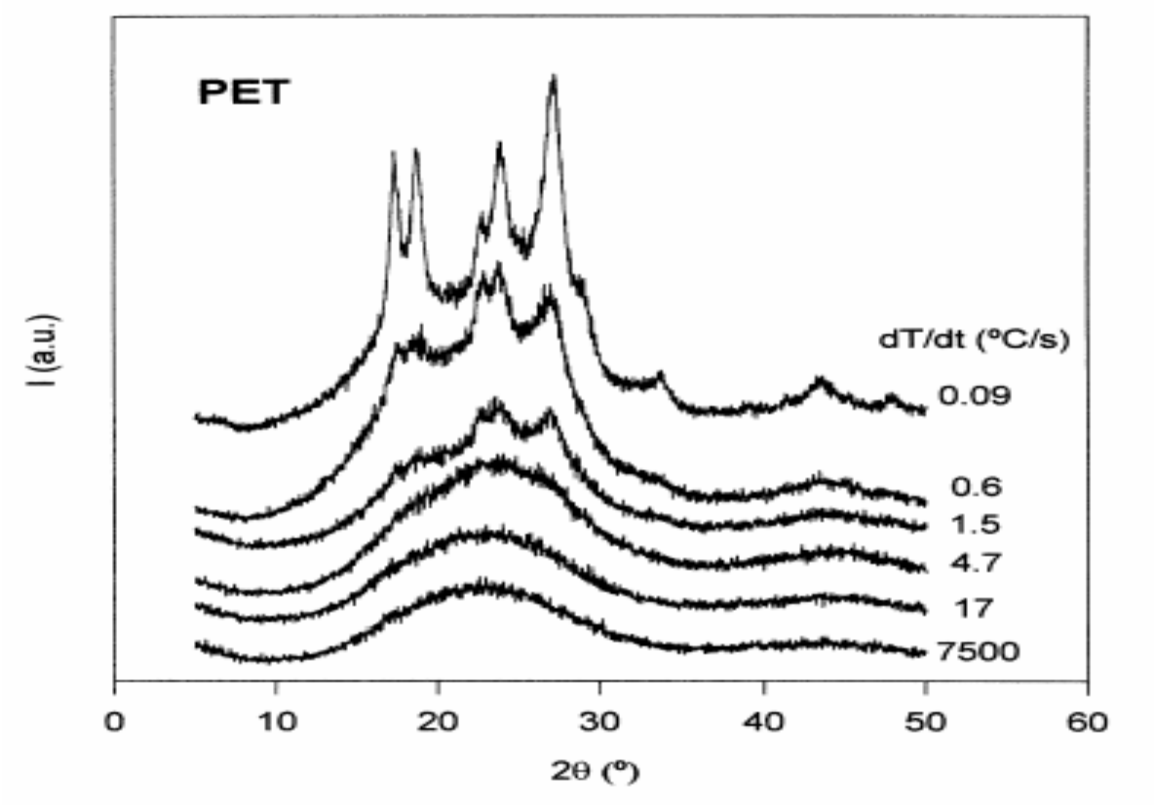

Figure 1.5. X-Ray diffractograms of thin PET film samples, cooled from the melt at different cooling rates, dT/dt [21]

A similar study of the crystallinity and physical characterization of PET using WAXD was done by Dhoot *et. al.* [22]**,** who examined biaxially oriented PET films to obtain their X-ray diffraction patterns. The diffractogram of one of their PET films is shown in Figure 1.6., and consist of a broad amorphous halo and peaks centered at 2θ = 16.6, 22.5, and 25.4° that are associated with PET crystallites. Vertical lines represent the peak locations expected for the (011), (010) and (100) reflections in PET. Also, the Herman's orientation function (f_c) was determined to be 0.875, which indicates a high degree of crystallite orientation in the plane of the film.

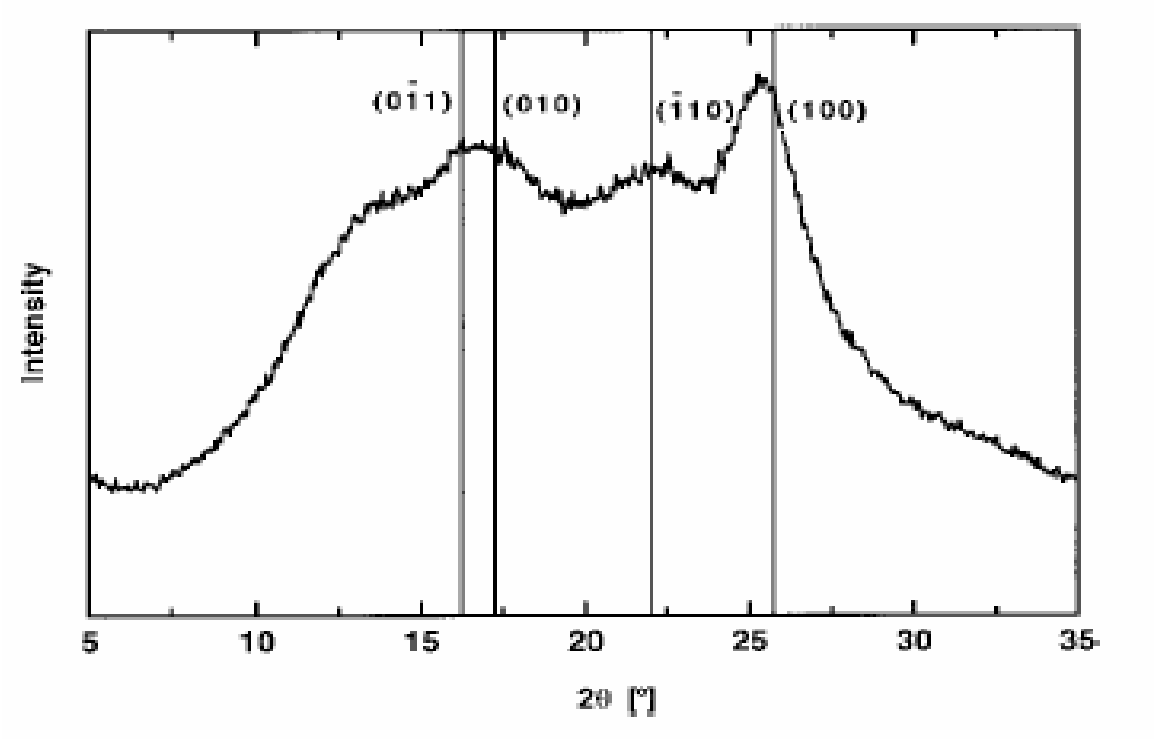

Figure 1.6. Wide Angle X-Ray Diffraction pattern of PET film [22]

1.3.1.4. Crystallinity Measurements by Density

Densities are measured on molded specimens by the Archimedes floatation method in a mixture of two different solvents, one having a lower density and the other a higher density than PET. The sample is suspended in the liquid and is allowed to equilibrate. Calculation of crystallinity by measuring the density of the polymer has motivated these studies. Weight Fraction crystallinity has been calculated in the literature [8] by using the following equation:

$$X_c = (\rho - \rho_a)\,\rho_c / (\rho_c - \rho_a)\,\rho = X_{c,v}\,\rho_c/\rho,$$

where ρ_c and ρ_a are the densities of crystalline and amorphous regions. The values of ρ_c, ρ_a used for PET were 1.515 and 1.335 g/cm^3 respectively [23 and 24]. X_c is the weight fraction crystallinity, $X_{c,v}$ is the volume fraction crystallinity, and ρ is the measured density of the sample.

1.3.2. Solvent Induced Crystallization

Several different methods have been tried to improve the crystallinity of PET. Crystallinity in PET can be induced by annealing and also by treatment with solvent. In terms of crystallization induced in the polymer by solvent, Wen Hao *Lee et. al.* [25] focused on the surface of the semi-crystalline polymer. The main aim of this work was to study crystallization induced in amorphous PET after it absorbed an organic solvent like acetone. FTIR was used to probe the conformational and molecular environment during crystallization of PET induced by the solvent. The induced crystallization was found to be a consequence of the decrease of the glass transition temperature (T_g) produced by reducing the activation energy for mobility and facilitating segmental motion. The intensity of the 973cm^{-1} band that corresponds to the "Trans" isomer of the O-C-C- group was found to be very sensitive to the ordered state of the polymer and was used in order to study the variation of crystallinity in the solvent-induced crystallization experiment. It was claimed that crystallization during the solvent transport process occurs in multiple phases as described in [20] and is a structural change which firstly involves the reorganization of the amorphous regions that occurs due to chain transport, secondly the reorganized amorphous regions emerge into well-aligned small crystallite structures, and finally lamellar thickening occurs leading to a well-defined crystal structure. It was also observed that the rate of crystallization increased with the increase in the temperature of the solvent.

Similar work by Fraeure *et. al***.** [26] was done in the direction of studying the crystallization behavior of PET. The study involved the solvent-polymer interaction in PET films prepared by a spin coating technique and water, isopropanol, and nitroethane as solvents. AFM and FTIR were used in order to understand the effects of solvent interaction at

the surface of the polymer film and to study the stress cracking phenomenon that results due to the induced crystallization. Different solvents were used in order to independently examine the effect of varying the solubility parameter of the solvent and of hydrolysis or esterification of the polymer by the solvent. Results indicate that stress cracking is initiated by the absorption of solvent by the polymer, with subsequent plasticization of the polymer. A transition from ductile to brittle nature occurs in the PET film and initiates the crazing and finally results in the cracking of the film. When the films are exposed to solvents which have solubility similar to the polymer, it was found that upon removal from the solvent, the polymer crystallinity increases, because exposure to solvent causes swelling and a decrease in the glass transition temperature and actually anneals the polymer. When the solubility parameter of the solvent is less than that of the polymer, hydrolysis of the polymer surface occurs and hence a decrease in crystallinity is observed by FTIR and AFM. So it was concluded that the increase and decrease in crystallinity of PET depends on the solubility parameter of the solvent it is exposed to.

A very recent study of the solvent-induced crystallization of PET was done by Ouyang *et. al.* [27,28]. There observations were carried out using Differential Scanning Calorimetry (DSC), optical microscopy, microscopic Fourier Transform Infrared Spectroscopy, and micro hardness measurements to examine the solvent-induced crystallization by the absorption of acetone in PET films. Their main assumption was that changing the surrounding medium to solvent molecules plasticizes the polymer and reduces the glass transition temperature by providing additional free volume. The extent of plasticization in the PET film was found to be directly proportional to the amount of solvent around the polymer molecules and the behavior is closely related to mass transport. The process of crystallization in this case was

also considered to be fully accomplished in three stages as assumed by Lee [25]. The first two stages are considered to be “primary crystallization” and the last stage is the “secondary crystallization”. DSC scans displayed exothermic crystallization peaks, whose areas decreased with the amount of amorphous regions, as shown in Figure 1.7, and represent the solvent-induced crystallization (SINC) process.

The DSC thermograms monitor the amount of residual amorphous phase, and the degree of solvent-induced crystallization could be estimated from the smaller areas of the crystallization peaks (peak 2 in Figure 1.7.) with increasing solvent treatment time. Peak 2 basically represents the amount of glassy core. All the above results indicate that the crystallization level in the polymer can be increased by making the polymer to interact with a solvent.

Annealing PET also has been used to increase the crystallinity. This is well described in the study of Huang *et. al.* [29], which mainly emphasizes the importance of the trans conformer to the annealing-induced crystallization in PET. They observed the trans-gauche ratio, the motion in different domains, and the growth in crystallization as a function of annealing temperature. The trans conformer was found to increase continuously with the increase in the annealing temperature, while the degree of crystallinity levels off during the later stages of annealing.

Koenig *et. al.* [30] observed the development of the “Trans” fraction during PET isothermal crystallization at low temperatures. The crystallization process was divided into two stages, one being the primary and the other the secondary stage. Conclusions made in this case were that the trans isomer fraction increases linearly with the annealing time.

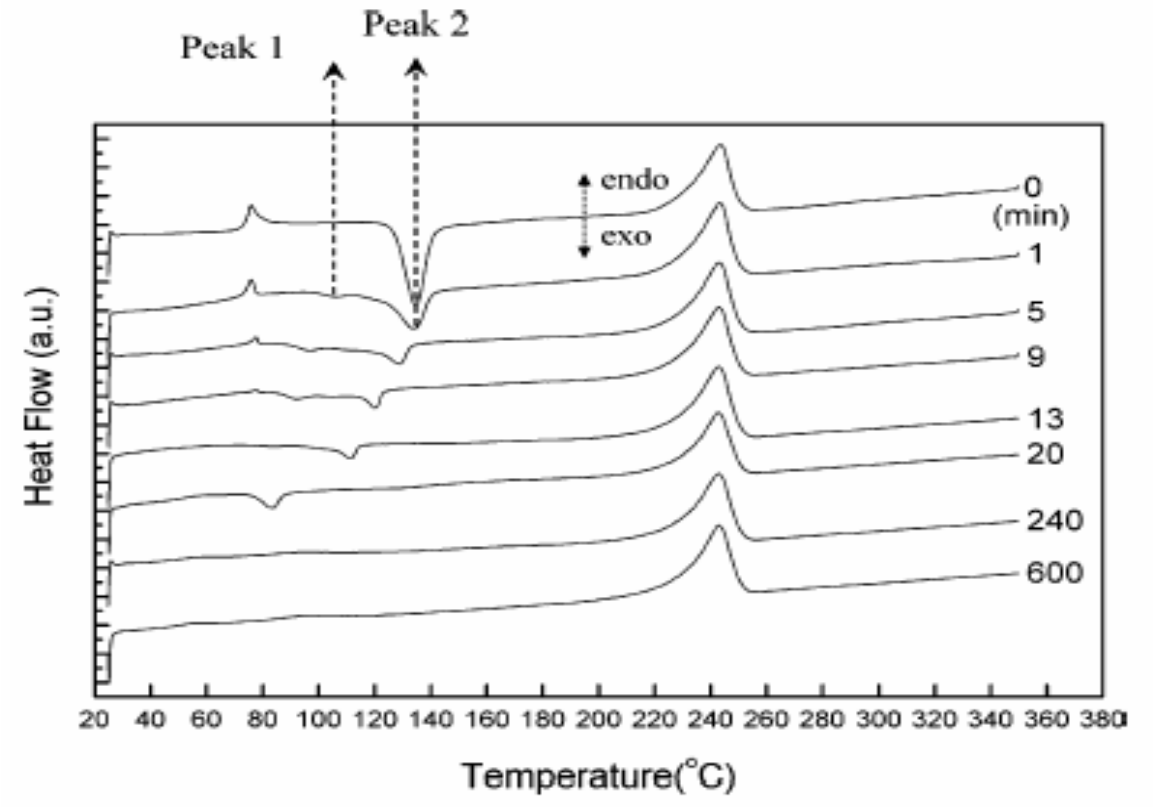

Figure 1.7. DSC curves of PET solvent-treated for different periods [25]

1.3.3. Permeability in PET Films

PET is widely used as films in packaging materials because it is light in weight and shatterproof. The permeability coefficient (P) of a permeant through a polymer is the product of its diffusion (D) and solubility (S) coefficients. D, or the diffusivity, is the speed of movement of a permeant and, therefore, characterizes how easily gas molecules can move from one position to another in the polymer. S describes the amount of gas permeant that dissolves in the polymer matrix [31]. Permeability of small gas molecules through PET films has to be reduced for it to be used in certain packaging applications. Permeability of gases can be reduced by decreasing the free volume within the polymer matrix, so that the movement of the gas molecules through the polymer matrix is impeded. The PET matrix

consists of amorphous and crystalline phases, and gas diffusion mainly takes place in the amorphous regions. Since there is a close packing of chains in the crystalline phase, the free volume available for transport of gas molecule decreases to such an extent that the crystalline phase is regarded as impermeable with respect to the more open, less dense amorphous phase. There is a practical need to improve the barrier properties of PET. Crystallization and orientation are used as two approaches for PET barrier enhancement. The efficient packing of chains in lamellar crystals or in the ordered regions of oriented PET reduces the available free volume to the extent that these regions are considered impermeable [23].

In the process of determining the permeability of oxygen through PET film, Slee and coworkers [32] observed that the volume of impermeable material increased upon drawing of the PET films, presumably due to the orientation of the chains, and hence lowered the oxygen permeability. In as-drawn samples, the impermeable units consists either of clumps of noncrystalline chains adopting the trans conformation of crystallites, whereas in the annealed material the permeability is related more closely to the concentration of crystalline material, because the majority of the trans conformers are in the crystalline regions there.

Similar work by Qureshi and coworkers [33] showed that orientation decreased the permeability of gas molecules in PET to almost one-third of the unoriented, amorphous polymer, because the diffusion coefficient as well as the solubility coefficient decreases. Stretching the film transformed the ethylene linkage from the gauche conformation into the trans conformation.

Some other studies that included the incorporation of impermeable phases, such as crystallinity or talc-platelets, into PET films have also been done [23]. Incorporation of Talc in the film did not affect permeability, but led to improvement in the mechanical properties.

Increasing the crystallinity in the PET samples decreased the amount of amorphous phase and the permeability of the gas molecules through the film correspondingly decreased.

A study on improving the permeability of PET film has been done by incorporation of comonomers like isophthalte, phthalate or naphthalate, and their incorporation gradually reduced the permeability [34]. Also some authors have modified PET with aromatic diester diamides to reduce permeability of PET to oxygen [35].

Some of the values of permeability measured for various gases in PET are presented in Table 1.5. These values have been taken from internet [36] and are the supplier data from Good Fellow.

In contrast to the previously mentioned studies, another group of workers led by Lewis *et. al.* [37] have examined the barrier properties of PET to mixtures of oxygen, carbon dioxide, and nitrogen for two different film structures; one an amorphous unoriented film and the other a biaxially oriented film that resembled closely commercially available products. This research was closer to practical reality, because, in general, simultaneous diffusion of different gases takes place through a film.

The permeant (gases) penetrates through the amorphous regions of the polymer and the crystalline regions of the polymer act as a hindrance to the flow of the gases. So, overall it can be concluded that higher the crystallinity of the polymer the smaller is the permeation of the gases through it.

Table 1.5. Permeability of different gases @ 25° C in PET film

Gases	Permeability Value X 10^{-13} $cm^3.cm.cm^{-2}.s^{-1}.Pa^{-1}$
CO_2	0.07 – 0.17
H_2	0.45
N_2	0.0034 – 0.0038
O_2	0.015 – 0.04
H_2O	100 - 115

1.4. Motivation

1.4.1. Background

The main aim of this research is to improve the properties of PET by using a simple precipitation method. We are trying to generate a PET with novel morphologies and unique properties that will be easy to process with retention of all the desirable qualities. Enhanced crystallinity levels are observed in our precipitated PET (ppt-PET). Throughout we compare the properties of as-received PET (ar-PET) with that of ppt-PET and investigate their differences both at the microscopic and macroscopic levels.

The initial motivation for this research was the improvement in the properties of PET observed by processing the polymer with cyclodextrins [38 and 39]. It had been observed that when polymers are made to form inclusion compounds (ICs) with cyclodextrins (CDs), and are then coalesced by removing the CD hosts, the processed polymers are found to behave differently than the as-received polymers [40], and this is particularly striking for PET.

In work done by T. A. Bullions *et. al.* [41], polymers were made to form noncovalent crystalline complexes with the small molecules hosts cyclodextrins, which act as the host for the guest polymer. Cyclodextrins (CDs) are cyclic oligosaccharides that are able to form non-covalent complexes/inclusion compounds (ICs) with various guest molecules [42, 43, and 44]. Based on the number of glucose units, CDs are classified as α-, β-, and γ-CDs. α-CD has 6 glucose units, followed by β-CD which has 7, and finally γ-CD has 8 glucose units [45], and Figure 1.8. presents their structures. CDs are water soluble due to their exterior hydroxyl groups, while the CD ring cavity is relatively hydrophobic compared to the outer surface. The average diameters of the doughnut-shaped cavities of α-, β- and γ -CD are ~ 5, 6

and 8.0Å, respectively. Since the inner cavities are hydrophobic, subject to cavity size restrictions, hydrophobic guest polymers like PET can also be included in CDs.

As described previously, ?-CDs are capable of forming an inclusion compound with PET [41]. In an inclusion compound the guest polymer chains occupy the narrow cylindrical channels created by the crystalline host CDs. Figure 1.9. shows an inclusion complex of cyclodextrins. The as-received CDs are packed in the form of a cage crystalline structure, which is less symmetric and represents the natural state of CDs [45]. As CDs form an inclusion compound with a guest polymer they adopt the channel crystal structure that is more symmetric and presents the state of CDs complexed with polymers (see Figure 1.9.).

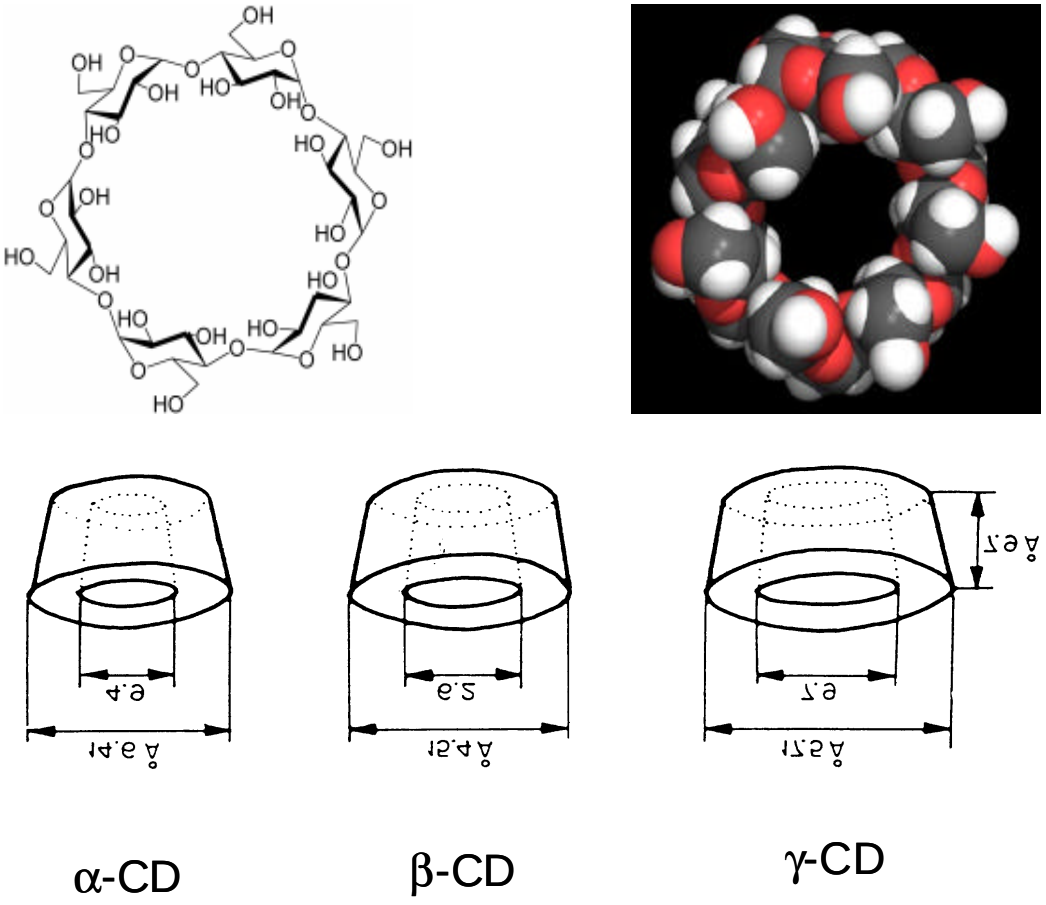

Figure 1.8. Schematic representation of a **-,** b **-,** g **-cyclodextrins**

The next step in the processing of polymers using their CD-IC's is the coalescence of the polymer. As is indicated clearly in Figures 1.9. and 1.10., the polymer chains are constrained to assume highly extended conformations and are segregated from neighboring polymer chains by the channel walls of the host crystalline CD lattice [41]. The polymer is isolated and made to assume extended, stretched conformations in these channel structures CD-ICs.

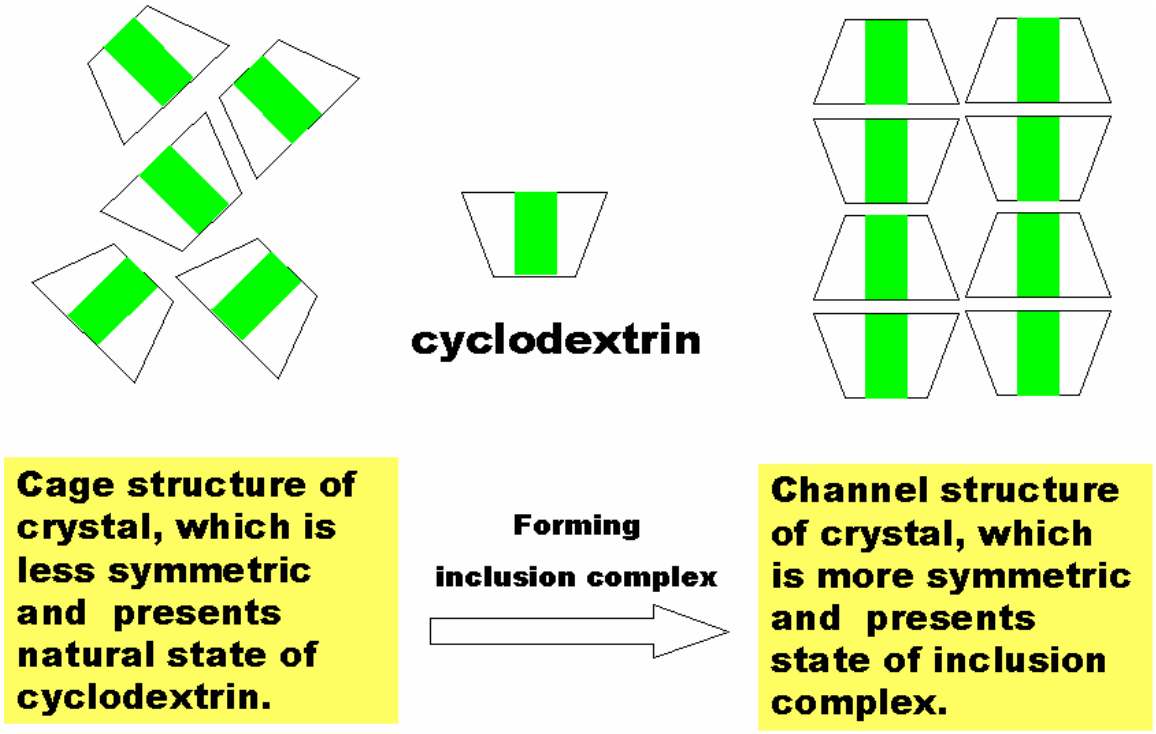

Figure 1.9. Schematic representation of the natural (cage structure) and inclusion complex of cyclodextrins

The main driving force behind the present work were previous investigations done by Wei *et. al*. on improving and restructuring the properties of PET [41,46]. There it was observed that crystallizable polymers coalesced from their molecular CD complexes reveal semi-crystalline characters that are observed to be distinct from samples crystallized from their completely

disordered solutions or melts. An extended-chain crystalline morphology for the IC-coalesced polymer samples is observed (Figure 1.10.). PET was processed using γ-cyclodextrin and has been found to organize differently. Some of the properties of PET that are expected to show a change were observed both microscopically and macroscopically and are described by the work in Bullions *et. al.* and Wei *et. al.* for PET [41,46].

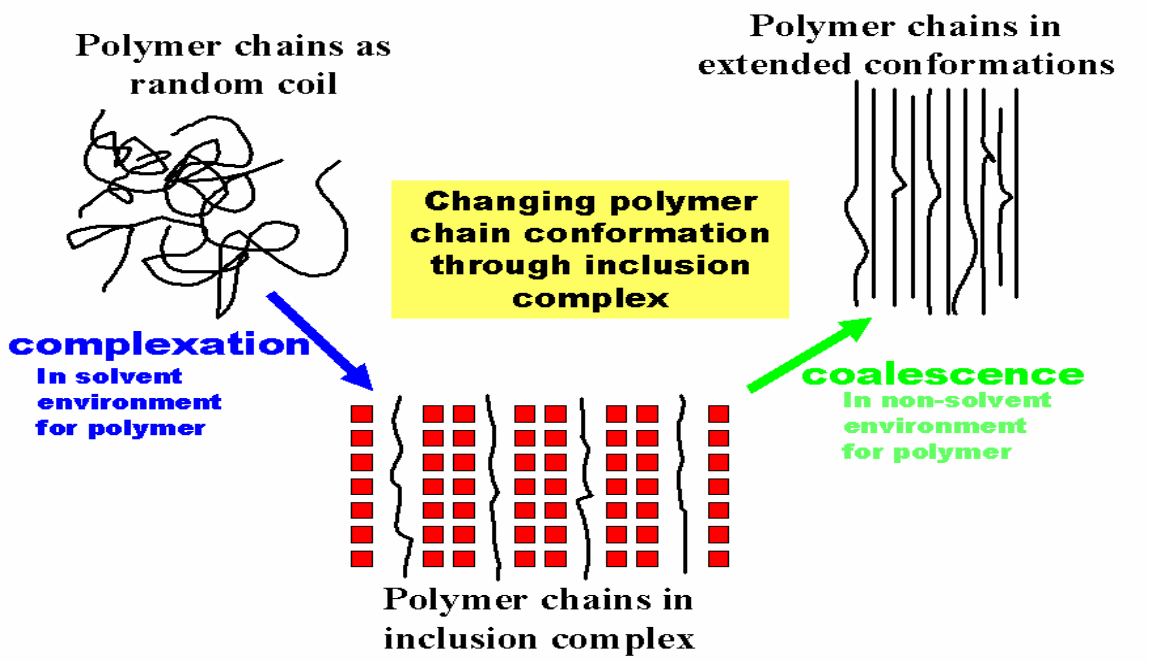

Figure 1.10. Representation of the coalescence of guest polymers from their cyclodextrin-inclusion compounds

Processing from its γ-CD-IC, the coalesced PET obtained was found to have much higher crystallinity than as-received PET. Repeated heating and cooling scans on the coalesced PET revealed an absence of both a glass transition and a crystallization exotherm upon heating, and, instead, just the presence of the melting endotherm was detected. On rapid cooling from the melt, a recrystallization exotherm is obtained in the case of coalesced PET, and it was concluded that the chains in the coalesced sample are organized differently than those in the as-received PET. The as-received PET can be quenched into predominantly amorphous material, whereas the coalesced PET cannot be obtained in a totally amorphous form. Figure 1.11. presents the results obtained using DSC, where the coalesced material is compared with the as-received, and solution- cast PET. The results of these DSC thermograms have been compiled in Table 1.6.

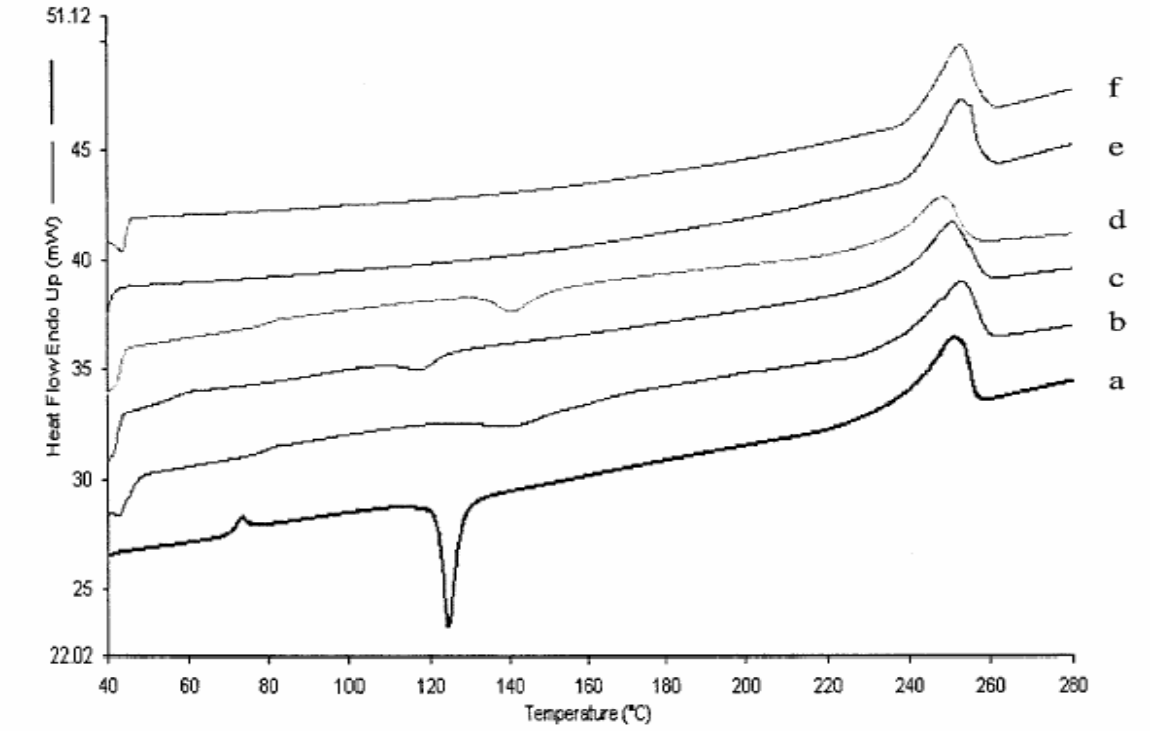

Figure 1.11. DSC scans of as-received PET runs I (a) and II (b), solution-cast PET runs I (c) and II (d), and IC-coalesced PET runs I (e) and II (f) [41].

Table 1.6. Heating Runs I and II DSC data for different PET samples [41]

Sample	Crystallization			Melting			Difference		
	T_g (°C)	Onset (°C)	T_c (°C)	ΔH_c (J/g)	Onset (°C)	T_m (°C)	ΔH_r (J/g)	$\Delta H_r - \Delta H_c$ (J/g)	W_c (%)
Pure PET run I	70.3	122.0	124.8	27.0	239.9	250.8	44.2	17.2	14.3
Pure PET run II	77.2	125.5	141.2	17.2	241.3	252.8	41.6	24.4	20.3
Cast PET run I	53.8	109.7	117.7	5.24	237.2	250.7	43.5	38.3	31.9
Cast PET run II	78.2	133.08	140.5	9.60	234.4	248.2	37.8	28.2	23.5
Coalesced PET run I	—	—	—	—	237.3	249.7	46.6	46.6	38.9
Coalesced PET run II	—	—	—	—	241.9	252.9	45.0	45.0	37.5

From the tabulated results above, it is clear that neither a glass transition nor crystallization are observed on heating the coalesced PET, and also the crystallinity values of the coalesced PET are higher than the as-received and the solution-cast PET samples.

FTIR observations and solid state ^{13}C NMR results on the coalesced PET were consistent with non-crystalline chains predominantly in the kink conformations, with gauche±, trans, gauche$^{\mp}$ ethylene glycol conformations, required by inclusion in the narrow γ-CD-IC channels. FTIR observations on the coalesced and the as-received PET indicated that the non-crystalline regions in the coalesced sample have different conformations, with improved order predominantly in the coalesced PET. There the chains are not nearly as randomly coiling and interpenetrating as those in the non-crystalline regions of the as-received PET, and hence do not evidence a glass transition.

WAXD studies indicated that the diffraction pattern for the coalesced material is different from that of the as-received PET. Diffraction peaks at $2\theta = 16.5$, 23.2 and 26.0° are found mostly in oriented samples of PET, such as uniaxially drawn PET fibers and films, and were found to be more pronounced in the coalesced PET.

All these results support the fact that the coalesced sample has an extended-chain crystalline morphology with stretched chain conformations also in the non-crystalline regions. The coalesced sample thus evidenced morphology, structure, chain conformations, and physical properties that are distinct from those generally observed for bulk PET samples, leading to rapid crystallization from the melt and to improved crystallinity.

1.5. Conclusions

It is clear from this literature review that many previous studies were done in order to understand the structures, behaviors, and properties of Polyethylene Terephthalate (PET) by employing different experimental probes, like DSC, FTIR, and WAXD. These instruments have been used to analyze the properties of PET with emphasis on the differences in the behavior observed by increasing the crystallinity in the PET either by annealing or by solvent-induction. The main reason for conducting the present research was that our precipitated PET (ppt-PET) appears to behave similarly to PET processed using ?-CD, yet is easier to process and can be obtained in larger amounts. Thus, the behavior of precipitated ppt-PET was studied using all the above mentioned characterization techniques.

With the improved crystallinity and different organization of chains expected in the precipitated material, ppt-PET should rapidly crystallize from its melt even at high cooling rates and hence may be more useful in certain applications, because as-received PET (ar-PET) is by nature a slowly crystallizing polymer. Improvement in the orientation of the non-crystalline chains is expected in ppt-PET, and preliminary results have led us to carry out further research in the direction of comparing the properties of ppt-PET (expected to be superior) to those of ar-PET.

2. Materials & Methods

2.1. Materials

- Polyethylene Terephthalate (PET), Trifluoro Acetic acid (TFA) and Acetone were obtained from Aldrich Chemicals.
- PET has an intrinsic viscosity of 0.59 dL/g (measured in a mixture of phenol / 1,1,2,2 tetrachloro ethane w/w 6:4, at room temperature)
- Viscosity average molecular weight of 18,000g/mol

2.2. The technique for forming Precipitated PET (ppt-PET)

Precipitated PET is prepared by a simple precipitation method (Figure 2.1.). In the course of sample preparation 3 gms of as-received PET (ar-PET) are dissolved in 50 ml of Trifluoro Acetic acid (TFA). The solution is heated to 50°C with simultaneous stirring for approximately 30 min. The heated PET solution is then precipitated by adding the solution drop wise into 150 ml of Acetone kept in a round bottom flask that is stirred at a high rate. A white precipitate appears. The precipitate is then washed, filtered and dried in a vaccum oven overnight at 40 °C to obtain dry precipitated PET.

Intrinsic viscosity observations of as-received and precipitated PETs show that the precipitation process has not resulted in degradation of PET molecular weight.

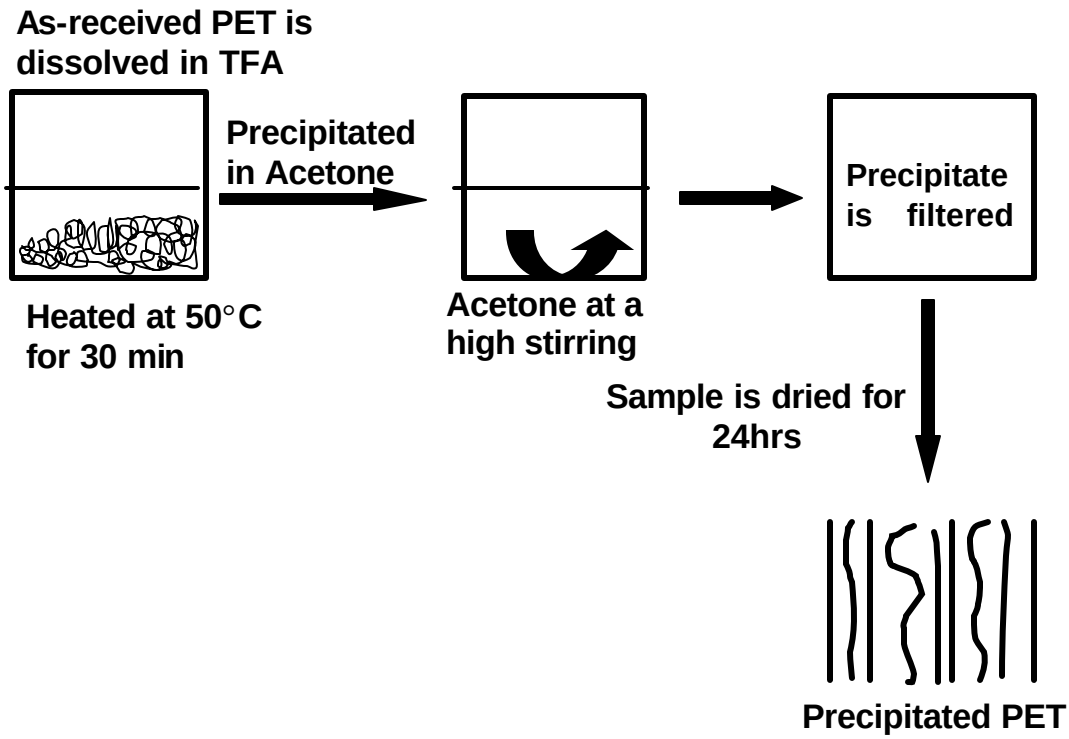

Figure 2.1. Schematic representation of the formation of Precipitated PET

3. EXPERIMENTAL TECHNIQUES

The behavior of the final product obtained by precipitating the polymer (PET) in acetone has to be confirmed to be different from the as-received PET. Confirmation that the precipitated PET (ppt.-PET) behaves differently from the as-received PET (ar-PET) can be done by comparing the Infrared spectrum obtained from the product of the attempted preparation with the spectra of the as-received material. The presence of absorption bands in the spectrum of the precipitated product that are shifted in frequency from the bands of the pure starting material and their improved resolution are usually taken as proof that the precipitated PET (ppt.-PET) behaves differently than that of the as-received PET (ar-PET).

Not only do IR results confirm that the ppt.-PET has a different morphology than ar-PET; but thermodynamic probes (like DSC, TGA) also offer information leading to some insights into the characteristics of ppt.-PET. The crystallinity levels in the two samples can be compared from their DSC thermograms, and their melting characteristics can also be obtained. X-ray diffraction analysis can offer us much detailed information about the crystal structure type, size, orientation, overall crystallinity, conformation, etc.

These experimental techniques and the procedures followed will be described in detail in the following sections.

3.1. Thermal Property Analyses

3.1.1. Differential Scanning Calorimetry

Differential Scanning Calorimetry (DSC) is mainly based on the principle that the thermal properties of the sample vary with changes in its structure and dynamics. DSC is a technique which profiles caloric heat loss or gain from a substance heated at a constant rate. It allows for the determination of the thermal properties, such as melting temperature, glass transition temperature, and other phase changes. It measures heat flow into (endothermic) and out of (exothermic) samples. It does so by measuring the power (mW) necessary to keep the sample and its pan at the same temperature as the reference pan. A prerequisite for using this instrument is knowledge of the thermal stability of the samples. As a polymeric sample is heated it absorbs energy and becomes plastic due to polymeric chain mobility, an endothermic process, and shows an increase in its heat capacity. When the amorphous regions in the polymer become crystalline, they do so accompanied by some energy release, i.e., an exothermic heat of crystallization. When the polymer reaches its melting temperature, it absorbs energy and its molten chains become mobile and disordered. All these transitions (fusion, crystalline structure transitions, vaporization, dissociation or decomposition reactions, oxidation and reduction reactions) can be recorded on a thermogram obtained from a differential scanning calorimeter.

DSC data were obtained using a Perkin-Elmer Model 7 Differential Scanning Calorimeter (DSC). Samples of 5–10 mg were used in all tests. The samples were sealed in aluminum pans designed for volatile materials and scanned by two heat/cool cycles between 25 and 280°C at a heating rate of 20°C/min and a cooling rate of 200°C/min. The instrument was calibrated before each set of scans with Indium or Tin depending on the temperature

range of interest. Nitrogen was used as the purge gas. The procedure that is employed for all the samples in our testing can be described as:

- Hold the sample for 1 min at 25°C
- Heat the sample from 25 to 280°C at 20°C/min
- Hold the sample in the melt for 10min
- Cool the sample from 280 to 25°C at 200°C/min
- Hold it at 25°C for 10 min
- Heat the sample from 25 to 280°C at 20°C/min

3.1.2.Thermo gravimetric Analysis

Thermo gravimetric Analysis (TGA) is a thermal analysis technique used to measure changes in the weight (mass) of the sample as a function of temperature and/or time. TGA is commonly used to determine polymer degradation temperatures, residual solvent levels, absorbed moisture content, and the amount of inorganic (noncombustible) filler in polymer or composite material compositions.

A simplified explanation of a TGA sample evaluation may be described as follows. A sample is placed into a tared TGA sample pan which is attached to a sensitive microbalance assembly and is subsequently placed into a high temperature furnace. The balance assembly measures the initial sample weight at room temperature and then continuously monitors changes in sample weight (losses or gains) as heat is applied to the sample. TGA tests can be run in a heating mode at some controlled heating rate, or isothermally. Typically weight loss profiles are analyzed for the amount or percent of weight loss at any given temperature, the amount or percent of noncombusted residue at some final temperature, and the temperatures of various sample degradation processes.

TGA is a useful technique for assessing the effectiveness of oven drying solution polymerized polymer samples. The volatilization of residual solvent is typically associated with the initial weight loss process in a TGA heating run, though in some cases, absorbed moisture may also be liberated over this same temperature range. After the initial solvent (or moisture) weight loss process, TGA profiles will typically plateau to some constant weight level until the polymer degradation temperature is reached. The weight fraction of residual solvent (or moisture) and the onset and maximum weight loss degradation temperatures are readily determined using TGA.

TGA data were obtained using a Pyris I Thermo gravimetric Analyzer (TGA). Samples of 5-10 mg were used in these tests. The samples were put inside platinum pans which were held in the heating furnace. The weight percentage of remaining material was recorded while the furnace was heating from 25 to 700°C at a heating rate of 20°C/min. A Curie point temperature calibration was performed using nickel and perkalloy. Nitrogen was used as the purge gas.

3.2. Fourier Transform Infrared Spectroscopy

3.2.1. FTIR using KBr Pellets

An infrared spectrum is characteristic of a particular compound providing information about its functional groups, molecular geometry and inter/intra molecular interactions. The infrared spectrophotometer provides a record of the infrared absorbency or transmittance of a sample as a function of frequency or wave number. The frequencies at which absorptions occur may indicate the type of functional groups present in the substance.

In FTIR the infrared beam passes through the beam splitter and after dividing, one portion is reflected by a stationary mirror. A laser light interferometer is used to get a zero retardation for a sampling interval, and a white light interferometer is used to get the zero retardation of the spectrum. Fourier transformation is used to convert the time domain signal into a frequency spectrum.

There are several basic techniques for examining the FTIR spectra of compounds. These include a neat preparation, liquid cells, KBr Pellets (Powdered samples were thoroughly mixed with KBr and pressed into pellets form), thin films on crystals and hot pressed films. A background spectrum is run using the same technique as the sample. The sample is run and the spectra printed. A library search is run and the best fit is matched from the available stored spectra.

Films were either placed directly in the sample beam using a magnetic film holder, or the film was sandwiched between two KBr pellets. KBr pellets were prepared by pressing finely grounded KBr powder in a hydraulic press at a pressure of 15,000 psi for approximately 10 mins. Absorbance Fourier Transform Infrared Spectra were recorded on a Nicolet 510p FTIR spectrometer (NCSU ID #205616) with Omnic software at frequencies from 600 to 4000 cm^{-1} with a resolution of $4cm^{-1}$, gain = 4, and scans = 64.

3.2.2. Microscopic FTIR

The variation of conformationally sensitive FTIR bands with temperature was studied using a Thermo Electron FTIR with Nexus 470 bench equipped with a Continum Microscope. The changes that take place in the absorbance of vibrational bands with increasing temperature were monitored. The films were prepared by pressing a very small amount of PET, so as to get the thinnest film possible. The films were sandwiched between two KBr pellets and then

exposed to the sample beam. The specifications that were used for these experiment were frequencies from 800 to 1500 cm^{-1}, with a gain = 4, velocity = 0.9494, sample compartment Right, μ scope % T, detector = MCT/A, Beam splitter = KBr. The measurements were obtained from an average of 64 scans with a resolution of 4 cm^{-1}. The temperature range that was selected for the study was from 25 to 280°C and the heating rate of 5°C/min was applied. A spectrum was collected every minute and the variations in the band intensities were observed. This was done over the whole of the temperature range until the sample melted. The sample was held in the melt for 2 hrs and then finally cooled back down to room temperature.

3.3. X-Ray Diffraction

The X-ray diffraction technique is used to determine the crystal structure of a polymer. X-rays are short wavelength electromagnetic radiation produced by the deacceleration of high-energy electrons in the inner orbital of atoms. The wavelength range of X-rays is from perhaps 10^{-5} Å to about 100 Å. Conventional X-ray diffraction is, however largely confined to the regions of approximately 0.1 Å to 25 Å. X-rays may be obtained by several different means:

- Bombardment of a metal target with a beam of high energy electrons;
- Exposure of a substance to a primary beam of X-rays to produce a secondary beam of X-ray fluorescence;
- Employment of a radioactive source whose decay results in X-ray photons that match the energy required to remove the electrons to the periphery of the atom.

The electrons excited by the absorption process may return to their ground state and cause emission of radiation. The scattering of the beam results in a diffraction pattern if the matter it passes through is crystalline. These diffraction patterns can be used to analyze the samples for the amount of crystallinity in them. Information about the crystal size can also be obtained from the diffractogram. Different crystals present in the sample show different peaks in the diffractogram. Each of the peaks in the diffractogram can be assigned Miller indices which describe the crystal type, i.e. triclinic, monoclinic, hexagonal, orthorhombic, tetragonal or cubic. The width of each of the peaks in the diffractogram is dependent on the crystal size.

The crystal size can be obtained by using the Scherrer equation:

$\delta(2\theta) = 0.9\lambda / (L\cos\theta)$, where θ = width of the peak at half-peak-height,

λ = wavelength of X-ray (1.5418 Å), L = crystal size, and θ = angle at which peak is located.

The amount of crystalline material present in the sample can be measured by calculating the area under the crystalline peaks and subtracting the area under the amorphous region. X-rays are very important in order to ascertain the structural properties of different substances.

Wide angle X-ray diffraction was recorded at ambient conditions on a Siemens type-F-X-ray diffractometer. The radiation source used was Ni-filtered, CuK_a radiation with a wavelength of 1.5418 Å. The supplied voltage and current were set to 30kV and 20 mA, respectively. Powdered samples were mounted on a circular sample holder with scotch tape, and the proportional counter detector collected data at a rate of $2\theta = 3° \text{ min}^{-1}$ over the range $2\theta = 5 – 40°$. The diffracting intensities were recorded every 0.1°.

3.4. Density Measurements

Density measurements were performed by constructing a density gradient column consisting of Toluene and Carbon Tetrachloride. Small pieces of film were placed in the column and were allowed to equilibrate for 10 min before the measurement of their heights in the column were taken.

3.5. Shrinkage Test

The study of the shrinkage of as-received and ppt-PET was carried out on the hot stage of the Microscopic FTIR (as described in section 3.2.1.). The hot stage is equipped with an optical microscope with a scale on it. The films were cut in ~ 0.5 cm squares. The films were placed over the hot stage and the temperature of the hot stage was increased from 25 to 280°C at a heating rate of 5°C. For every 5°C increase in temperature, an image of the film was taken and the length of the film was measured.

3.6. Melt Viscosity Measurements

Viscosity tests on both the PET's were carried out using the Thermo Haake Poly Lab 4.1 (Minimelter) instrument. The counter rotating, twin-screw Minimelter was preheated from room temperature to 280°C, and then the pellets of PET were fed in to the extruder and allowed to melt. The polymer stays in the molten form inside the extruder for approximately 12 mins and then the molten polymer is vented out from the exit valve.

3.7. Stress-Strain Measurements

The stress and strain measurements were carried out using the SINTECH Instron Tensile Tester. The films that were tested were made by pressing the pellets in a hot press that was heated to 280°C so as to completely melt the polymer, and the pressure applied was 5000 psi. The ASTM standard D 882 was used for testing the films. Testing conditions for the films were as follows: Lab temperature was 21.11 °C (~70 °F) and the RH was 65 %, gage length was 15 mm, load cell was of 5 lb, and the speed of the load cell was 1 in/min.

3.8. Atomic Force Microscopy

Tapping mode AFM images were obtained at ambient conditions using a NanoScope Dimension 3000 (Digital Instruments) AFM. Phase images were recorded using the retrace signal with a Si tip and the scan rate was in the range 0.5 – 1.5 Hz. AFM images of samples at 2-D resolutions of 4×4 μm are presented here.

3.9. Static Absorption of Carbon Dioxide in PET

A sorption system was employed to probe the structure of PET, consisted of an electronic balance capable of recording sample weight changes and a computer for data collection. The sample is hung from one side of the balance beam and a counterbalance made of aluminum foil is placed on the opposite side of the beam. The system used here is static in nature, because gas is introduced in a closed chamber at a fixed total pressure. Additional gas is introduced in the chamber to increase the gas pressure up to a maximum of one atmosphere (~760 torr), and is designed for sorption of gases like carbon dioxide (CO_2). Figure 3.1. shows a schematic diagram of the static gravimetric balance designed for sorption of gases at

pressure below one atmosphere. Gas is introduced in the reservoir with the valve between the balance chamber and reservoir closed. Once the pressure equilibrates in the reservoir, the valve is opened to allow gas to penetrate the sample. For this work CO_2 gas was used, because it is inert. Approximately 0.5 gms of PET film is hung on the Cahn 2000 gravimetric balance. The balance chamber was evacuated until no sample weight loss was recorded. An interval sorption experiment was performed in which CO_2 gas was initially introduced in the balance chamber at approximately 100 torr, then the mass gain was monitored until the sample mass reached equilibrium. The pressure was then increased by about 100 torr and again equilibrium was established. This was repeated up to a pressure of one atmosphere.

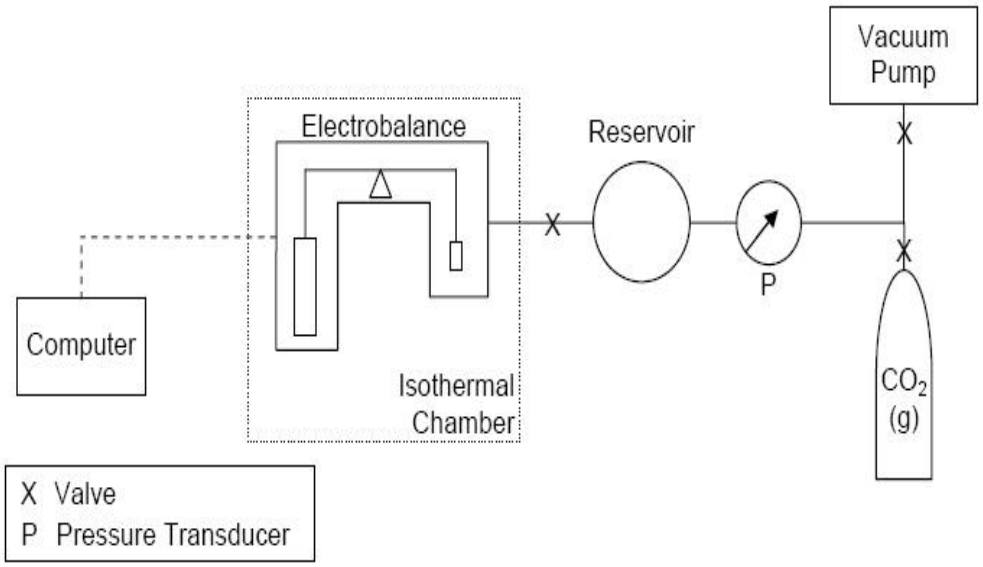

Figure 3.1. Static gravimetric absorption apparatus

3.10. Fiber Testing

PET fibers were obtained by an extrusion process, where the polymer pellets were melted in and extruded from the Minimelter, and were then drawn, followed by quenching and winding over a rotating roller. Though the fibers are not fully drawn, there is likely some orientation in the formed fibers. Stress-strain tests on these fibers were performed using an SINTECH testing device that was also used for testing PET films. Single filaments of the PET fiber were used for testing and the specimen was prepared by mounting the fibers on a rectangular cardboard frame using tape. The fiber with the cardboard was mounted in the grips of the SINTECH and then the cardboard support was cut to allow free movement of the specimen. A gauge length of one inch and a strain rate of 20%/min was used. Six to eight specimens were tested in each experiment and the data presented is the average of all the samples.

4. Results & Discussion

PET has been a polymer material of interest for many years. It is commercially used in the production of fibers, films, yarns and in packing materials. My research has been focused on the study of Polyethylene Terephthalate that is modified using a simple precipitation method. In the precipitation method the as-received PET (ar-PET) is dissolved in Trifluoro acetic acid and is precipitated in Acetone (as described in section 2.2.). The nature of the precipitated PET (ppt-PET) has been the focus of my study, because the PET obtained via the precipitation method is found to behave similarly to PET processed using γ-CD. In PET-γ-CD-IC, the guest polymer chains are confined to narrow, cylindrical channels created by the host, small-molecule lattice, where the polymers are highly extended, as a consequence of being squeezed, and are separated from neighboring polymer chains by the channel walls of the host (cyclodextrins). Coalescence of PET from its γ-CD-IC resulted in solid PET with a significantly reorganized structure leading to different properties. In order to characterize ppt-PET, the use of all the instruments described in section 3 was employed, to study the difference in the behaviors of as-received and precipitated PET. Though the ppt-PET was formed using the as-received PET pellets, precipitated and as-received PETs behaved all together differently.

4.1. Thermal Properties

4.1.1. Differential Scanning Calorimetry Results

4.1.1.1. As-received & Precipitated PETs

As-received and precipitated PETs were tested for their thermal properties by using a DSC. The testing conditions and the methods used are described in section 3.1.1. Figure 4.1. represents the DSC thermograms of as-received PET with two heating and one cooling cycle recorded at a heating rate of 20° C/min and a cooling rate of 200° C/min. Similarly Figure 4.2. shows the DSC thermograms for the precipitated PET. Both the thermograms have been generated in the same way and the operating conditions are the same for the two PETs.

In the thermograms of the as-received PET (Figure 4.1.) we see that the first heating scan shows a glass transition (T_g) at 82.4°C, which is followed by a crystallization exotherm at around 144.5°C, and then finally the melting endotherm follows at 257.5°C. The sample is held at 280° C for some time so as to completely melt the polymer and remove every trace of crystals. On cooling at a high rate the material is quenched into an amorphous material. The second heat of the material that follows after the rapid cooling behaves in the same manner as observed in the first heat, except the peaks are found to be a little displaced from their previous positions. This shift may be the result of the thermal history of the polymer which is erased after the polymer completes a heating and a cooling cycle. The crystallinity values in the case of as-received PET have been calculated based on the method described in [41].

$X_c = \Delta H_{m,\,obs} / \Delta H_{m\,o}$, where $\Delta H_{m,\,obs} = \Delta H_f - \Delta H_c$ and ΔH_f is the enthalpy of melting, ΔH_c is the enthalpy of crystallization, and ΔH_{mo} = 120 J/g is the enthalpy of melting of 100% crystalline PET [9].

For as- received PET Run I

$(\Delta H_f - \Delta H_c) = 41.3 – 27.6= 13.7$

$X_c = 13.7 / 120 = 0.114$

$\% X_c$ (Run I) $= 0.114 * 100 = 11.4$

Similarly for the Run II of the ar-PET

$(\Delta H_f - \Delta H_c) = 40.5 – 29.0 = 11.5$

$X_c = 11.5 / 120 = 0.095$

$\% X_c$ (Run II) $= 0.095 * 100 = 9.5$

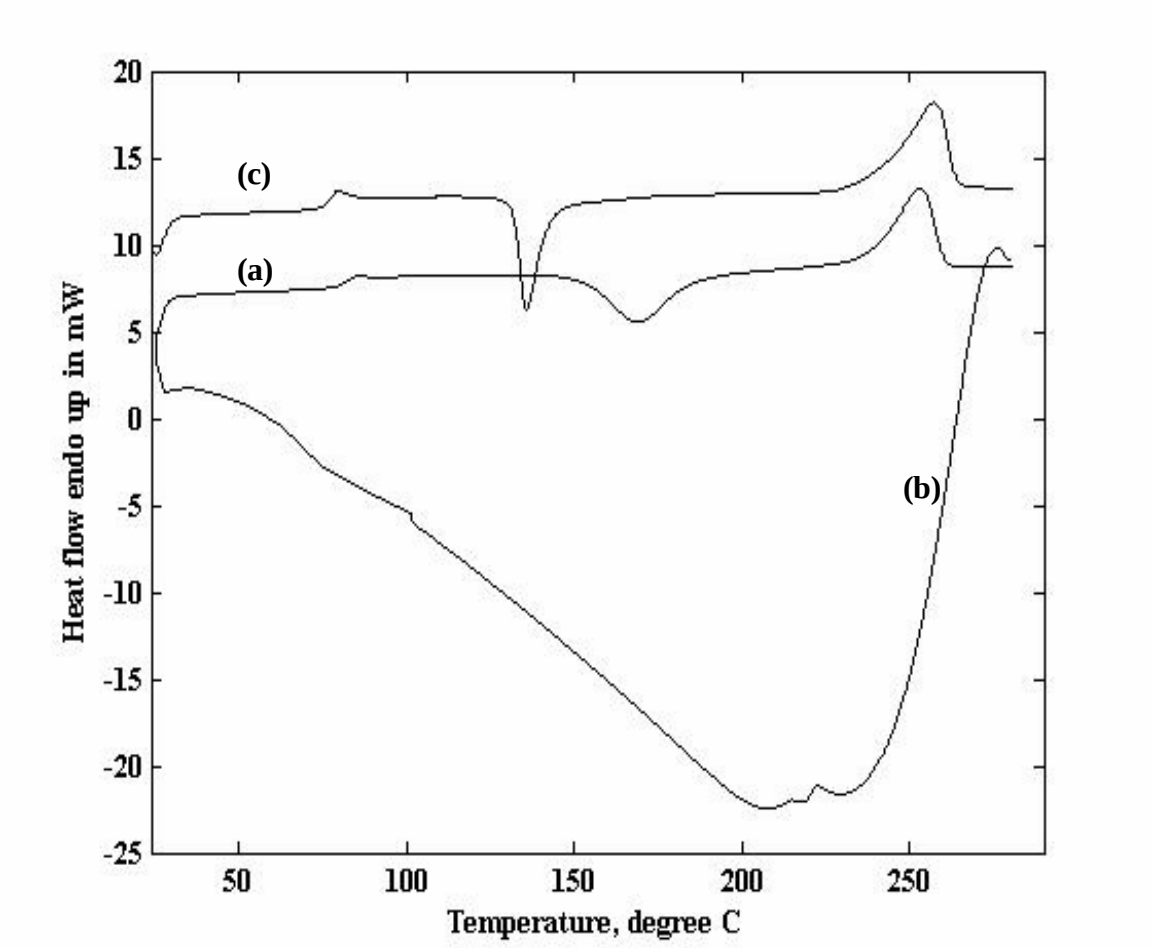

Figure 4.1. DSC thermogram of as-received PET. (a), (c) first and second heating scans and (b) cooling scan.

The results of the DSC thermogram and the calculated crystallinity have been summarized in Table 4.1.

Table 4.1. First and second heating scans of as-received PET

Sample	T_g in °C	T_c in °C	ΔH_c in J/g	T_m in °C	ΔH_m in J/g	X_c in %
Ar-PET run I	82.4	144.5	27.6	257.5	41.3	11.4
Ar-PET run II	81.7	161.4	29.0	256.3	40.5	9.5

Figure 4.2. represents the precipitated PET DSC scans. In its first heating scan ppt-PET neither shows a glass transition temperature nor a crystallization exotherm, the scan only exhibits a melting endotherm. However, unlike ar-PET after the melting of precipitated PET, it is difficult to quench the resultant PET melt into an amorphous PET, instead the melt rapidly recrystallizes during the attempted quench, and again on the second heating cycle it shows a behavior similar to the first heating scan and exhibits only a melting endotherm. The behavior is unchanged even with multiple heating and cooling cycles and is also unaffected by holding it in the melt for a longer period of time. All these preliminary results indicated that the precipitated PET behaves in the same manner as PET coalesced from its γ-cyclodextrin inclusion compound [46].

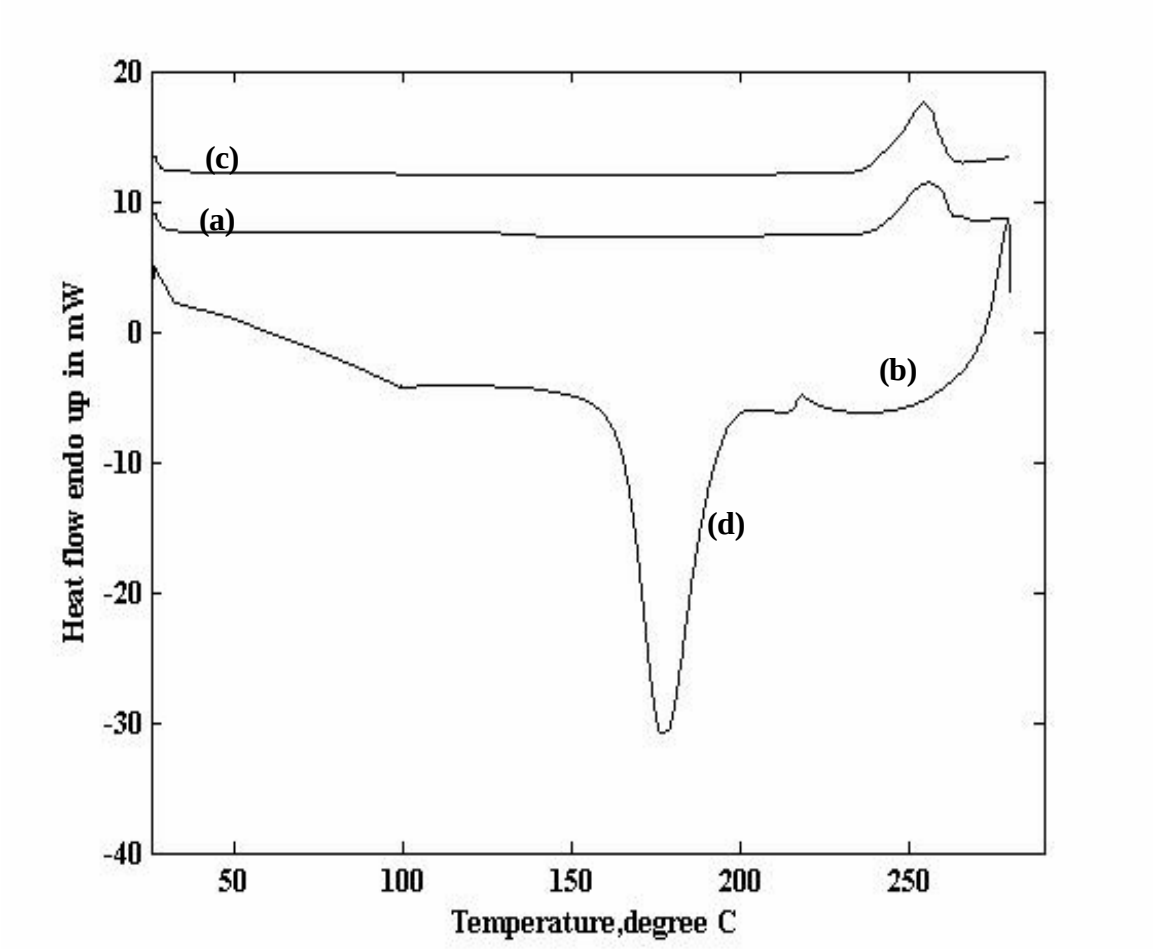

Figure 4.2. DSC Thermogram of precipitated PET. (a), (c) first, second heating and (b) cooling scans. (d) - Recrystallization exotherm observed in the case of precipitated PET (ppt-PET) on rapid cooling from the melt which is not found to be present in ar-PET on cooling the melt at a high cooling rate (200° C/min).

Following the same procedure for the calculations of crystallinity, the crystallinity values for the ppt-PET are:

% X_c (Run I) = (41.3 / 120) * 100 = 34.4

% X_c (Run II) = (46.9 / 120) * 100 = 39.1

The DSC results for the ppt-PET are given in Table 4.2.

Table 4.2. First and second heating scans of precipitated PET

Sample	T_g in °C	T_c in °C	ΔH_c in J/g	T_m in°C	ΔH_m in J/g	X_c in %
Ppt-PET Run I	-	-	-	255.6	41.3	34.4
Ppt-PET Run II	-	-	-	253.9	46.9	39.1

4.1.1.2. Annealed as-received PET

As-received PET pellets were annealed at 120°C for 20 min in vaccum oven so as to increase the crystallinity level. This was done in order to have a material for comparison that will have approximately the same level of crystallinity as that of the ppt-PET. This will lead to two different PET's with the same level of crystallinity. Figure 4.3. represents the DSC thermogram of the annealed ar-PET and Table 4.3. gives a brief summary of the DSC thermogram and the crystallinity levels of this material. The crystallinity values were calculated using the same method as done for the as-received and precipitated PET.

Table 4.3. First and the second heating scans of the annealed ar-PET

Sample (Annealed ar-PET)	T_g in °C	T_c in °C	ΔH_c in J/g	T_m in°C	ΔH_m in J/g	X_c in %
Run I	-	-	-	257.6	40.3	33.6
Run II	-	-	-	256.8	46.5	38.7

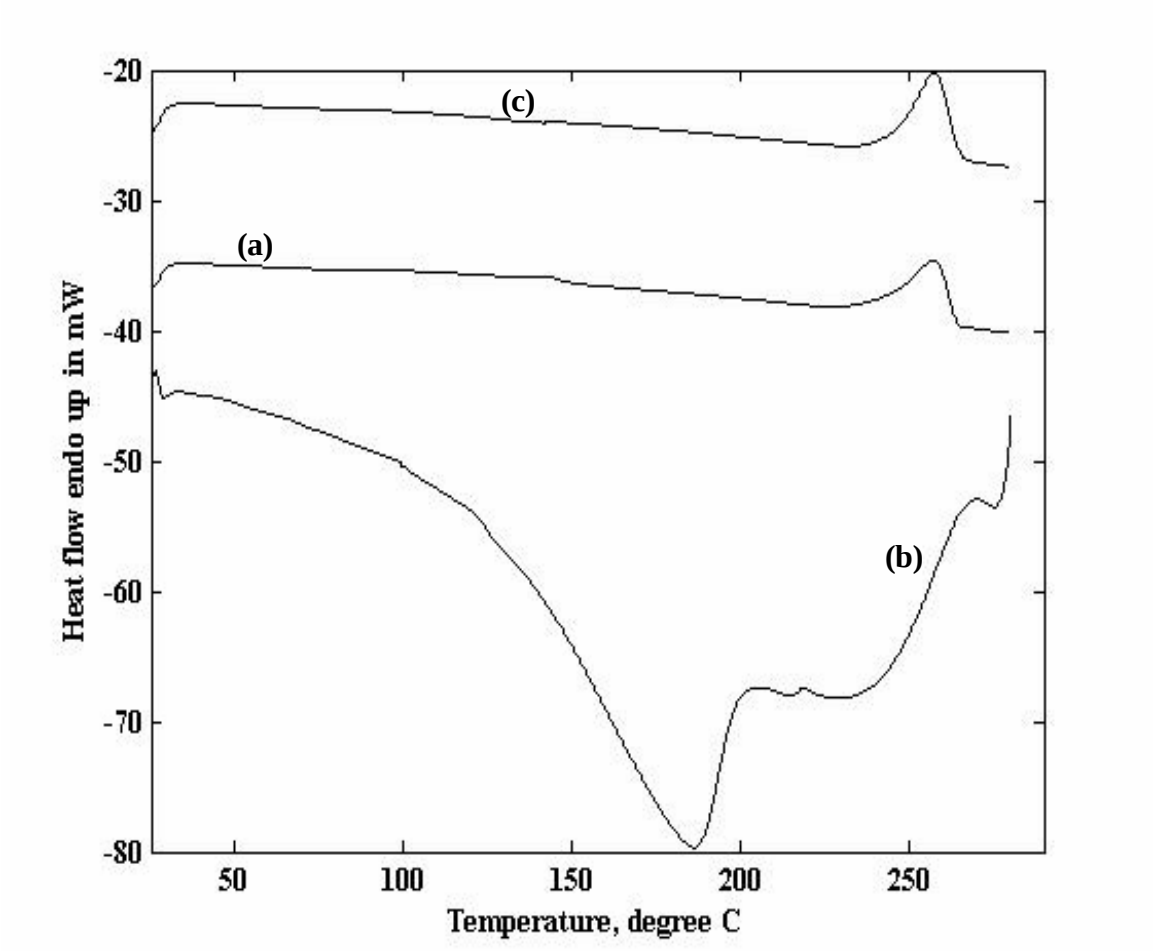

Figure 4.3. DSC thermogram of annealed as-received PET. (a), (c) first and second heating scans and (b) cooling scan.

4.1.1.3. Solvent Induced Crystallization in ar-PET vs. ppt-PET

As extensively covered in the literature, we observed that the crystallinity of the polymer can be improved by plasticizing the polymer through emersion in a solvent [25, 26 and 30]. As described in section 2.2. of materials and methods, we stated the use of acetone to precipitate the ar-PET. We tried to study the crystallization induced by acetone in the ar-PET film by soaking the film overnight in acetone. Figure 4.4. shows a DSC thermogram showing a comparison of the acetone soaked ar-PET and the ppt-PET films. Here it is evident that the first heating scan (a) of the ar-PET film soaked overnight in acetone neither exhibits a glass transition nor a crystallization exotherm and shows only a melting endotherm, similar to the first heating scan (c) of the ppt-PET. Immediately after melting the sample is rapidly cooled at a very high cooling rate and is then again subjected to a heating cycle and this second heating scan of the ar-PET soaked in acetone, thermogram (b), behaves in a different manner than that of the second heating scan of the ppt-PET, thermogram (d). In curve (b), the thermogram evidences a glass transition peak, a crystallization exotherm and a melting endotherm. The first heating scan of the ar-PET soaked in acetone (a), is different from that of its second heating scan (b). The first heating scan is the result of the plastcization of the polymer that increases the mobility of the chains by reducing the activation energy hindering their mobility, thereby inducing crystallization. This is evidenced by no glass transition or crystallization exotherm during the first heating, but this nature is not retained as proved by the second heating scan of the acetone soaked film. However, In the case of the ppt-PET we observed that the nature of the thermogram obtained is unchanged even after repeated heating and cooling cycles. Table 4.4. describes the results obtained.

Table 4.4. Comparison of the Acetone soaked ar-PET and ppt-PET

Sample		T in °C	T_c in °C	ΔH_c in J/g	T_m in°C	ΔH_m in J/g	X_c in %
Ppt-PET	Run I	-	-	-	255.6	41.3	34.4
	Run II	-	-	-	253.9	46.9	39.1
Acetone soaked ar-PET	Run I	-	-	-	255.1	42.2	35.2
	Run II	82.0	159.8	20.7	252.7	35.2	12.1

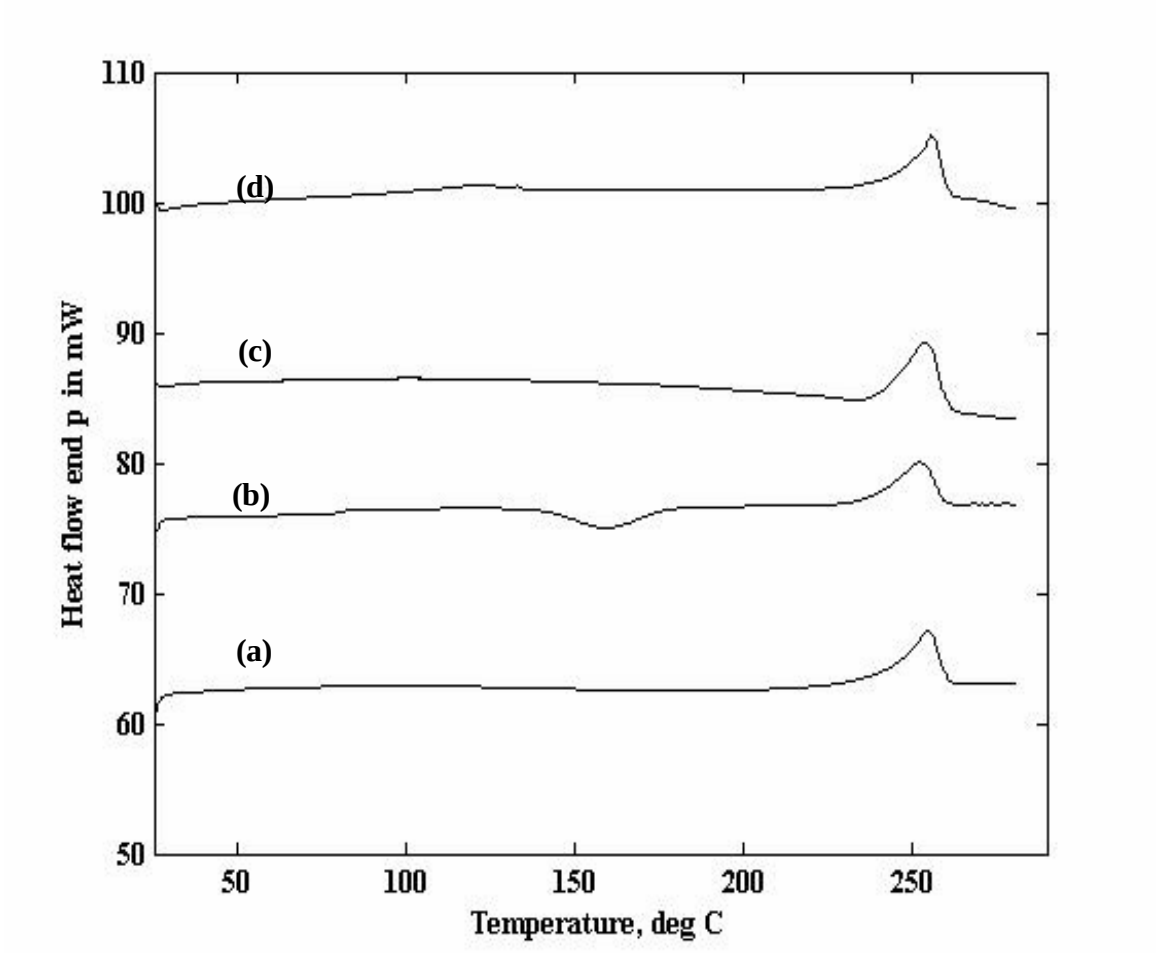

Figure 4.4. Comparison of the DSC thermograms (a) First heating scan of the acetone soaked ar-PET, (b) Second heating scan of the acetone soaked ar-PET, (c) First heating scan of the ppt-PET, (d) Second heating scan of the ppt-PET

4.1.1.4. DSC Results of the blending of precipitated and as-received PET's

The aim behind this approach was to determine the minimum amount of ppt-PET that can be blended with the ar-PET with retention of ppt-PET behavior. This process is expected to minimize the use of ppt-PET and still retain its properties. The behavior of the blends (with different proportions of ppt-PET and ar-PET) was observed with DSC for the purpose of determining how much precipitated PET is needed to produce a PET sample that crystallizes rapidly and maintains structural integrity.

We blended ppt-PET and the ar-PET in proportions (ppt/ar-PET) 20-80, 40-60, 50-50, 60-40, and 70-30. The thermal behavior of all blends with different ratios of ppt and ar-PET was examined by DSC. The next section illustrates the results observed for all these blends with different mole fractions of the constituent materials.

Preliminary results indicated that blends containing ≥ 50 % ppt-PET can in fact rapidly crystallize i.e. if a blend had 50 mol% or more of ppt-PET, then it is observed to have more crystallinity and also recrystallizes rapidly upon fast cooling.

4.1.1.4.1. Blend of ppt:ar-PET in the ratio of 20:80

Figure 4.5. shows the DSC thermogram of the blend in the proportion of 20:80. As is evident from the thermogram the blend behavior is dominated by the nature of the ar-PET. The blend shows a glass transition endotherm and a crystallization exotherm and is followed by a melting endotherm. No trace of recrystallization is observed during rapid cooling from the melt (nature of ar- PET) and the blend quenches into an amorphous material. The second heating scan behaves in the same manner as the first heating scan.

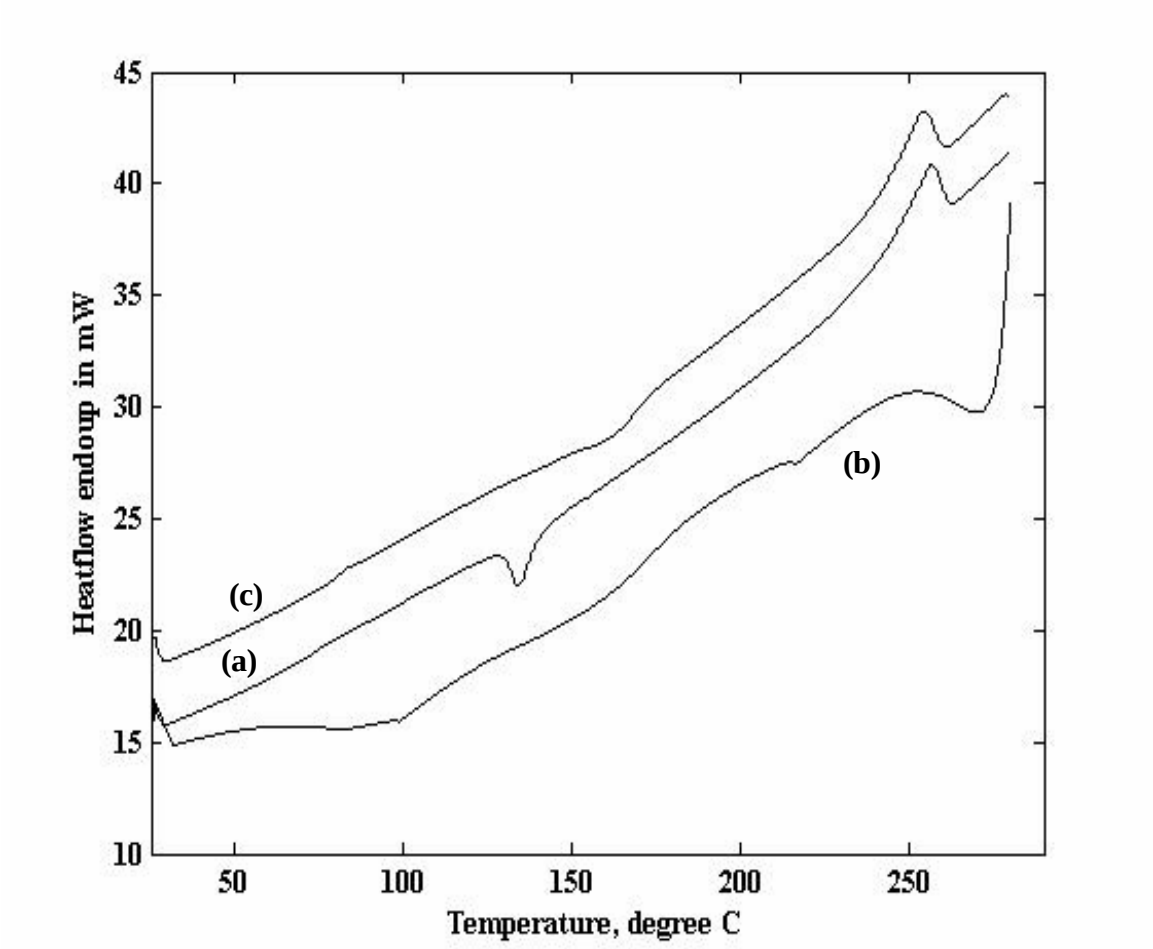

Figure 4.5. DSC Thermograms of blend of ppt - / ar-PET in the ratio of 20/80. (a),(c) first, second heating and (b) cooling scans.

4.1.1.4.2. **Blend of ppt:ar-PET in the ratio of 40:60**

The next thermogram is of a blend that had 40 % precipitated PET and 60 % as-received PET. This blend still has the as-received characteristics dominating in its behavior. It still has a T_g, a crystallization exotherm and does not recrystallizes on rapid cooling. Figure 4.6. describes the thermograms of this blend.

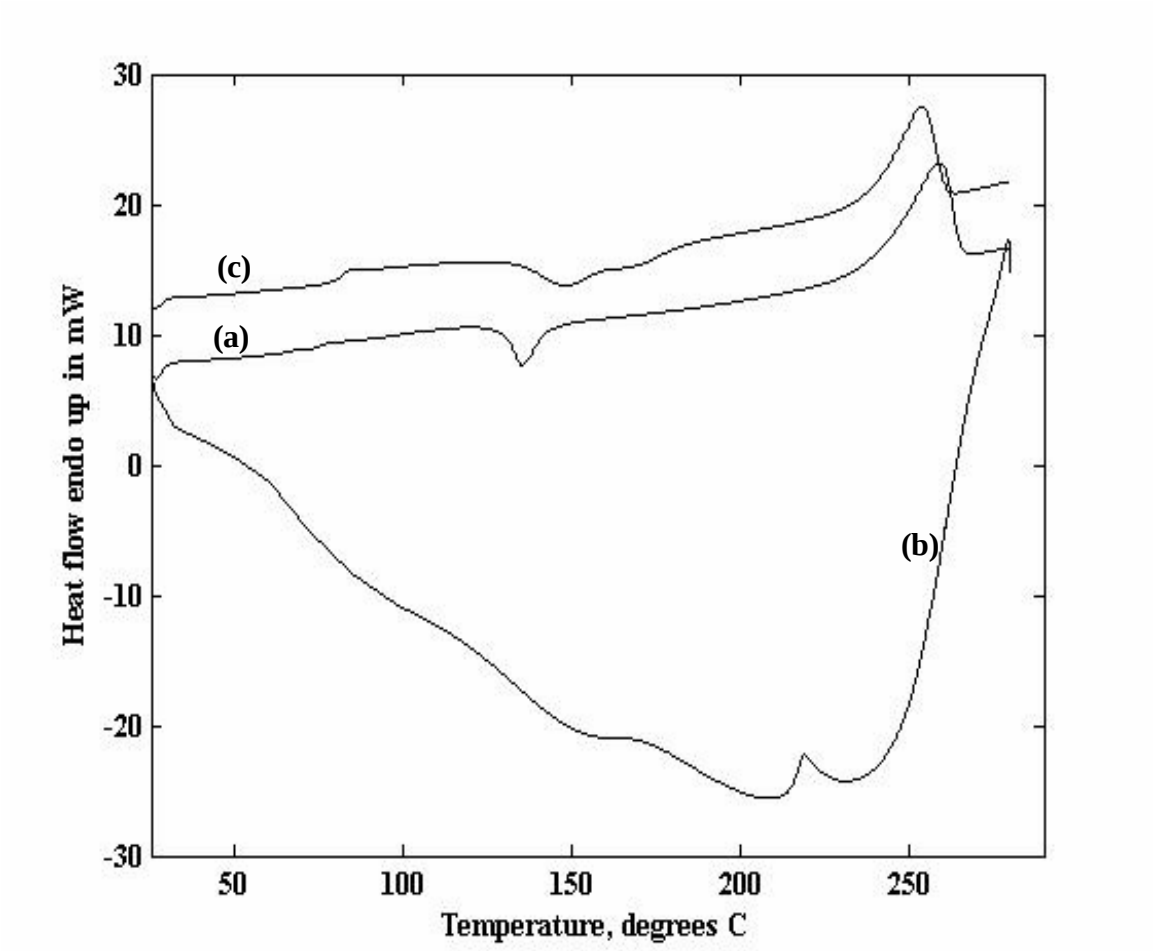

Figure 4.6. DSC Thermogram of blend of ppt / ar-PET in the ratio of 40/60. (a), (c) first, second heating and (b) cooling scans.

4.1.1.4.3. Blend of ppt:ar-PET in the ratio of 50:50

Figure 4.7. is the DSC thermogram of the blend of the ppt:ar- PET in the ratio of 50:50. The blend is observed to behave somewhat like pure ppt-PET. The first heating scan (a) of the blend is similar to the heating scan of ppt-PET. Also, the cooling scan of the blend (b) shows a recrystallization during fast cooling from the melt. After one cycle of heating and cooling the second heating scan (c) is found to show a small crystallization exotherm.

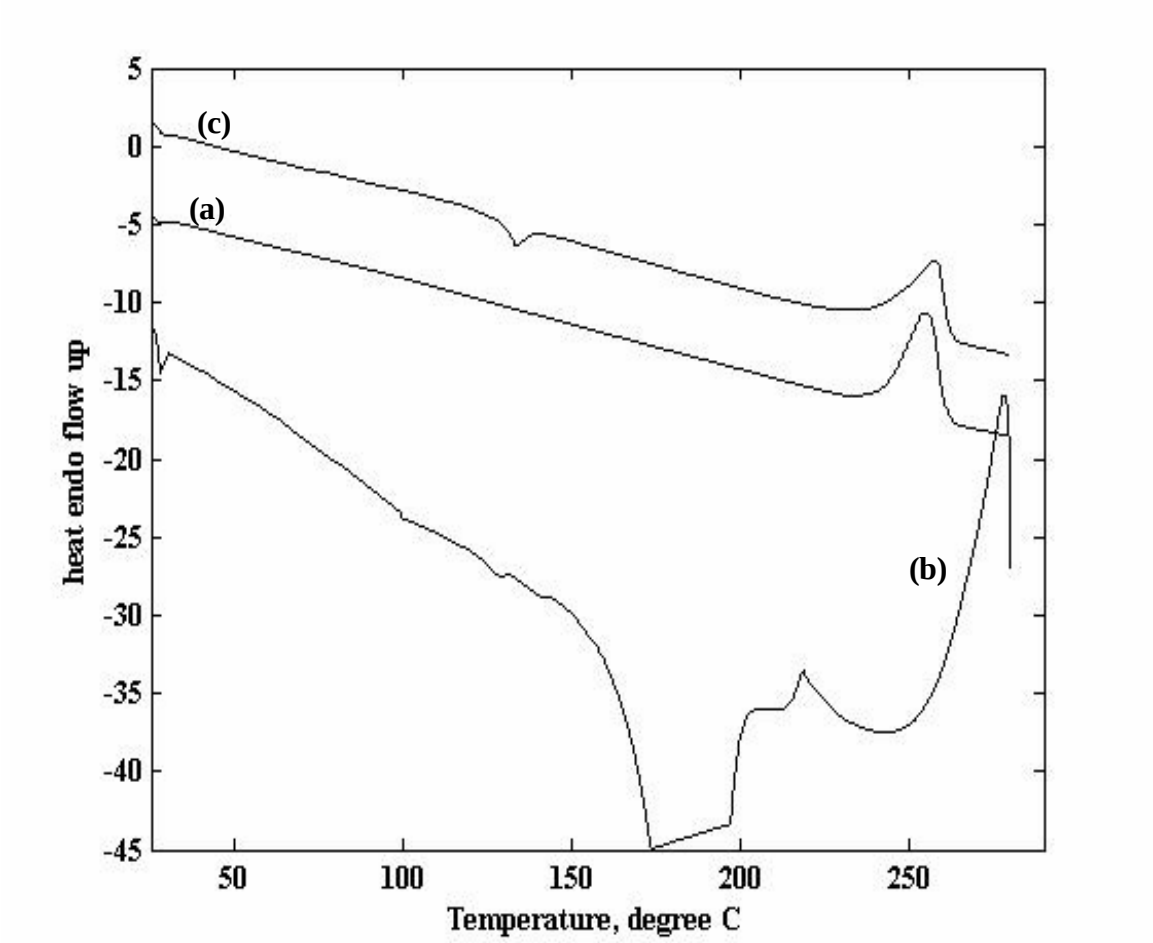

Figure 4.7. DSC Thermogram of blend of ppt / ar-PET in the ratio of 50/50. (a), (c) first, second heating and (b) cooling scans.

4.1.1.4.4. Blend of ppt:ar-PET in the ratio of 60:40

Figure 4.8. is just an extension of the blend results. This is a blend where the ratio of the precipitated PET to that of the as-received is 60:40. This blend behaves in the same manner as a 50:50 blend, with not much difference in their behavior. The blend is not yet found to fully behave like the precipitated PET. As-received PET behavior is observed in the thermogram.

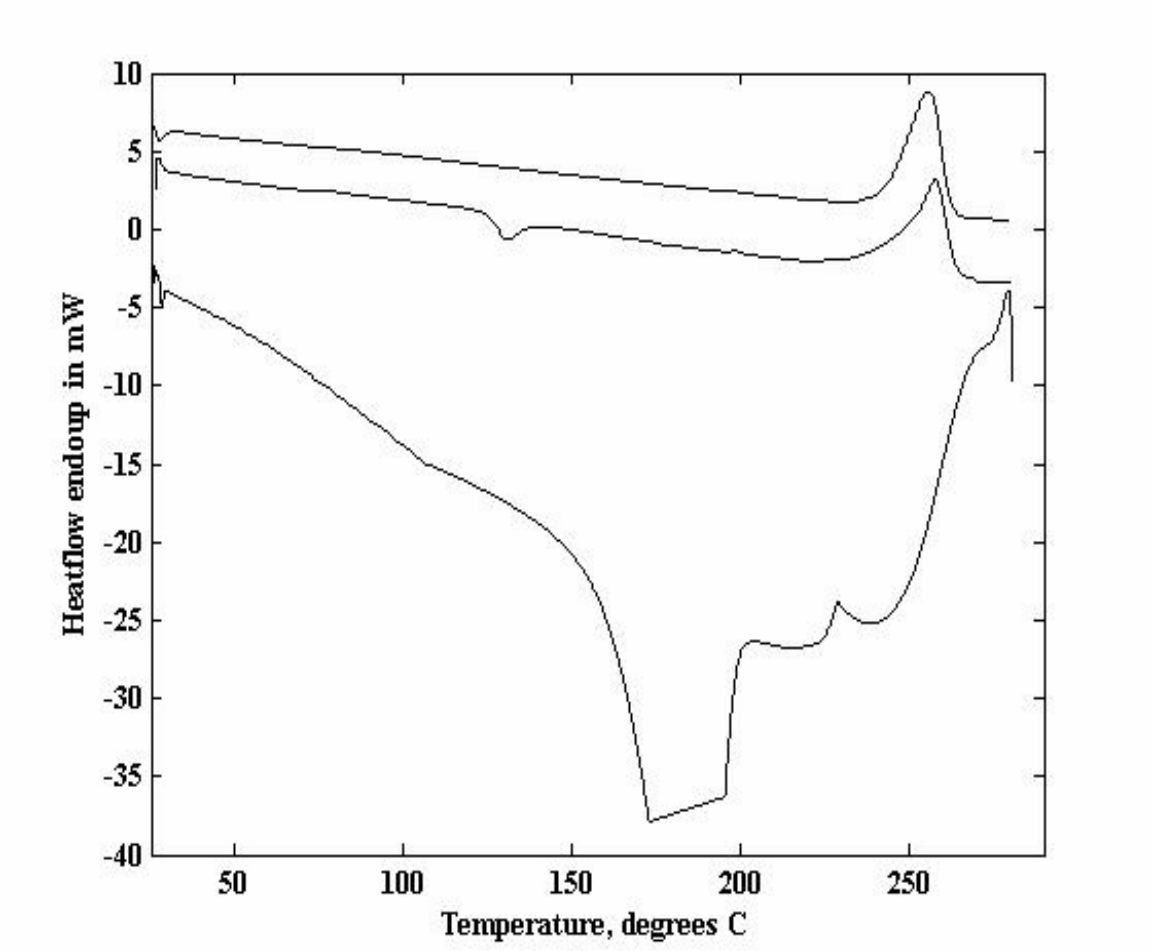

Figure 4.8. DSC Thermogram of blend of ppt / ar-PET in the ratio of 60/40. (a),(c) first, second heating and (b) cooling scans.

4.1.1.4.5. Blend of ppt:ar-PET in the ratio of 70:30

The thermogram for the blend consisting of 70 % ppt-PET and 30 % ar-PET is shown in Figure 4.9. As it clearly evident from the DSC thermogram, this blend shows a behavior that is typical of the ppt-PET. The double melting peak observed in the second heating scan of the 70:30 blends may be due to the two distinct crystal populations as described by Tan *et. al.* [12]. This is due to the recrystallization phenomenon of initial crystal morphology that is characteristic of the prior crystallization history.

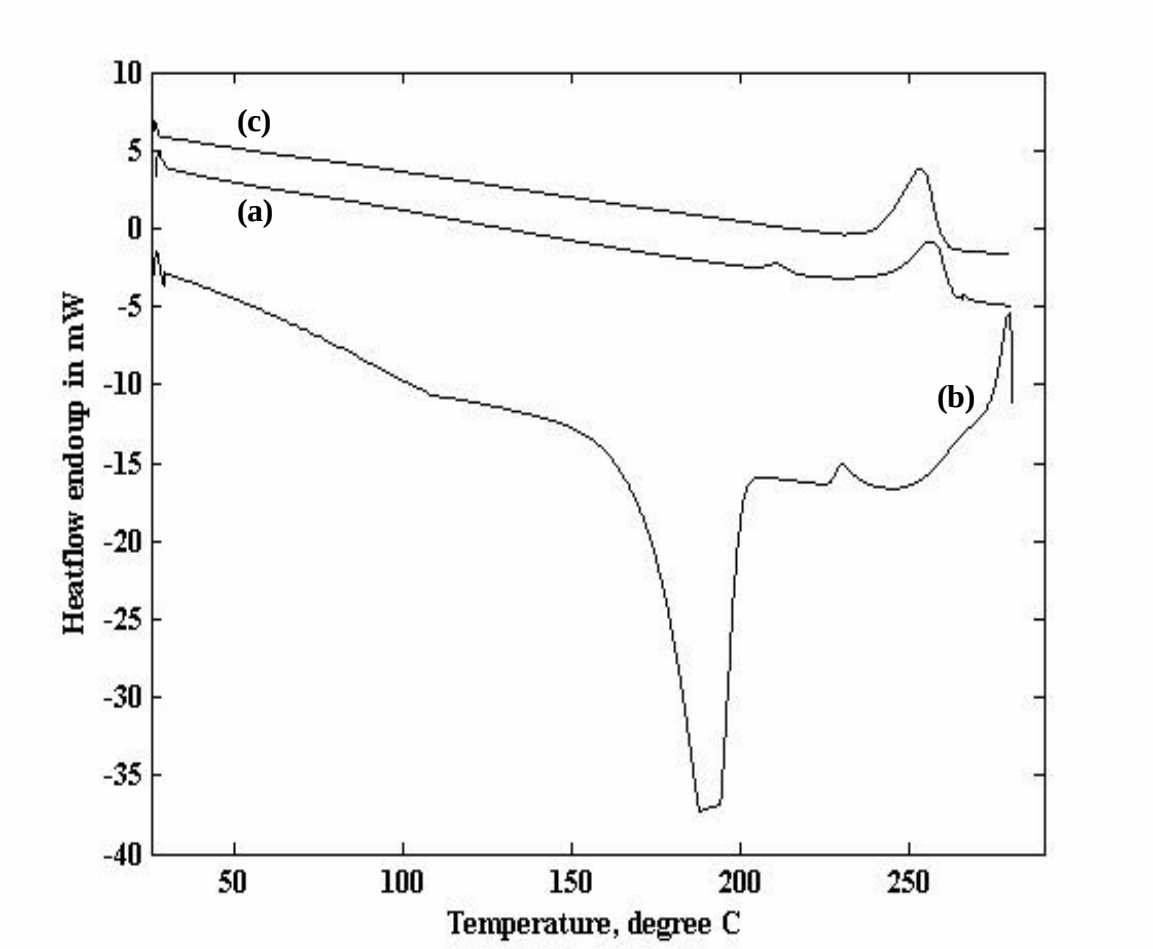

Figure 4.9. DSC Thermogram of blend of ppt / ar-PET in the ratio of 70/30. (a),(c) first, second heating and (b) cooling scans.

4.1.1.5. Discussions of the DSC Results

The DSC thermograms for the ppt-PET are found to be different than those of the ar-PET. In the first heating scan absence of the glass transition temperature in the ppt-PET thermogram is indicative of the fact that the non-crystalline regions in the ppt-PET are organized differently than those of the ar-PET. The glass transition temperature of a polymer depends on the amorphous regions of a polymer and its absence in ppt-PET indicates an order and orientation of the chains even in the non-crystalline regions. The second heating scan that follows after immediately cooling from the melt is carried out mainly to erase the thermal history of the polymer, because as mentioned previously the behavior of PET is dependent on its thermal history [11, 12]. After the first heating and subsequent rapid cooling from the melt, neither a glass transition nor a crystallization exotherm is obtained in the second heating scan. The second heating scan of the ppt-PET still behaves similarly to the first heating scan (with just a melting endotherm) and hence this confirms the fact that melting completely and holding the polymer in the melt has not erased the reorganization achieved by precipitating PET.

During the cooling scan of the two PET's it is clearly observed from Figures 4.1. and 4.2. that the ar-PET can be quenched into a predominantly amorphous material, whereas the rapid cooling of the ppt-PET shows a recrystallization exotherm which indicates that even on cooling ppt-PET at a high rate, an amorphous melt capable of being quenched is not achieved. Immediately after melting the ppt-PET chains are organized differently than those of the ar-PET, and holding in the melt has failed to disrupt this organized structure. Successive heating and cooling of the ar-PET and ppt-PET produced some changes in the

enthalpies and the peak temperature of melting etc, but a melt capable of being quenched has not been achieved in the case of ppt-PET.

Also when we compare Tables 4.1. and 4.2. we can conclude that the crystallinity level in the case of precipitated PET is much higher than that of the as-received PET, as the ppt-PET does not evidence a crystallization exotherm on the heating scan.

The above evidence obtained for the ppt-PET indicates the similarity between the ppt-PET and the coalesced PET. The thermal behavior of coalesced PET is observed to be the same as that of the ppt-PET. The coalesced PET thermogram does not exhibit a T_g nor T_c, but just a melting endotherm [8, 41]. We thus have evidence that even, though the precipitated and coalesced PET are processed using different techniques, there exists a close similarity in their thermal behaviors and presumably their structures..

In summary, the thermal behavior of ppt-PET samples suggest crystalline characters and melt crystallized morphologies that are different from normal samples, and there exist close similarities in thermal behaviors of precipitated and coalesced PET's.

As far as the blending of the ar-PET with the ppt-PET is concerned the main objective was to reduce ppt-PET usage, but with retention of the characteristics of the ppt-PET. From the results of blending of the two PET's, we concluded that more than 50% of the ppt-PET is required in order to make the blend crystallize rapidly. Overall we observed that a blend having more than 60 mole % of precipitated PET will provide a blend with structural integrity and with thermal properties similar to ppt-PET.

We carried out a brief study on the crystallization induced in a polymer due to the presence of solvent molecules around it. This was done in order to confirm that the reorganization of chains and the crystallization behavior observed in ppt-PET is different

from that induced by the soaking of the ar-PET film in acetone overnight [25-28]. Presence of solvent around PET decreases the T_g in ar-PET by reducing the activation energy for mobility, facilitating segmental motion and resulting in crystallization. The ppt-PET behavior is consistent with repeated heating and cooling scans, but this was not true with the films where crystallization was induced by acetone. This may be due to the loss of the solvent plasticizing effect in the polymer. Heating at a continuous rate in DSC must have relaxed the chains and the polymer snaps backs to its original behavior. The ppt-PET chains are organized differently and hence it does not behave like the ar-PET even after performing multiple heating scans.

4.1.2. Thermo gravimetric Analyses

4.1.2.1. As-received & Precipitated PET

Figures 4.10. and 4.11. shows the TGA scans for the as-received and precipitated PETs. The testing conditions were the same for both, as described in section 3.1.2. We can see that the ar-PET decomposes at around 365.2° C and the ppt-PET decomposition starts at 360.8° C. The two PET's scans look alike in terms of their behavior around their decomposition temperatures.

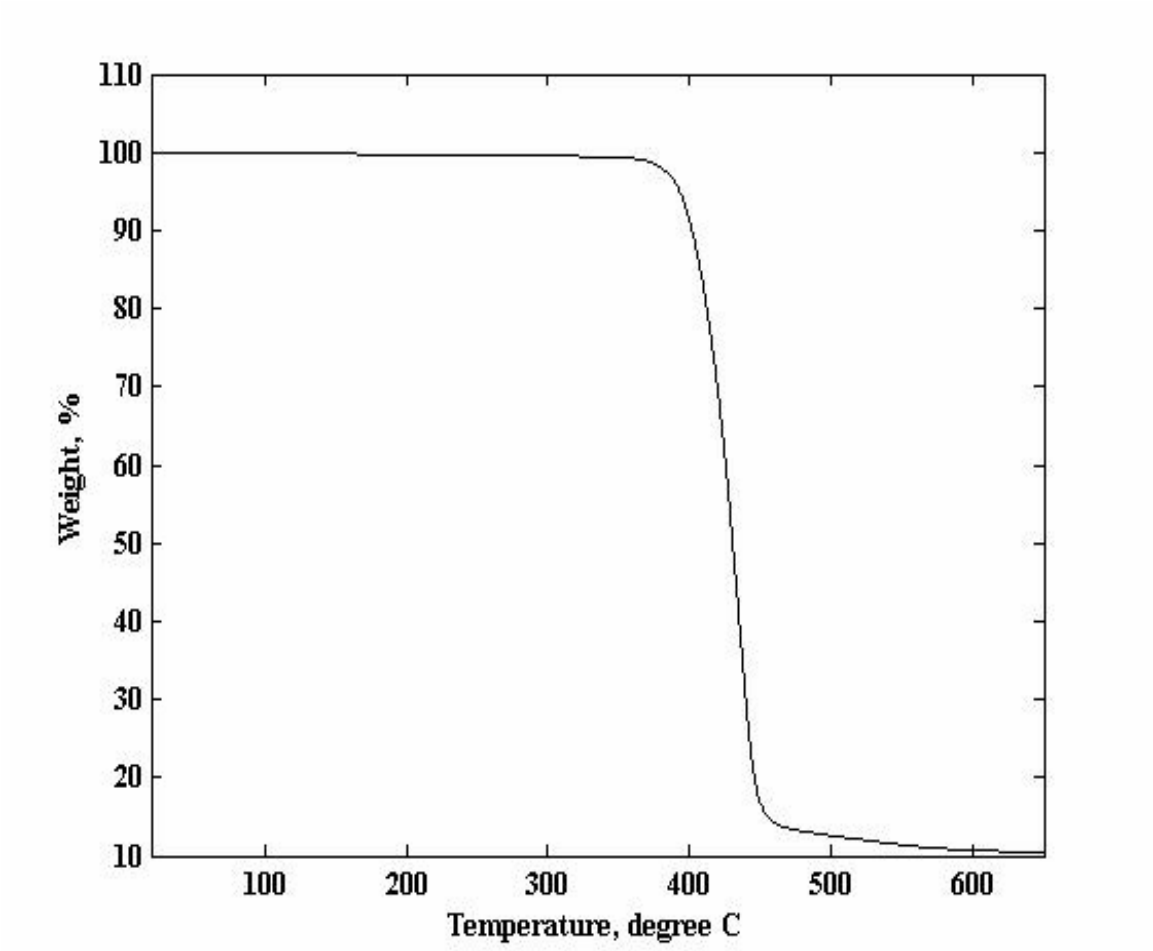

Figure 4.10. TGA thermogram of as-received PET

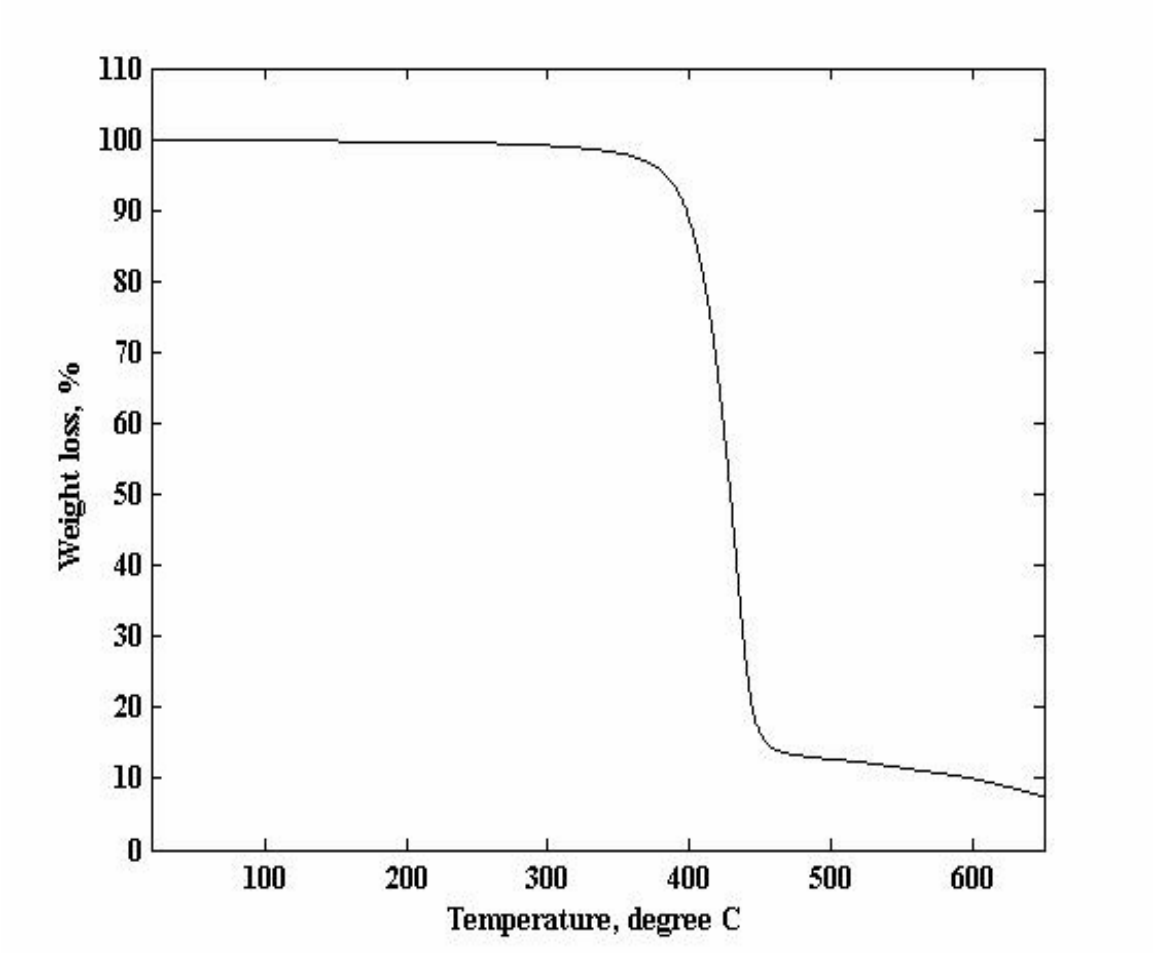

Figure 4.11. TGA thermogram of precipitated PET

4.1.2.2. Discussion of TGA results

The TGA scans for as-received and precipitated PET samples reveal very similar thermal stabilities despite apparent differences in their morphologies. These similar decomposition temperatures indicate that dissolving of the polymer (ar-PET) in acid (TFA) to obtain ppt-PET is not resulting in the breakage of chains as no trace of acid is found in the processed sample. No evidence of low temperature weight loss is observed in the precipitated PET, as the presence of acid is almost nil in the processed sample. TGA results of ppt-PET are the same for PET obtained via coalescence from its ?-CD-IC.

4.2. Fourier Transform Infrared Spectroscopy

4.2.1. FTIR with KBr Pellets

Fourier Transform Infrared Spectroscopy for the two PET's (ar-PET and ppt-PET) was done by making a KBr pellet of the two as described in section 3.2. The FTIR spectra of ar- and ppt-PET's in the region from 700 to 2000 cm^{-1} are presented in Figure 4.12. The spectra appear similar, but careful examination of the two reveals some differences between them. FTIR's of precipitated and coalesced PETs are nearly identical, and are more highly resolved than the spectrum of the ar-PET. This is the consequence of greater crystallinity and order in the non-crystalline regions. The 973 cm^{-1} band is considered to correspond to the

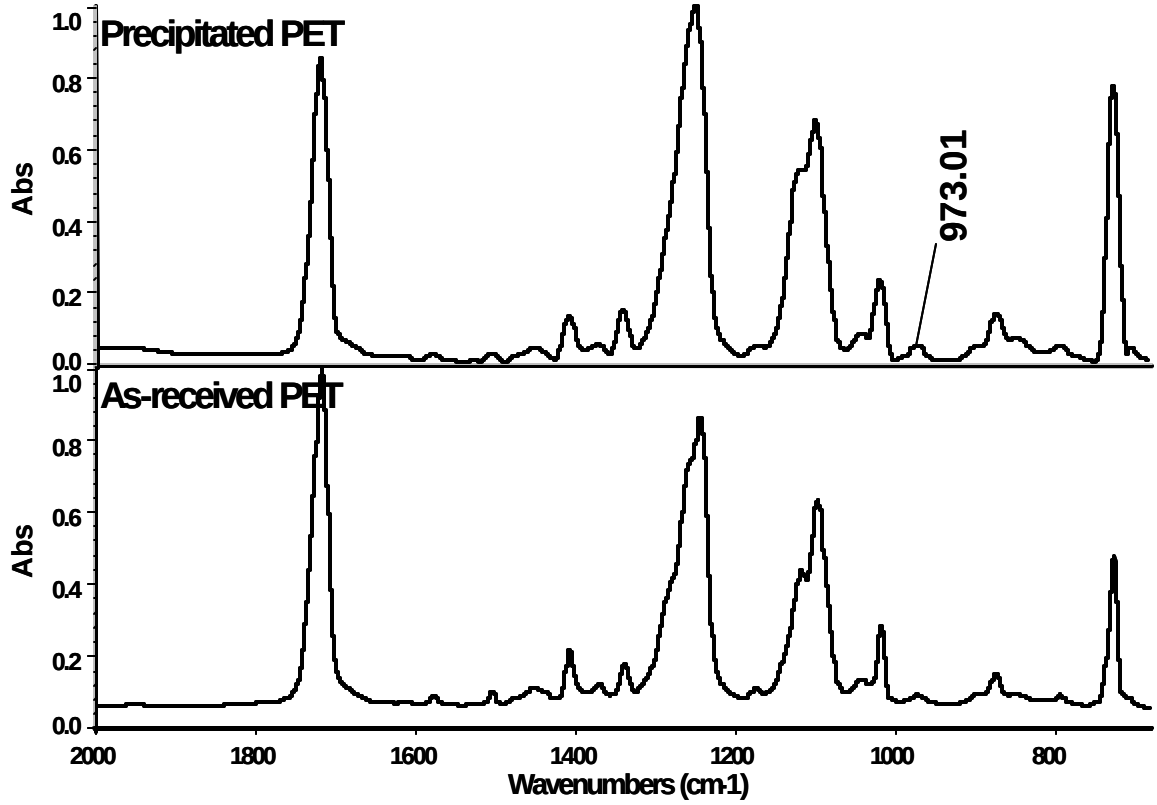

Figure 4.12. FTIR spectra of as-received and precipitated PET

-CH_2-O stretching vibration of the trans unit in the ethylene glycol linkage [20], and is found to be present in the ppt-PET at room temperature. The ar-PET sample does not show the presence of the 973 cm^{-1} band at room temperature.

4.2.2. Microscopic FTIR

In order to carry out an in depth study of the variation of the trans and gauche bands in PET with temperature, a microscopic FTIR study was carried out on very thin films of PET as described in the section 3.2.1. This was done with the aim to monitor the variation of the conformationally sensitive FTIR bands as the temperature increases. The bands that are mainly used for analysis and were based on previous studies carried out on thin films are the bands observed at 973, 1340 and 1370 cm^{-1} [14, 17 and 19]. Figure 4.13. shows the variation of the 973 cm^{-1} band with temperature for the two PET's. As clearly observed there, the trans conformer is present in substantial amount in ppt-PET and corresponding to the crystal structure, whereas in the case of ar-PET the trans band introduces itself at around the crystallization temperature of the polymer (approximately120°C) and starts to disappear as the sample reaches the melting point.

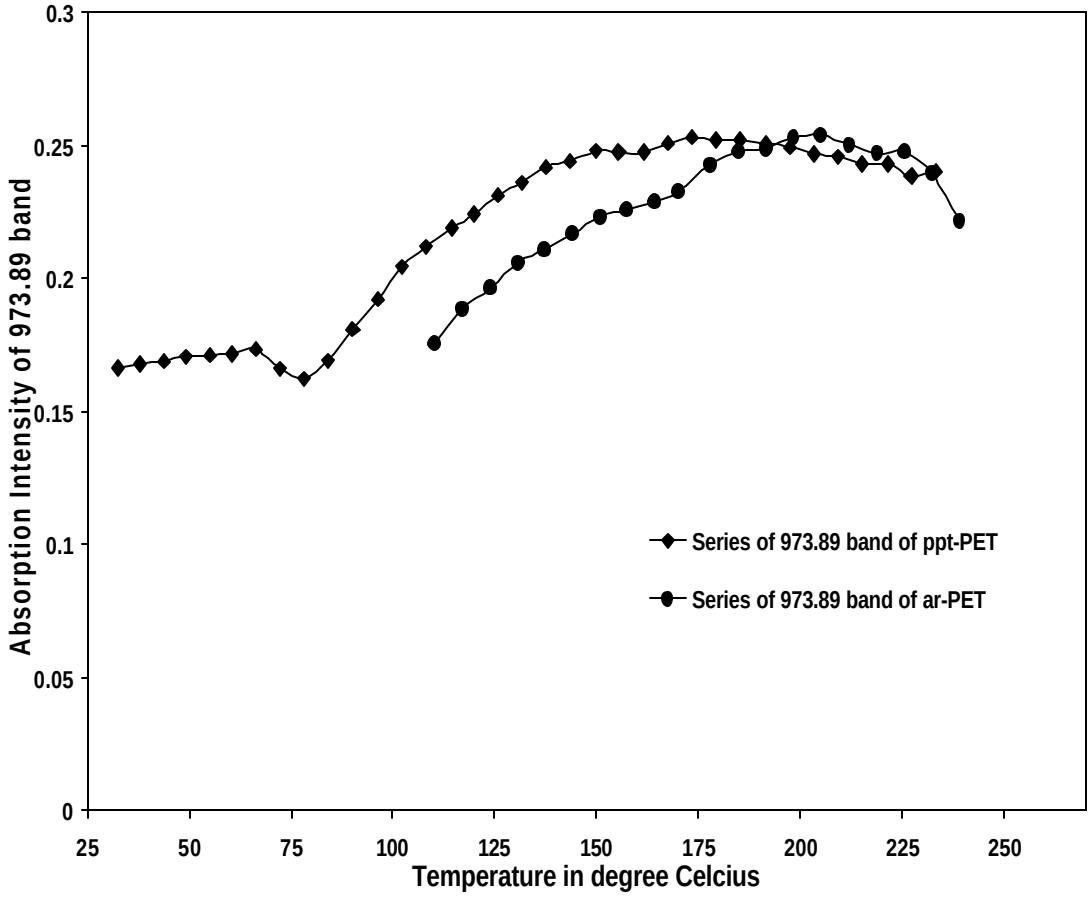

Figure 4.13. Absorption intensity of the 973 cm^{-1} band vs. Temperature.

As mentioned above the 1340 and 1370 cm^{-1} bands correspond to the wagging of the ethylene unit in trans and gauche conformations. These bands are found to show a greater change in intensity on crystallization and with changes in temperature. Using these bands, an attempt was made in order to calculate the % trans conformer in the two PET's and compare them with respect to the variation in temperature.

The equation used for the calculation is:

$$T = A_{1340} / (A_{1340} + 6.6 * A_{1370}) \quad \text{[17]},$$

where A_{1340} and A_{1370} are the integral absorbances of 1340 and 1370 cm^{-1} bands, respectively. % trans conformer calculated for both the PET's with increasing temperature are presented in Table 4.5.

Table 4.5. Temperature dependence of the % Trans conformer in ar- and ppt-PETs

Temperature in °C	% Trans conformer of Precipitated PET	% Trans conformer of As-received PET
32.3	25	13
43.7	25	12
55	24	12
66.3	23	12
78.3	22	11
90.2	22	10
108.2	25	12
114.2	25	14
125.9	25	19
137.8	26	24
143.6	26	25
155.6	26	26

4.2.3. Discussion of FTIR Results

The trans band (973 cm^{-1} band) is found to be present in the ppt-PET, and the band is considered to correspond to crystallinity in the polymer. Ppt-PET is expected to be more crystalline, as reflected by the 973cm^{-1} band. This result is in accordance with the DSC results of ppt-PET being significantly more crystalline than the ar-PET. The absorption intensity of the 973 cm^{-1} band initially rises and finally levels off for ppt-PET. But for ar-PET it is only introduced in the crystallization temperature range and then it increases slightly for some time and finally it disappears as the crystals start melting and the trans conformer transforms to gauche as the polymer changes to an amorphous form.

From Table 4.5. it is clear from the 1340 cm^{-1} band, that the % of trans conformer in the ppt-PET is approx ~ 25% throughout the heating scan, whereas the trans conformation % for the ar-PET is just ~13% initially and only reaches 25 % at around the crystallization temperature of PET (between 120 - 145°C). % of trans fraction in ppt-PET is almost double the % of trans conformer in the ar-PET. This leads us to decide that the ppt-PET is more crystalline than the ar-PET. The ar-PET film can be characterized as nearly amorphous (as % trans conformer is less than ~15%). Difference in the % trans conformer below 120°C may be due to the occurrence of deorientation/relaxation of the PET chains with increase in temperature through the T_g.

4.3. Wide Angle X-Ray diffraction

4.3.1. As-received PET

The X-ray diffraction pattern for the as-received PET was obtained from an analysis of PET powder as described in section 3.3. Figure 4.14. shows the powder diffraction pattern of the ar-PET. The diffraction pattern for the ar-PET shows a broad amorphous halo that is centered at approximately $2\theta = 21.3°$. From this value of 2θ, using Braggs law ($\lambda = 2d\sin\theta$), the d spacing of the amorphous material is estimated to be at 4.16? .

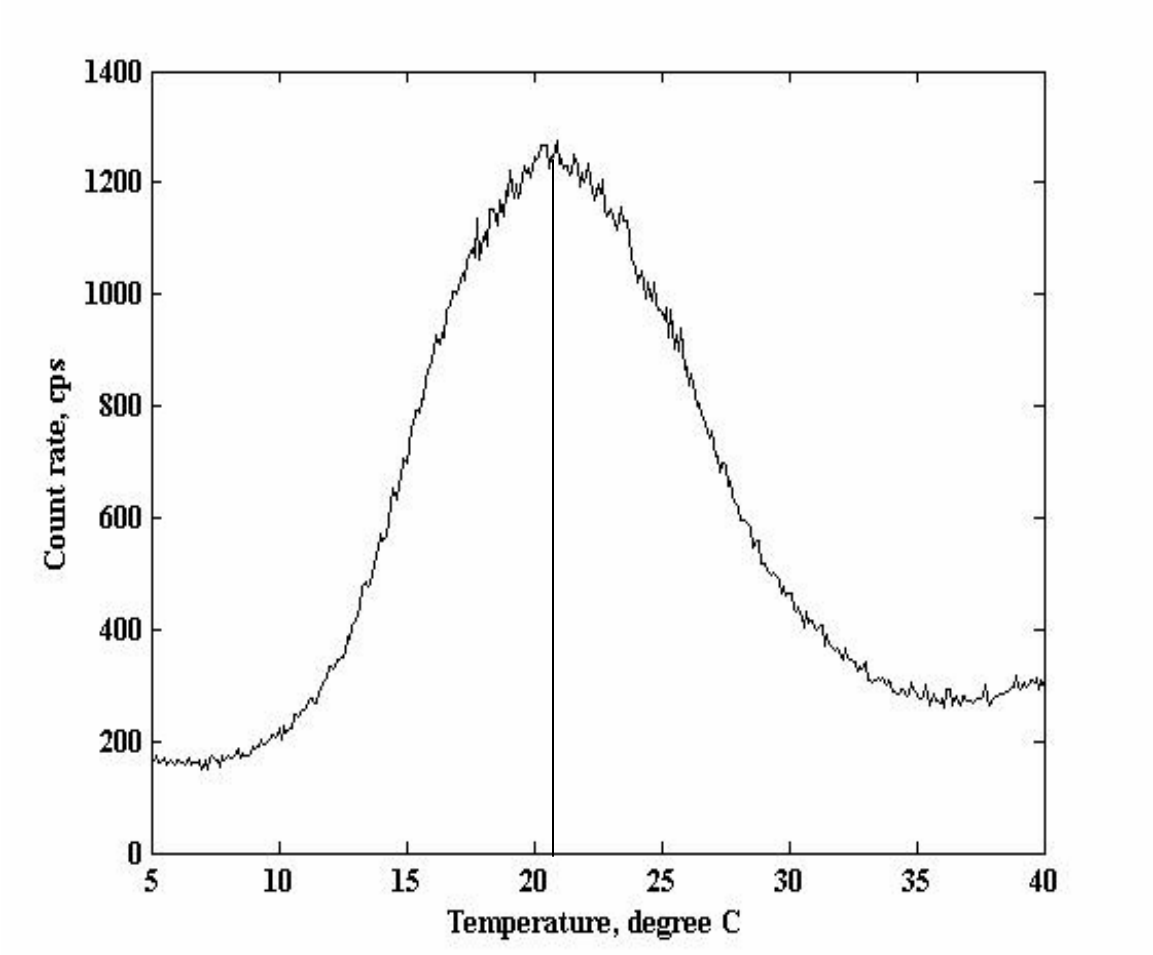

Figure 4.14. Wide Angle X-Ray Diffraction pattern of as-received PET

4.3.2. Precipitated PET

Figure 4.15. shows the WAXD pattern of the ppt-PET. The ppt-PET was formed from the same batch as ar-PET. Strong diffraction peaks centered at 2θ = 17.1, 22.6 and 26.2 ° are observed. The vertical lines in Figure 4.15. represent values of WAXD peak locations expected for the (0i1), (010) (i10) and (100) reflections in PET [47].

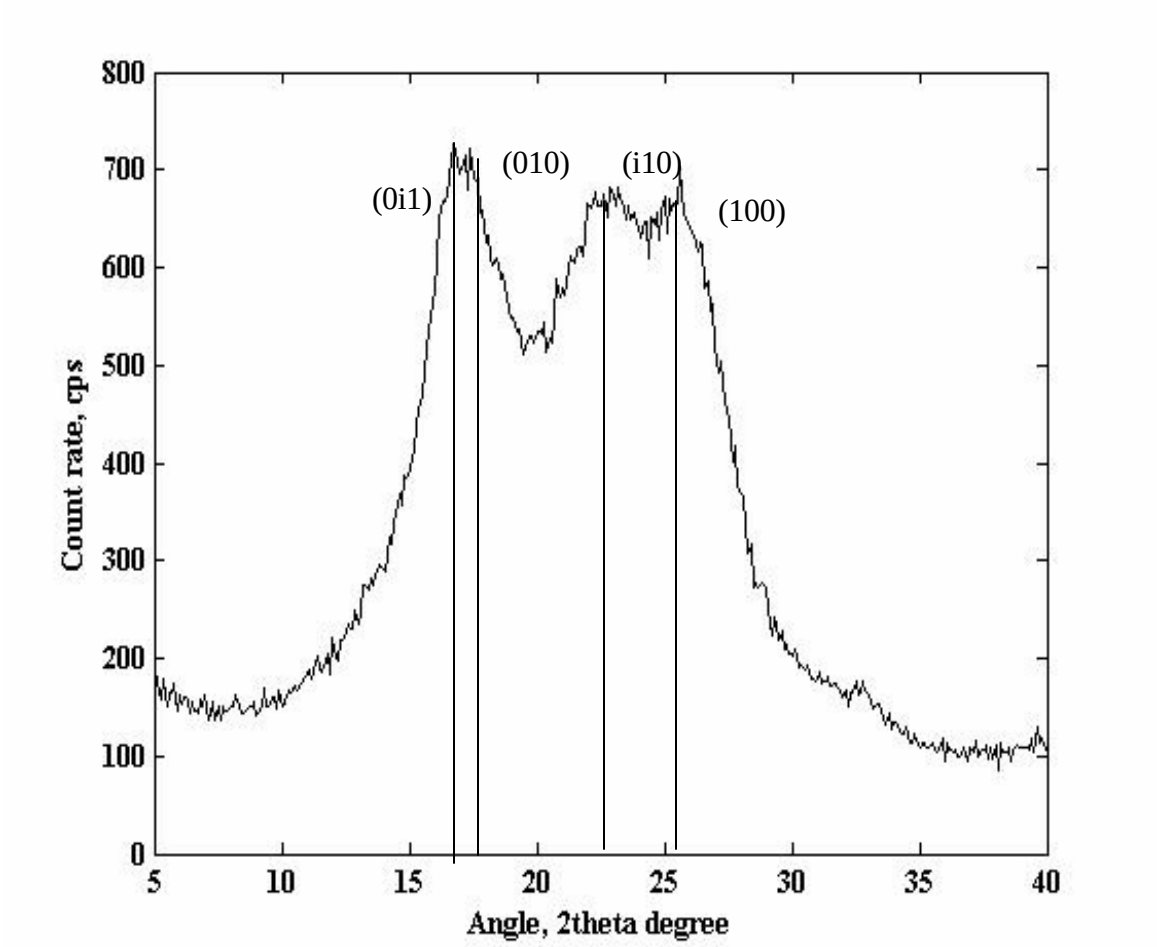

Figure 4.15. Wide Angle X-ray Diffraction pattern of precipitated PET

4.3.3. Annealed as-received PET

As-received PET was annealed in a vaccum oven at 120°C for 20min. This was done in order to have a sample of ar-PET with a level of crystallinity equivalent to that of the ppt-PET. Figure 4.16. shows the WAXD pattern of the annealed ar-PET sample. Strong diffraction peaks centered at 2θ = 17.8, 22.8 and 26.2° are observed.

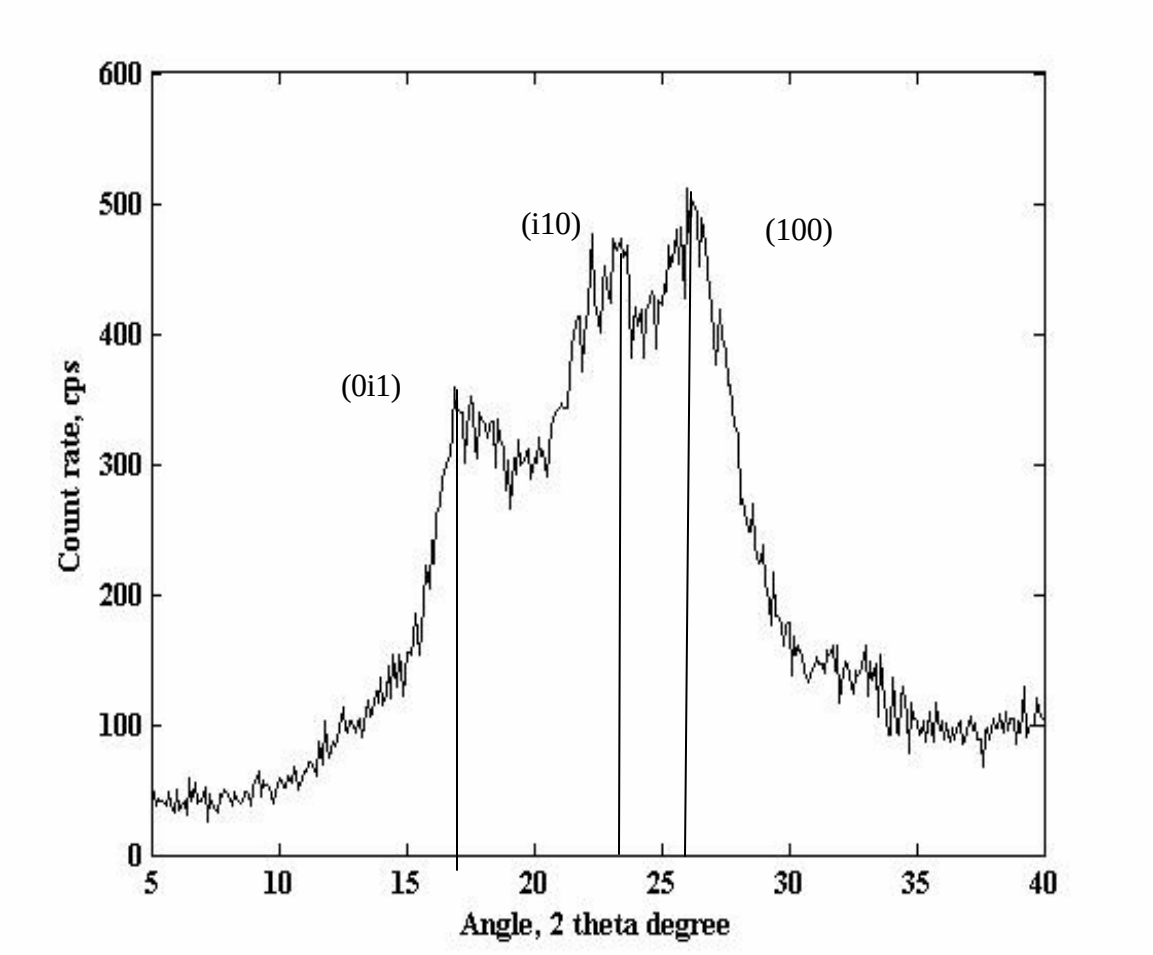

Figure 4.16. Wide Angle X-ray Diffraction pattern of annealed ar-PET

4.3.4. Calculation of Crystallinity by X-Ray

Crystallinity is estimated from the WAXD spectrum using the following relation:

$X_c = (I_c / I_c + K * I_a) * 100$, where I_c and I_a are the integrated areas under the sharp crystalline peaks and the broad amorphous halo, respectively. K is the calibration constant which takes into account that the intensities associated with the crystalline peaks occur at different angular distributions than the amorphous halo. K is assumed to be unity [22].

On the basis of the diffractogram obtained in Figure 4.14. the apparent weight % crystallinity for the ar-PET is calculated to be:

$X_{c,\ ar\text{-}PET} = (12601 / 12601 + 204760) * 100$

$X_{c,\ ar\text{-}PET} = 5.8\ \%$

Similarly the crystallinity value for ppt-PET in Figure 4.15. can be calculated as:

$X_{c,\ ppt\text{-}PET} = (5558.4 / 5558.4 + 11642) * 100$

$X_{c,\ ppt\text{-}PET} = 32.3\ \%$

Also, the crystallinity value for annealed ar-PET can be calculated as:

$X_{c,\ annealed\ ar\text{-}PET} = (3206.3 / 3206.3 + 7004.8) * 100$

$X_{c,\ annealed\ ar\text{-}PET} = 31.4\%$

The above calculations indicate that ppt-PET has a greater amount of crystallinity when compared to ar-PET and also that annealed ar-PET has almost the same level of crystallinity as the ppt-PET.

4.3.4. Discussion of X-Ray Diffraction Results

The crystallinity values obtained from WAXD are lower than the crystallinity values obtained by DSC by nearly a factor of two for ar-PET. One reason for this might be that K is different from unity and should be calculated from WAXD data for two different samples of known crystallinities. The assumption here is that all crystallites contribute to I_c and only chains in the amorphous regions contribute towards I_a. Another reason for this lower value may be due to the presence of a transition region of finite width between the amorphous and crystalline regions instead of a sharp interphase and hence this transition region tends to lower the crystallinity estimate done by WAXD.

Diffraction peaks at 2θ = 17.1, 22.5, 26.2 °, which have been assigned to (010), (i10) and (100) lattice planes, are evident in the diffractograms of ppt-PET in the Figure 4.15. These are the strongest reflections present in the previous crystallographic studies of PET [48]. The (100) peak is found to be present in oriented samples, such as uniaxially drawn PET fibers and films and is also pronounced in ppt-PET. It appears that the ppt-PET has crystallized with a higher level of orientational order than the ar-PET. This reflects a highly ordered environment from which the ppt-PET is crystallized, with respect to the randomly coiling environment dominant in ar-PET samples.

Results of the X-ray diffraction obtained for ppt-PET are found to be very similar to that observed for coalesced PET, where the (100) peak is also more clearly observed [41]. X-ray results have confirmed our assumption that, though processed differently, there exists (both microscopically and macroscopically) a strong similarity between the organization of PET chains in ppt and coalesced samples.

4.4. Density Measurements

4.4.1. Densities of PET films

The density measurements on three films of PET were carried out using the method described in section 3.4. The aim was to measure the amorphous density of the films. The three films used for the measurements were

a) Precipitated PET film

b) As-received PET film

c) As-received PET film annealed at 120°C for 20 min that had the same level of crystallinity as ppt-PET (according to DSC and X-ray measurements).

The precipitated PET film was observed to have the highest density value of 1.3670 g/cm^3, followed by the density value obtained for the annealed film of ar-PET, which was 1.3497 g/cm^3. The ar-PET film was found to have the lowest density of 1.3442 g/cm^3.

The annealed ar-PET film, with almost the same level of crystallinity indicated by DSC and X-ray as ppt-PET, was used for analysis so as to compare the amorphous regions in the two samples. Variations in the two values indicate a difference in the chain packing and orientation in their amorphous regions.

The volume fraction crystallinity (X_c) is also calculated from density values obtained according to:

$X_c = (\rho - \rho_a) / (\rho_c - \rho_a)$, where ρ, ρ_c and ρ_a are densities of the semi-crystalline polymer sample, wholly crystalline PET, and wholly amorphous PET, respectively. We have used the widely reported amorphous and crystalline density values of 1.335 and 1.515 g/cm^3 [23, 24] respectively. The values of crystallinity for all the films have been calculated in the same manner as above and are presented in Table 4.6.

Table 4.6. Crystallinity from density measurements

Sample	Density in g/cm^3 (ρ)	Volume fraction crystallinity (X_c)	Overall crystallinity in %
Precipitated PET film	1.3670	0.178	17.8
Annealed as-received PET film	1.3497	0.082	8.2
As-received PET film	1.3442	0.051	5.1

The main purpose for studying the film densities was to draw a comparison among the three in terms of their crystallinity values and amorphous/non-crystalline densities. The crystallinity level determined from film densities in the case of ppt-PET film is higher by a factor of two than the annealed ar-PET film and by over a factor of three compared to that of ar-PET. The crystallinity values obtained are much lower than the crystallinities obtained from the DSC and X-ray results, though they support the fact that the ppt-PET has a higher level of crystallinity than ar-PET.

We also tried to compare the ρ_{nc} and ρ_a value for the ppt-PET and the annealed ar-PET films, respectively, by comparing the X_c values obtained from the ppt- and annealed ar-PET films. ρ_{nc} is the density of the non-crystalline regions in the ppt-PET. This was done in order to draw a comparison between the amorphous/non-crystalline regions of the two PETs, though the crystallinity levels of both PET's (ppt-PET and annealed ar-PET film) are similar (DSC,X-ray), there exist a difference in the amorphous/non-crystalline parts of the two samples. This attempt would redefine ρ_a. Differences in the crystallinity values may be due to the differences in the value of the density of 100% amorphous or non-crystalline regions in

the polymers (ρ_a and ρ_{nc}), as ρ_a ? ρ_{nc}. The values for ρ_a and ρ_{nc} were obtained by using the volume fraction crystallinity (X_c) calculation from the equation given above, where the X_c value obtained from annealed ar-PET was used and $X_{c,\ ppt\text{-}PET} \sim X_{c,\ annealed\ ar\text{-}PET}$

For ppt-PET, the calculated ρ_{nc} was obtained from:

$0.082 = (1.3670 - \rho_{nc}) / (1.515 - \rho_{nc})$, with $\rho_{nc} = 1.354$ g/cm^3, compared to the standard ρ_a = 1.335 g/cm^3 assumed for annealed ar-PET.

The density of the non-crystalline portions of ppt-PET (ρ_{nc}) is higher (~1.4 %) than the density of the amorphous regions in annealed ar-PET (ρ_a). In fact ρ_{nc} calculated in this manner for ppt-PET is higher than the overall density ρ of the annealed ar-PET film.

4.4.1. Discussion of density measurements

Three films, two as-received and one precipitated PET were made by quenching the films immediately in cold water after melting, followed by annealing one of the ar-PET films at 120°C for 20 min. The main aim was to draw a comparison among the amorphous/non-crystalline densities of the PET films. Crystallinity determinations using film densities indicated that there exists a difference in crystallinity levels in all three films. This result is the same as obtained by DSC for the precipitated and as-received PET's. The ppt-PET cannot be quenched into a totally amorphous form, but a certain amount of crystallinity still remains even after quenching the film from the melt. The reason for this can be the fact that the chains in the amorphous/non-crystalline region are organized differently than that of the ar-PET and the annealed ar-PET

Amorphous/non-crystalline phase densities of these PET samples cannot be assumed to be the same. One reason for the difference in the values of density observed with these

three films might be that the orientation of the chains in the case of ppt-PET is higher than in the ar-PETs as was also observed by other methods (FTIR, X-ray). Orientation should increase amorphous/non-crystalline phase density due to the transformation of some gauche conformers to trans conformers. In contrast, crystallization decreases the amorphous/non-crystalline phase density due to constraints placed on amorphous chain segments attached to chain segments in crystals.

The ppt-PET has a higher value of density for its non-crystalline phase, because there the chains are more extended and tightly packed, and possibly more oriented (X-ray results), with a higher trans conformer content (FTIR results).

The value of ρ_{nc} obtained for ppt-PET is higher than the density measured for the annealed ar-PET. This is likely due to the orientation and order induced by our precipitation procedure in the non-crystalline regions of ppt-PET.

High precision and accuracy is needed for determining the densities of films. This inaccuracy might be a reason for the difference in the crystallinity values calculated from the densities, and they are not found to be in agreement with that of the DSC and X-ray results. Density calculations can be carried out again and confirmed by using a column designed especially for PET.

4.5. Comparison of PET crystallinities

This section involves a comparison of ar-PET and ppt-PET in terms of their % crystallinity obtained by using Differential Scanning Calorimetry, Wide Angle X-Ray Diffraction, and Density Measurements. Table 4.7. presents a comparison of the crystallinity levels in different PETs. All of the methods used indicated that ppt-PET has a higher level of crystallinity than ar-PET, and a different type of organization exists in the ppt-PET sample, because the differences persist even after melt quenching.

Table 4.7. Comparison of the crystallinity values for the two PETs obtained using different methods

Methods Used	% X_c of As-received PET	% X_c of Annealed As-received PET	% X_c of Precipitated PET
DSC	9.5	38.7	39.1
X-Ray	5.8	31.4	32.3
Density	5.1	8.2	17.8

Precipitated PET and annealed as-received PET have very similar crystallinity values when measured by DSC and X-ray, but the crystallinity values from density measurements differ substantially, with the ppt-PET having a much higher crystallinity than the annealed ar-PET, because the non-crystalline regions of the ppt-PET are denser than the amorphous regions of the annealed ar-PET (see section 4.4.1.). It has been observed in the studies done by Koenig *et. al.* that the crystallinity measurements carried out by density measurements varies with that of the DSC and the X-ray results.

4.6. Film Shrinkage Tests

4.6.1. Shrinkage Results

The two PET films were examined under the optical microscope to observe their shrinkage behavior at varying temperatures (section 3.5.). The observations carried out on the ar-PET and the ppt-PET films were normalized by the original lengths of the two films.

Figure 4.17. shows the film shrinkage–temperature curves. The film samples were heated from room temperature till they melt. With increase in temperature, shrinkage increases strongly. The shrinkage for ar-PET film reveals a transition at about 81°C, near its T_g. Change in the shrinkage, actually expansion of ar-PET is observed again at around 120°C, and is related to the beginning of its crystallization.

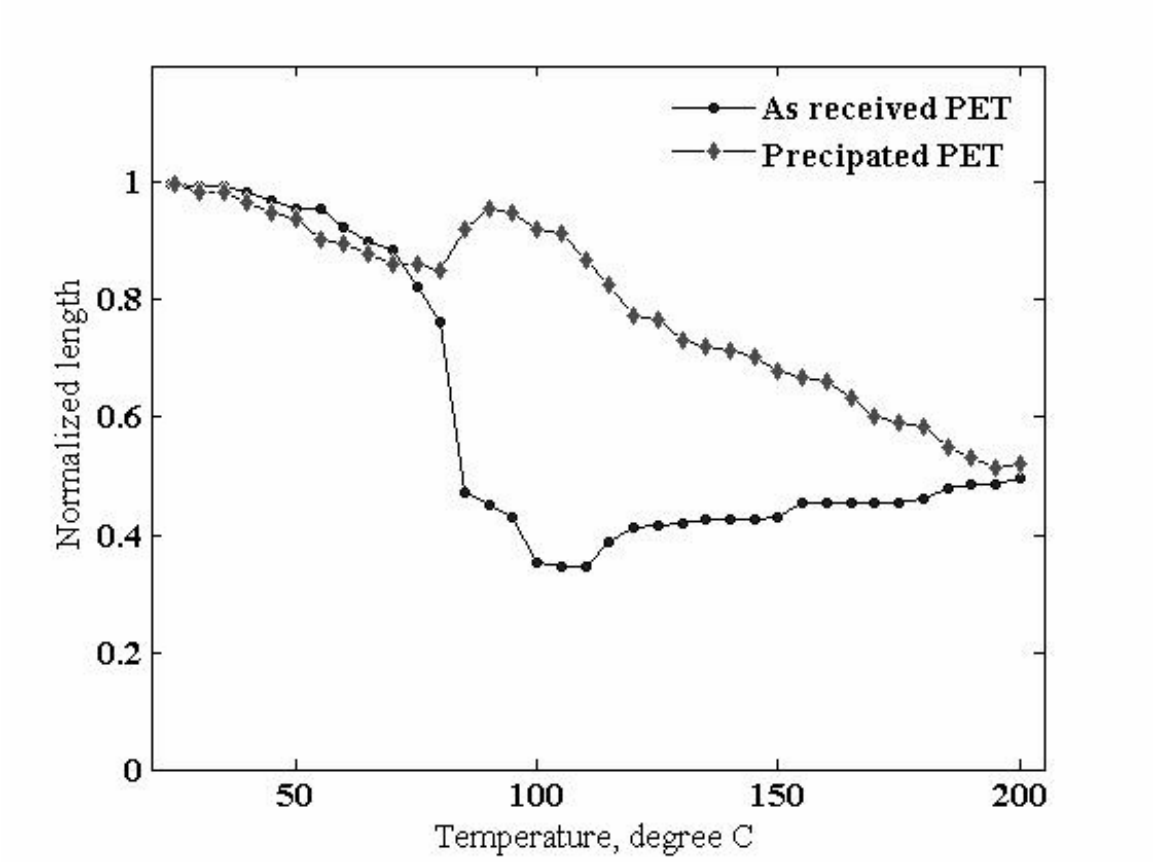

Figure 4.17. Shrinkage test for the two PET's

4.6.2. Discussion of film Shrinkage Results

Initially on heating, both films are observed to behave similarly. At room temperature both of them start to gradually shrink almost equally, till the temperature of ar-PET reaches its glass transition temperature (T_g ~ 80°C). Here the film contracts abruptly (as observed in Figure 4.17.). This may be due to the fact that at T_g the chains become mobile and they are able to contract from their more extended melt pressed configuration, whereas the ppt-material still continues to shrink, but an abrupt shrinkage is not observed for this material. These results support the fact that a T_g for the ppt-PET is not observed using the DSC. This increase in shrinkage with increasing temperature for ar-PET is due to a rise in the molecular mobility with temperature, which enables conformational changes [50]. The shrinkage for the ar-PET increases more than a factor of 2 from 23.8 % to 52.9 % as the sample temperature changes from 80 to 85°C, whereas during the same temperature interval shrinkage for the ppt-PET is not found to show much variation.

The ar-PET continues to shrink till it reaches its crystallization temperature (T_c ~120°C), where the ar-PET chains tend to extend as they are crystallized. The ppt-PET does not exhibit this kind of behavior. It continues to shrink uniformly with not much change over the whole of the heating scan, because this sample shows neither a T_g nor a T_c.

4.7. Melt Viscosity Measurements

4.7.1. Melt Viscosity Results

In order to further characterize the two materials macroscopically, melt viscosity measurements were carried out using the Minimelter as described in section 3.6. Figure 4.18. shows the comparison of the viscosity vs. time plot for the two PETs. In the course of measuring the viscosity we observed that the viscosity of the ppt-PET is always less than that of the ar-PET even when both samples are held in the melt for a longer period of time, say 12 minutes.

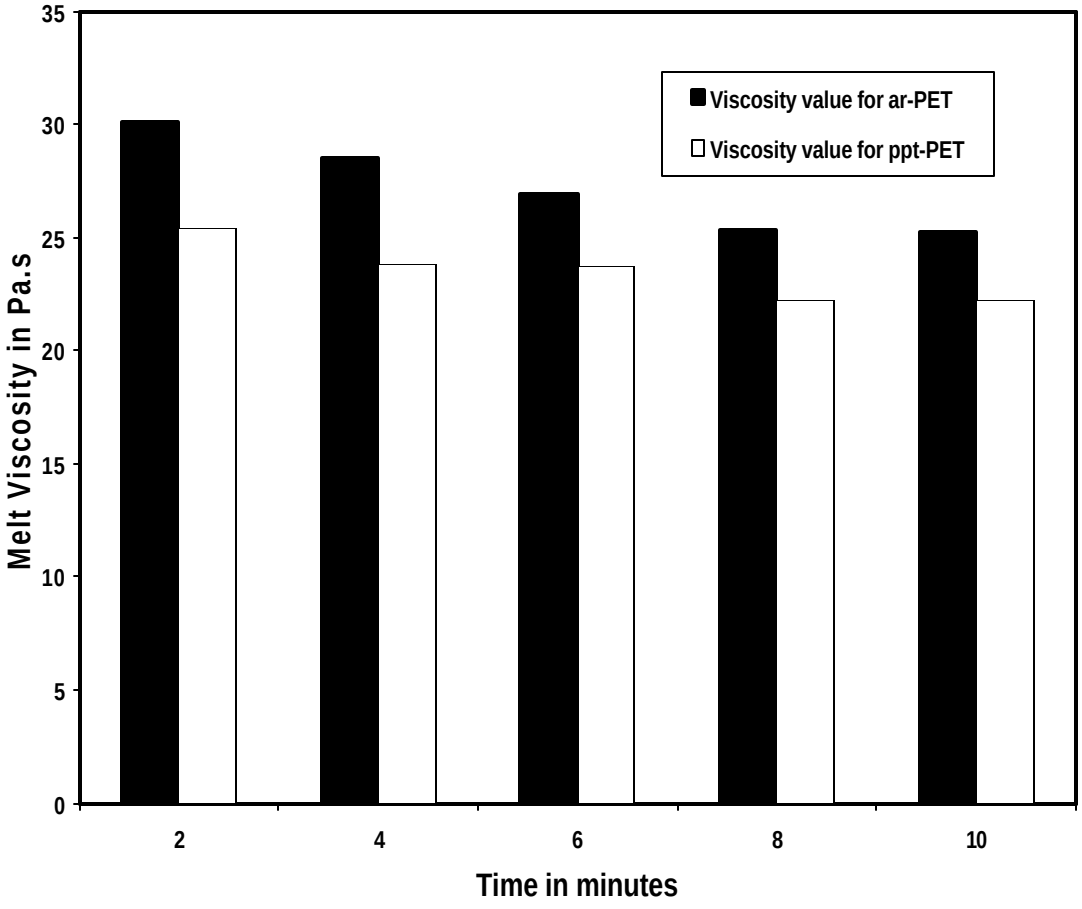

Figure 4.18. Viscosity measurements of the two PET's using a Minimelter

4.7.1. Discussion of Viscosity Measurements

From the graphs in Figure 4.18. it is clear that the melt viscosity changes with time in the case of the ppt-PET are less than that of the ar-PET. After some time the viscosity of the two materials attains a constant value. These observations were carried out in order to study the rheological properties of the two materials. We can draw the conclusion that the ppt-PET will be easier to process in the melt, because it is less viscous. Thus, the two PET's are found to differ macroscopically in the melt.

4.8. Stress-Strain Measurements

4.8.1. As-received PET

In order to study the qualitative behavior of the two films, stress-strain measurements were carried out. Figure 4.19. shows the results of the stress-strain tests for ar-PET, which exhibits yielding and necking and high extensibility before failure, behavior characteristic of amorphous polymers observed below T_g. Sample 1, Sample 2, and Sample 3 are film strips that were tested under the same conditions, so as to observe the reproducibility of the data.

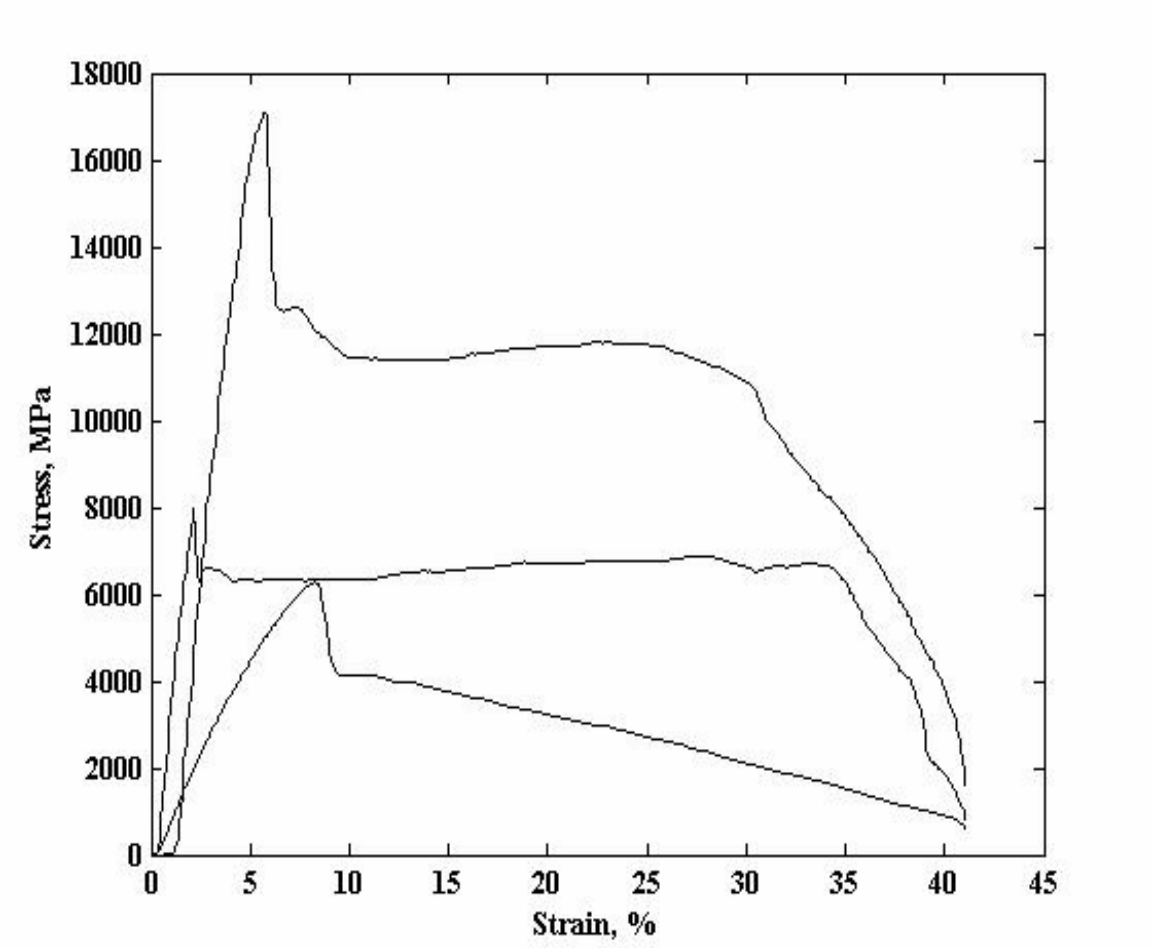

Figure 4.19. Stress and Strain behavior of ar-PET films

4.8.2. Precipitated PET

Similarly Figure 4.20. depicts the behavior of the ppt-PET film. It behaves distinctly different than the ar-PET film. Ppt-PET shows a rigid behavior, more like a semi-crystalline polymer, such as isotactic polypropylene.

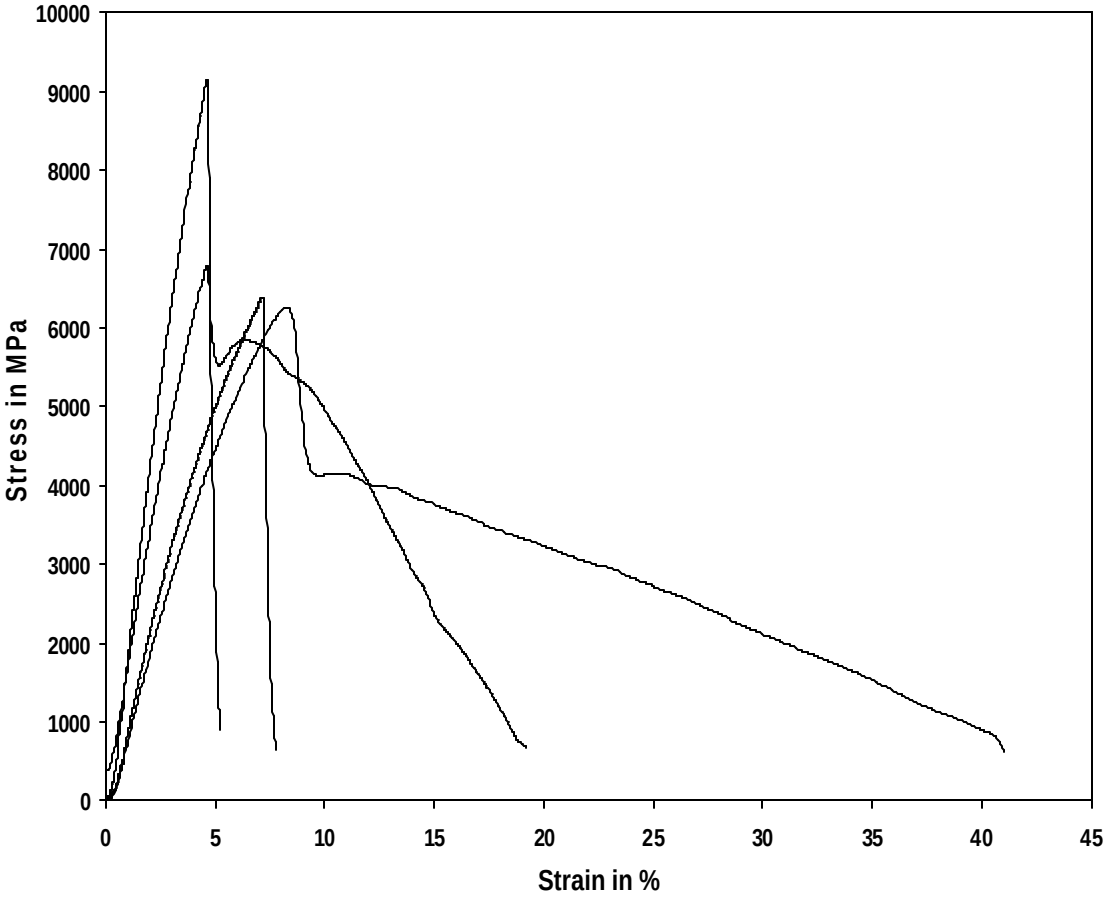

Figure 4.20. Stress-Strain behavior of ppt-PET

4.8.3. Discussion of the Stress-Strain behavior

The nature of the stress–strain curve of a polymer depends on the conditions of testing. A polymer can show all the features of a glassy brittle solid, an elastic rubber, or a viscous liquid depending upon the time scale of measurements, which depend upon the conditions of testing. All our stress-strain tests were carried out at room temperature (~22°C) well below the glass transition temperature of PET (~81°C). At temperatures below the glass transition (T_g), which is the case here, typical stress-strain curves of PET show a yield point at the low strain rate employed here. This is what is observed in the stress-strain curve of ar-PET (Figure 4.19.). This behavior of ar-PET films is due to cold drawing of the polymer. In the case of ar-PET, initially the load rises rapidly, up to the yield point. With further elongation, the curve shows a plateau where the load stays at a constant level and large plastic deformation is achieved in this region (necking). After the plateau region there is a region of alignment and ordering. The polymer chains are aligned resulting in a higher degree of orientation in the direction of deformation, and this orientation leads to strain-induced crystallization (crystallization occurring during orientation). After the plateau region the load rises steadily with further elongation and finally failure is found to occur. The stress-strain behavior indicates that the chains in the ar-PET film are not initially aligned and oriented, and hence after the yield point exhibit a plateau region, where the chains orient themselves and eventually cease to orient and finally break [49]. Ar-PET exhibits the usual tough plastic behavior of predominantly amorphous polymers strained below their T_g's.

The behavior in the case of ppt-PET film (Figure 4.20.) is observed to be quite different than that of ar-PET. It shows an increase in the load at first and shows a yield point, but does not show the presence of a plateau region. Strain-induced crystallization in not

observed as the chains are not able to further orient themselves. This may be due to the preexisting high orientation and order in ppt-PET. Even the film shrinkage results confirm the fact that strain-induced crystallization is not observed in ppt-PET to the extent observed in the ar-PET films. Ppt-PET is already sufficiently crystallized that it does not crystallize during orientation. Ppt-PET fails at much reduced extension showing a rigid behavior similar to semi-crystalline polymers.

4.9. Atomic Force Microscopy

4.9.1. As-received & Precipitated PET films

AFM was done in order to study and determine the morphologies of the two PETs. This was carried out on both films of PET that were crystallized from their melts. When the oscillating AFM probe is scanned along the surface of the film the soft amorphous material is more compliant than the harder crystalline material, which results in a phase difference between the soft and the hard regions of the sample and hence provides a distinct contrast between the two phases.

Figure 4.21. (a) shows the AFM image of the ar-PET., which shows a somewhat featureless morphology. The structure of the ar-PET can be differentiated into amorphous and crystalline regions. The ar-PET exhibit some lamellar structures in the spherulites, which can be visualized both edge and flat on due to lamellar twisting. If we consider the brighter portions of the image to be crystalline (with a higher Young's Modulus than the surrounding areas) and the darker ones to be the amorphous regions, then in the ar-PET we observe a very uneven distribution of the bright and the dark regions [26].

Similarly Figure 4.21. (b) is the AFM image of the ppt-PET film that has been made in the same way as that of the ar-PET. Ppt-PET shows the presence of spherulites very clearly and they are evenly distributed. Crystal orientation does not follow a specific direction, but instead the spherulites are randomly aggregated. Ppt-PET shows a high density of branching and hence crystalline features are dense.

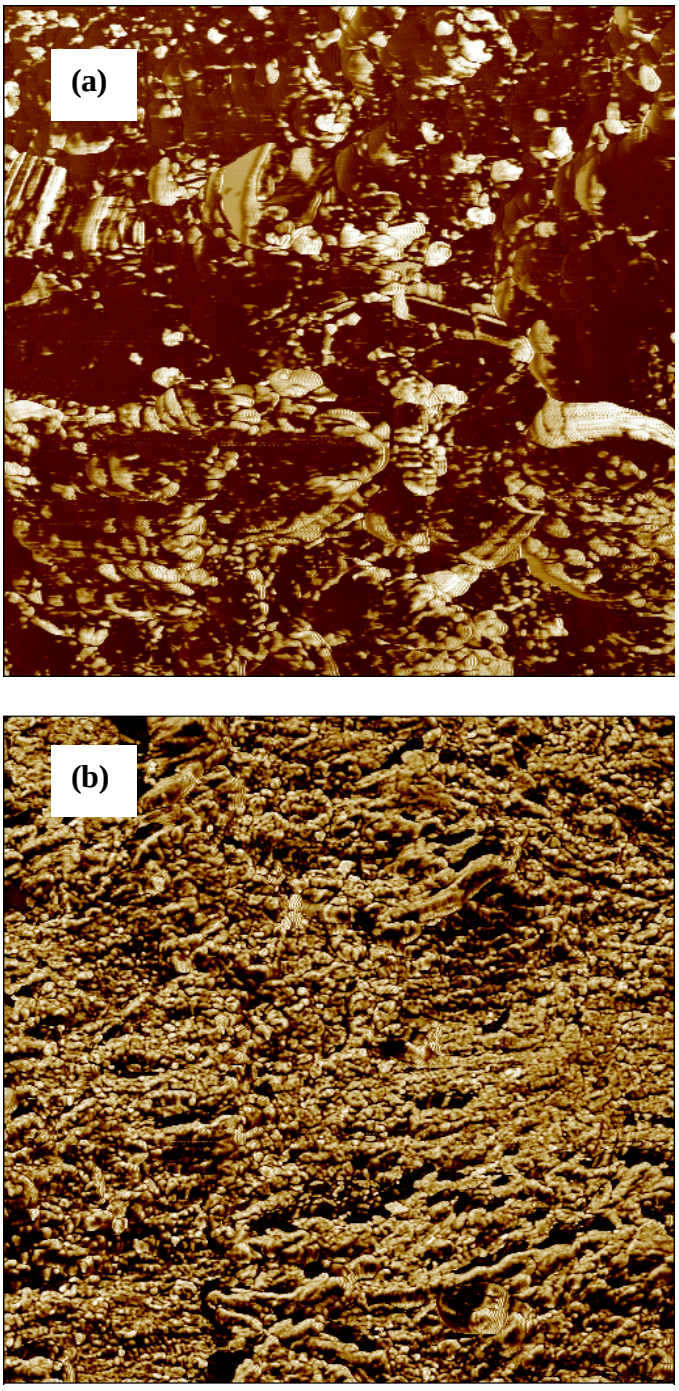

Figure 4.21. AFM images with 2-D resolutions of 4´4 ㎛ of (a) As-received PET and (b) Precipitated PET.

4.9.1. Discussion of AFM Images

Observations of the morphology by Atomic Force Microscopy were done on ultra thin sections, assuming that the observations made at the surface may be extrapolated to bulk. AFM is used to determine the surface morphology of the samples and it can be concluded that the crystallization does initiate at the surface for the ppt-PET. Bulk crystallinity of PET has been evaluated by comparing the relative intensity of the 1340 cm^{-1} band by Microscopic FTIR (section 4.2.2). The intensity was found to be higher for the ppt-PET, as compared to the ar-PET, so we can conclude that crystallization has occurred in the bulk also.

As crystallization is related to microstructural properties, from the above images we can conclude that ppt-PET has all together a different morphology and crystallizes differently than ar-PET. Even in the state where both materials have been rapidly cooled from their melts, ppt-PET has a much larger number of small spherulites evenly distributed compared to the larger spherulites of ar-PET. Spherulites of the ppt-PET appear to be cropping out from the surface. Microscopically the two films behave differently.

4.10. Absorption of Carbon dioxide by PET

4.10.1. Static Absorption of Carbon dioxide by PET

At sub-atmospheric pressures, CO_2 has a very low solubility in most polymers. The small amount of CO_2 that is dissolved tends to reside in voids or free volume that are present. Hence, the sorption of CO_2 may be used as an indicator of the amount of free volume in a given sample. Free volume exists in the interstitial sites between PET molecules. CO_2 sorption is explored here as an indirect probe of this free volume.

Figure 4.22. shows the sorption isotherm behavior of carbon dioxide in ar-PET film. The test has been carried out as described in section 3.9. The isotherm shown is at 30° C and at a pressure of 314 torr.

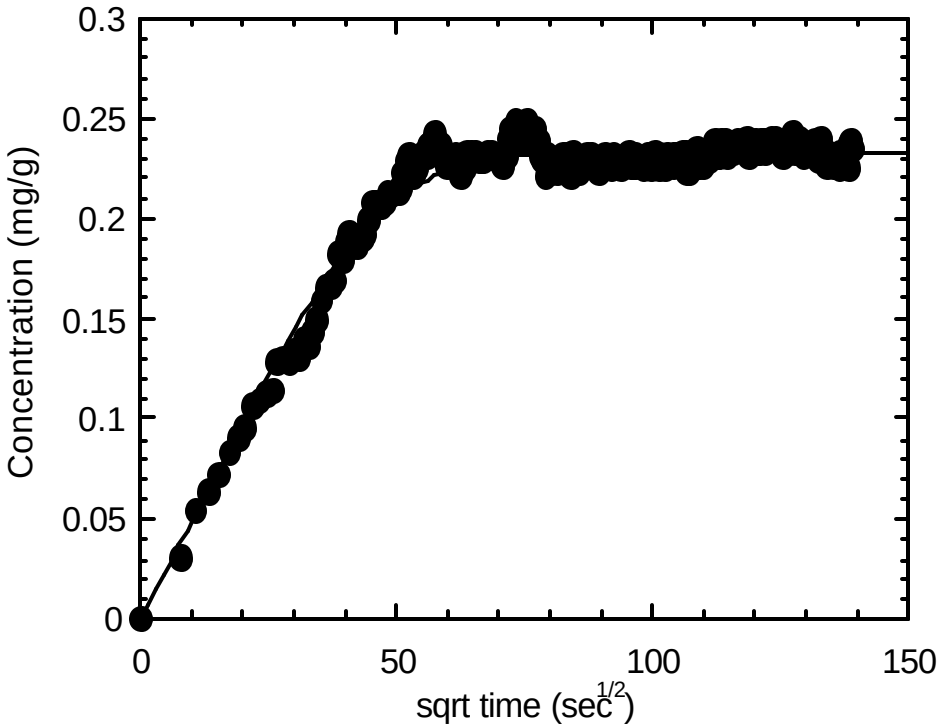

Figure 4.22. Carbon dioxide sorption in ar-PET at T=30° C and P=314 torr

Figure 4.23. shows the sorption behavior of the carbon dioxide in ppt-PET. In both Figures the isotherms were obtained under the same conditions.

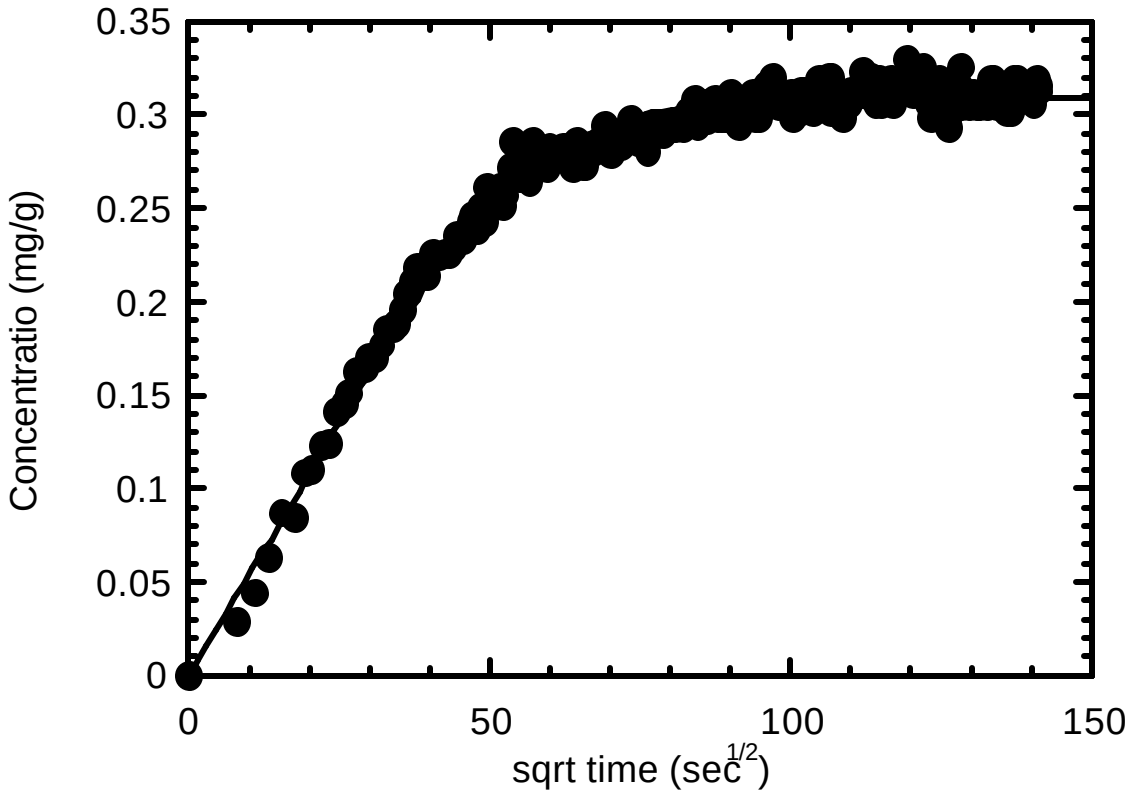

Figure 4.23. Carbon dioxide sorption in ppt-PET at T=30° C and P=314 torr

Figure 4.24. shows a comparison of the sorption isotherms of carbon dioxide in ar- and ppt-PETs observed at different values of pressure at 30º C. Ar-PET begins approaching an asymptotic absorption of approximately 1.6 moles of CO_2 per mole of ar-PET, at 510 torr CO_2, while ppt-PET behaves in a similar manner at low values of pressure, but continues to absorb gas beyond this pressure, with no indication of leveling. The shape of the isotherm, for the ar-PET in Figure 4.24. is typical of that for a glassy polymer, while the isotherm observed for ppt-PET is not. (CO_2 absorption at 510 torr in ppt-PET should be remeasured to

determine whether or not the increased CO_2 absorption at this higher pressure shown in Figure 4.24 is real.)

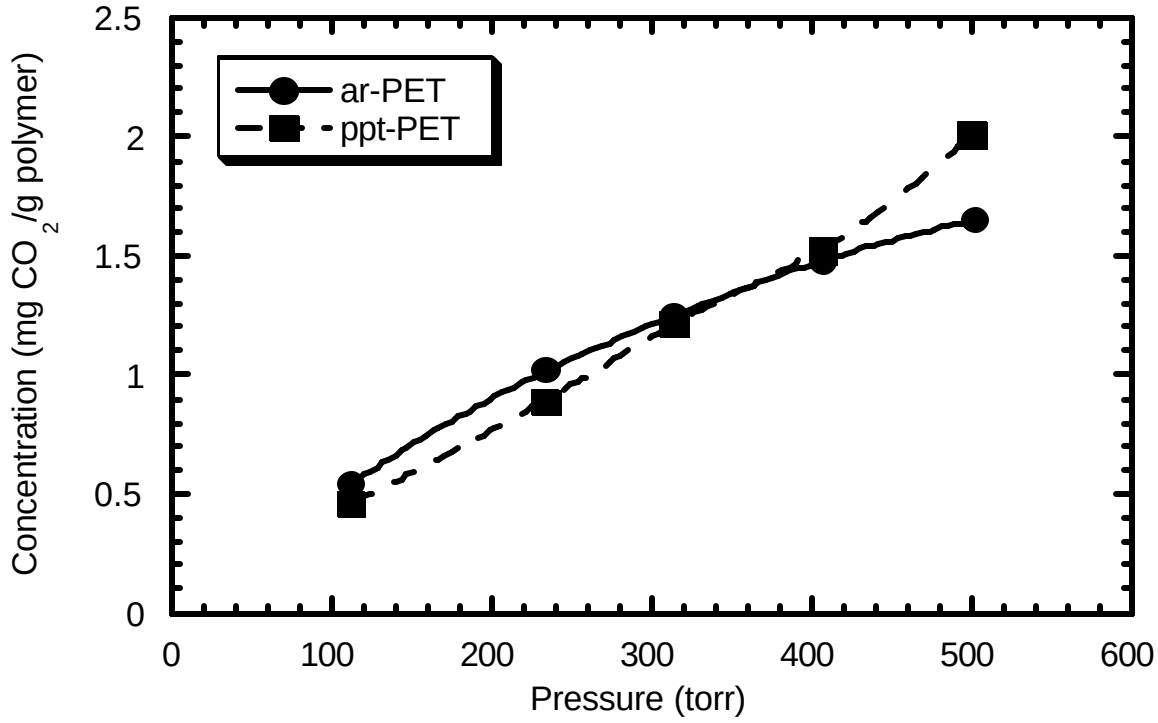

Figure 4.24. Sorption isotherms for CO_2 in as-received and precipitated PETs at 30° C

Figure 4.25. shows a comparison of the diffusion coefficients measured for CO_2 in the as-received and precipitated PETs. At all, but the lowest pressure (100 torr), the diffusion coefficient CO_2 in the precipitated PET is found to be less compared to that of the as-received PET. With an increase in pressure the diffusion coefficient of CO_2 in the ppt-PET decreases initially, but then attains a constant value, whereas the ar-PET shows an increasing value of diffusion coefficient with increasing pressure, though the diffusion coefficient of CO_2 in ar-PET at 510 torr needs to be remeasured to confirm the trend seen in Figure 4.25.

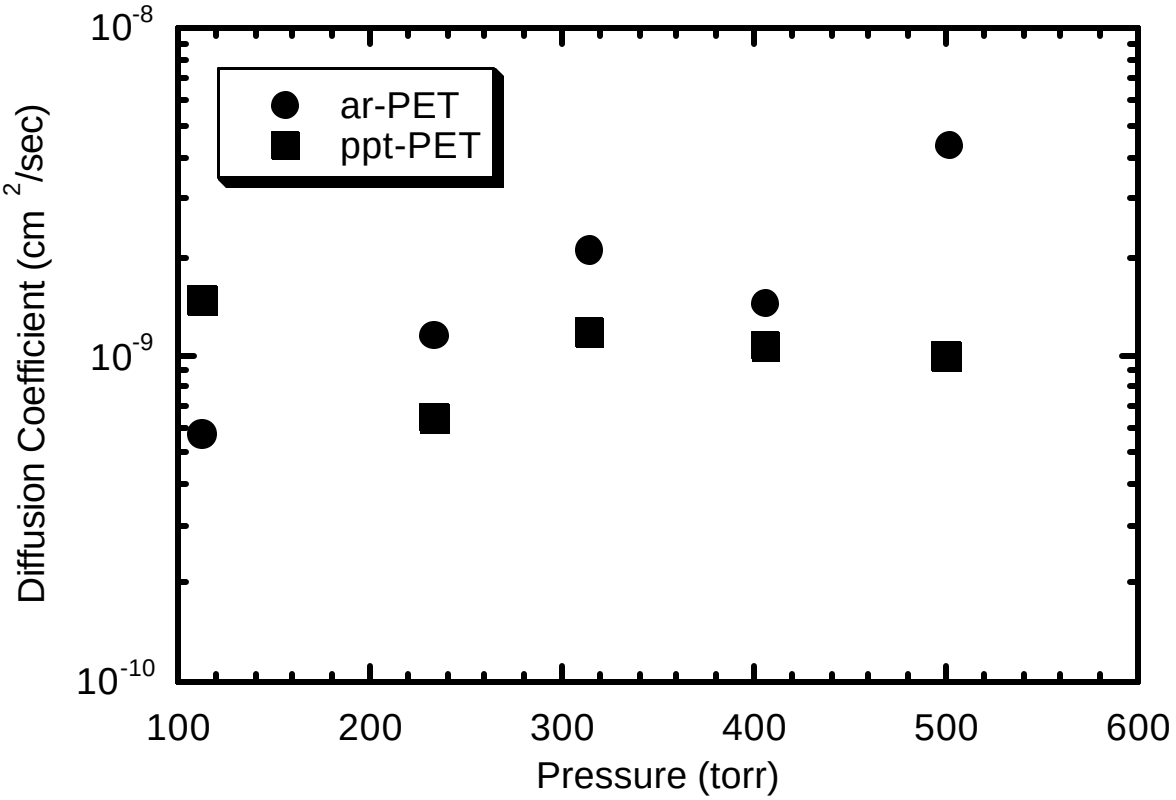

Figure 4.25. Comparison of the diffusion coefficients for as-received and precipitated PETs.

Table 4.8. shows the values of the CO_2 diffusion coefficients and solubilities observed at different pressures for the as-received and precipitated PETs.

Table 4.8. CO_2 solubility and diffusivity in PET films

Pressure in torr	As-received PET		Precipitated PET	
	Diffusivity $X10^{-9}$ in cm^2/sec (D)	Solubility in mg of CO_2/gm of polymer (S)	Diffusivity $X10^{-9}$ in cm^2/sec (D)	Solubility in mg of CO_2/gm of polymer (S)
100	0.58	0.04	1.47	0.09
200	1.16	0.05	0.64	0.06
300	2.11	0.11	1.16	0.12
400	1.44	0.14	1.07	0.16

4.10.2. Discussion of sorption of carbon dioxide by PETs

In this section we theoretically analyze the sorption of carbon dioxide in PET films. In the past most studies of gas sorption in PET have concluded that PET obeys the dual-mode sorption model [52, 53]. The dual-mode sorption model can be described as:

$C_e = C_D + C_H = k_D p + C_H' bp / (1 + bp)$ [52], where C_e is the total penetrant concentration determined in the sorption experiment, C_D is the soluble concentration due to Henry's-law constant, p is the partial pressure of the penetrant at equilibrium, b is the hole affinity constant of the gas for the Langmuir sites, and C_H' is the hole saturation constant of the polymer for the gas in the Langmuir's sorption mode.

One reason for the increased absorption by ppt-PET shown in Figure 4.24 at high CO_2 pressures, if it is real, may possibly be due to greater free volume than ar-PET, resulting in higher sorption levels. Additionally, this could be due to CO_2 molecules adsorbing on the external surfaces of the sample, because higher sorption levels can be attributed to higher surface areas. The AFM images in Figure 4.21.(b) show that the surface morphology of ppt-PET appears more uniform, but with a finer scale of heterogeneities than the ar-PET film surface. Thus, the ppt-PET sample may have a larger surface area, which is consistent with its slightly higher CO_2 sorption level at high gas pressures.

Precipitated PET is found to be nearly 40% crystalline, whereas the as-received PET is only 10% crystalline (DSC results) and so the ppt-PET is expected to show a lower value of CO_2 absorption as compared to that of the ar-PET. Increase in the crystallinity level of a polymer should reduce its ability to absorb gases. Since absorption of gases in polymers is usually attributable to their amorphous regions, the non-crystalline regions in ppt-PET, that act as a barrier for gas absorption at low pressure, might, at higher pressures, allow more gas to penetrate. This may be the reason that ppt-PET shows a higher value of sorption with an increase in CO_2 pressure.

The average diffusivity value (D_{avg}) calculated for ppt-PET (1.08 cm^2/sec) is smaller than that for ar-PET (1.32 cm^2/sec). This may be due to the fact that the ppt-PET has more highly oriented and more tightly packed chains in its non-crystalline regions. Modification of ar-PET to form ppt-PET might restrict the molecular motions of PET chains that occur in the non-crystalline regions [51]. Small increases in density are normally found to cause a reduction in the solubility and the diffusivity of gases in polymers [54, 55]. An increase in

the density of the polymer raises the activation energy for the diffusion of gases and hence gives a lower value for the diffusion coefficient, consistent with our density measurements.

The rigid closely-packed polymer chains in the non-crystalline regions of ppt-PET are quite different from those in the amorphous regions of typical semi-crystalline glassy polymers. In the latter case the less dense amorphous regions are found to play an important part in the sorption uptake and the transport of gases through the polymer sample.

From the nature of the solubility and the diffusivity curves of a polymer film, its permeability can be estimated. The permeability coefficient (P) of a permeant through a polymer is the product of its diffusion (D_{avg}) and solubility coefficients (S), $P = S \times D_{avg}$. S is normally dominated by the degree of crystallinity and usually increases as X_c is reduced. Solubility of CO_2 in PET is not found to vary much. D is dominated by the mobility and packing of polymer chains in the amorphous/non-crystalline regions, but not by their quantities. Thus, we expect D to be lower for ppt-PET than ar-PET. Table 4.9 presents the permeabilities of CO_2 in ar- and ppt-PETs. These permeability values are in the range of those mentioned in Table 1.5 (0.07 – 0.17), with some deviation from our data at high pressures.

Table 4.9. CO_2 permeabilities in PET films

Sample	D_{avg} in cm^2/sec	Permeability values X 10^{-13} $cm^3.cm.cm^{-2}.s^{-1}.Pa^{-1}$			
		100 torr	200 torr	300 torr	400 torr
As-received PET	1.32	0.05	0.06	0.15	0.19
Precipitated PET	1.08	0.1	0.07	0.13	0.18

We are planning to measure the CO_2 permeabilities (CO_2 sorption as a function of time and pressure) of annealed ar-PET, which has the same level of crystallinity as ppt-PET (DSC and X-ray results), to isolate the contrasting behaviors of their, respective, amorphous and non-crystalline regions. The annealed ar-PET film is similar to the ar-PET film, but with a much higher level of crystallinity. With a higher crystalline fraction and the usual amorphous regions we expect the solubility, diffusivity, and permeability of CO_2 in the annealed ar-PPT to be reduced, similar, and smaller than in the ar-PET film. Preliminary sorption measurements on annealed ar-PET film are consistent with these expectations.

4.11. Fiber testing of PET's

4.11.1. DSC results of the fibers

4.11.1.1 As-received PET

Figure 4.26. represent the DSC thermograms of the as-received PET fiber. The fiber thermogram resembles that of the ar-PET DSC scans in Figure 4.1. It shows the same trend with the glass transition followed by a crystallization exotherm and a melting endotherm. Table 4.10. presents a summary of the different peaks obtained in the DSC thermograms of ar-PET fiber. Comparing the crystallinity values from Tables 4.1. and 4.9. for ar-PET, the % crystallinity values X_c obtained for the ar-PET fiber are somewhat higher than that of the normal ar-PET pellets.

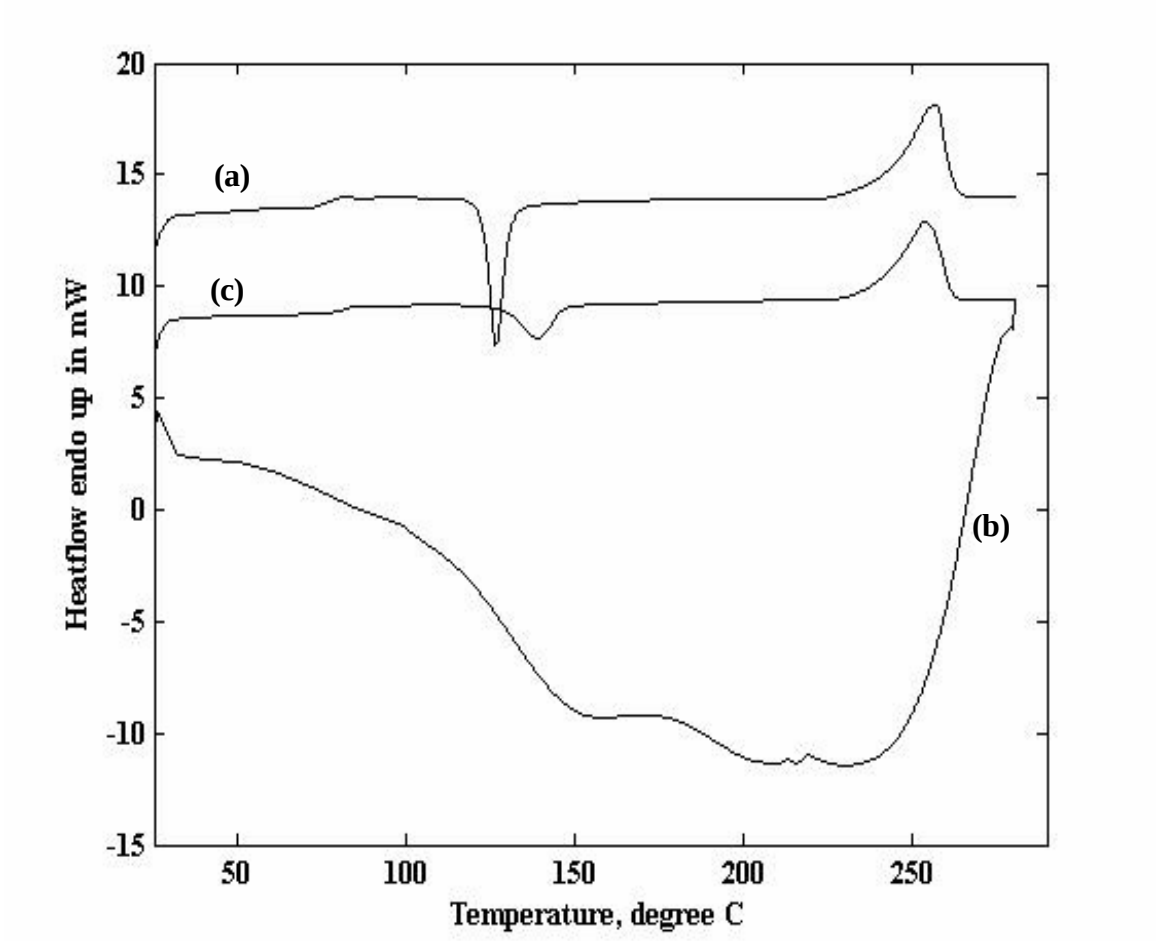

Figure 4.26. DSC Thermograms of ar-PET fiber. (a), (c) first, second heating and (b) cooling scans.

Table 4.10. Summary of the first and the second heating scan of ar-PET fiber

Sample	T_g in °C	T_c in °C	ΔH_c in J/g	T_m in°C	ΔH_m in J/g	X_c in %
Ar-PET Run I	77.7	126.6	29.9	257.5	50.2	16.9
Ar-PET Run II	81.6	139	12.7	254.1	42.8	25.1

4.11.1.2. Precipitated PET fiber

Figure 4.27. shows the DSC thermograms of the ppt-PET fiber that is made as described in section 3.10. The DSC thermogram of the ppt-PET fiber is similar to that of the thermogram in Figure 4.2. for the ppt-PET powder. The only difference between the two is seen in the first heating scan of the ppt-PET fiber, where the presence of a crystallization peak that is not observed in the scan of the ppt-PET powder in Figure 4.2 is evident. It does not, however, exhibit a crystallization exotherm in the second heating scan. The cooling scan and the second heating scan of the ppt-PET fiber are identical with the respective scans in Figure 4.2. of the ppt-PET powder. Table 4.11. shows a summary of the different peaks obtained in the DSC heating thermograms of ppt-PET fiber. The ppt-PET fiber does exhibit a recrystallization exotherm on cooling from the melt at a very high cooling rate (characteristic of ppt-PET and not observed in the ar-PET). Also, the crystallinity values X_c are high for the ppt-PET fiber.

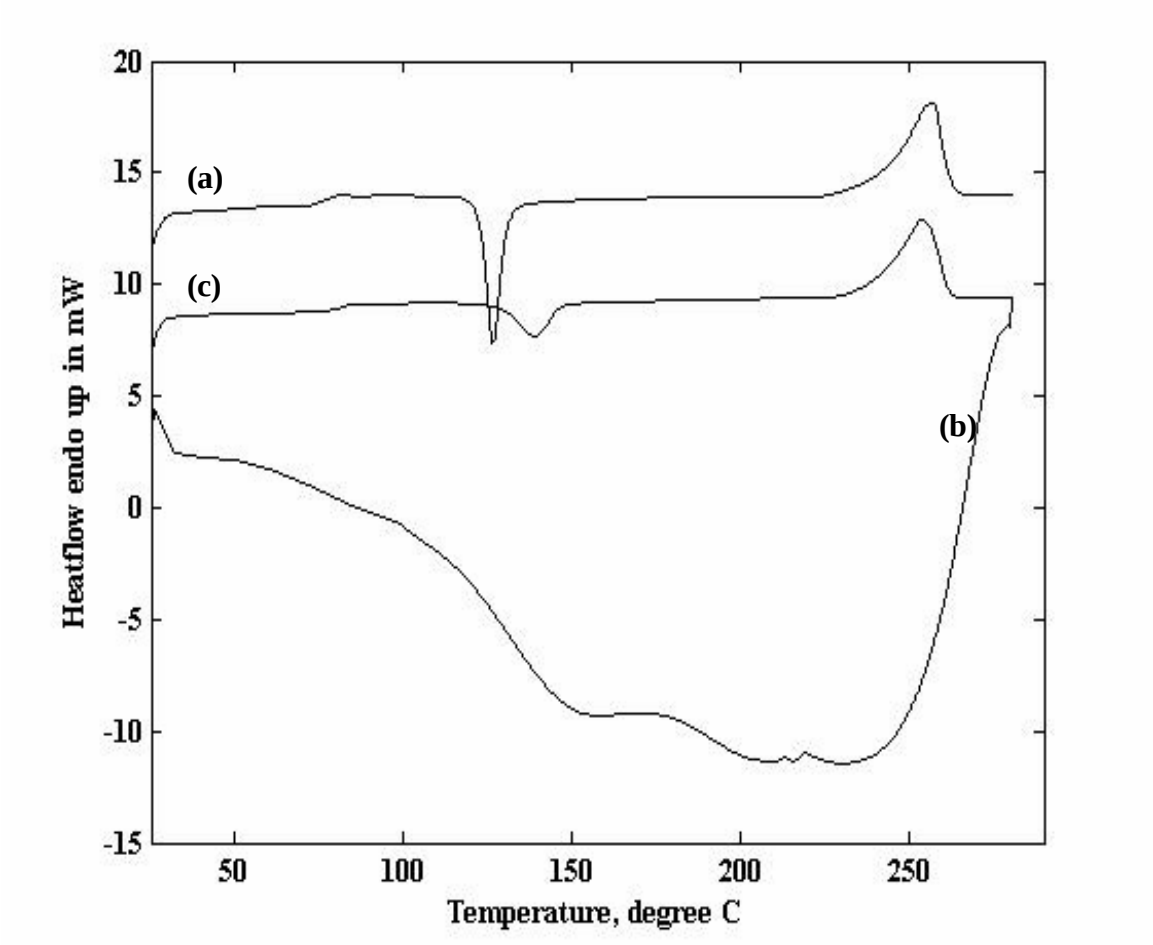

Figure 4.27. DSC Thermograms of ppt-PET fiber. (a),(c) first, second heating and (b) cooling scans.

Table 4.11. Summary of the first and the second heating scans of ppt-PET fiber

Sample	T_g in °C	T_c in °C	ΔH_c in J/g	T_m in°C	ΔH_m in J/g	X_c in %
Ppt-PET Run I	72.8	123.9	15.4	256.5	45.8	25.3
Ppt-PET Run II	-	-	-	250.8	48.1	40.1

4.11.2. Discussion of the fiber behavior (DSC)

The DSC thermograms of the ar-PET fiber as described above are found to exhibit the same trend as the ar-PET pellets. Melt obtained from the first heating scan of the ar-PET fiber, quenches into a totally amorphous form. The crystallinity values obtained in the case of the ar-PET fiber is somewhat higher than that of the pellets. One reason for this behavior may be that while extruding the fiber from the melt the chains in the amorphous region of the polymer might have been partially aligned and orientated resulting in their more facile crystallization.

The ppt-PET fiber differs in terms of its first heating scan from that of the ppt-PET powder, while the rest of the thermograms are the same. One possibility is that after melting and drawing into fibers, the ppt-PET either loses its usual melt characteristics and behaves more like ar-PET or impurities are present while processing the polymer. In the former case ppt-PET after melting should behave like ar-PET and cooling the melt at a high cooling rate should not yield a recrystallization exotherm and must be capable of being quenched in to a totally amorphous material. The second heating scan should then also yield a T_g and a crystallization exotherm, but these are not observed in the cooling and the second heating scans of the ppt-PET fiber. So the second possibility, the presence of some impurity in the sample that acts as sites for the nucleation of crystals and which disappears as the polymer undergoes one complete cycle of heating and cooling, becomes more plausible.

4.11.3. Load-Extension measurements on fibers

4.11.3.1. As-received PET fiber

The fibers were tested as described in section 3.10. The ar-PET load-extension behavior is shown in Figure 4.28. Three distinct behaviors are observed. Below elongation of 2.5% the fibers exhibit a linear stress-strain relationship. After that region the fibers are found to undergo instability in yield, where multiple necks are observed in the sample. A region of constant load drawing is then found as the multiple necks merge into a continuous neck that then propagates through the entire gauge length (1 inch here). This is then followed by a sharp rise in the load as the material experiences redraw and strain hardens till failure.

The load-extension behavior in Figure 4.28. can be interpreted with reference to the work of Bechev and Mishinev [56], who carried out tensile tests on PET filaments. At a few percent elongation and at a similar load, materials regardless of the degree of relaxation, show a plateau region in which a fiber deforms without any increase in tensile load. This characteristic is observed in the stretching of the ar-PET fiber. The plateau region represent orientational draw, and the length of the plateau depends upon the amount of the disordered material present in the sample. The greater the length of the plateau region the greater is the amount of disordered material. Since the fiber is not drawn fully, it shows some variations on extension.

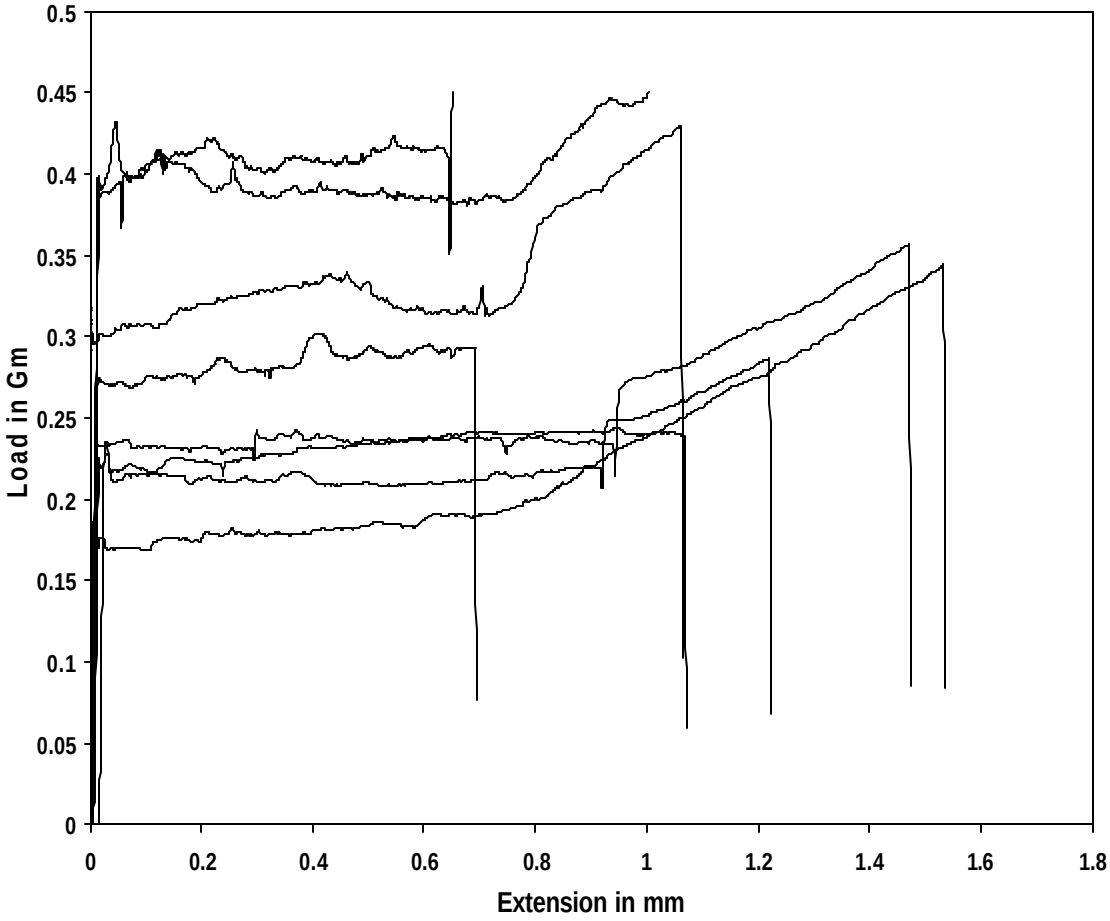

Figure 4.28. Load–Extension curves of ar-PET fibers

4.11.3.2. Precipitated PET Fiber

The ppt-PET fiber response to extension is shown in Figure 4.29. Here it is clearly visible that the load-extension curves of the ppt-PET fibers are quite similar to one another. The shapes of the curves indicate a closeness to brittle rather than to the ductile behavior of ar-PET fibers.

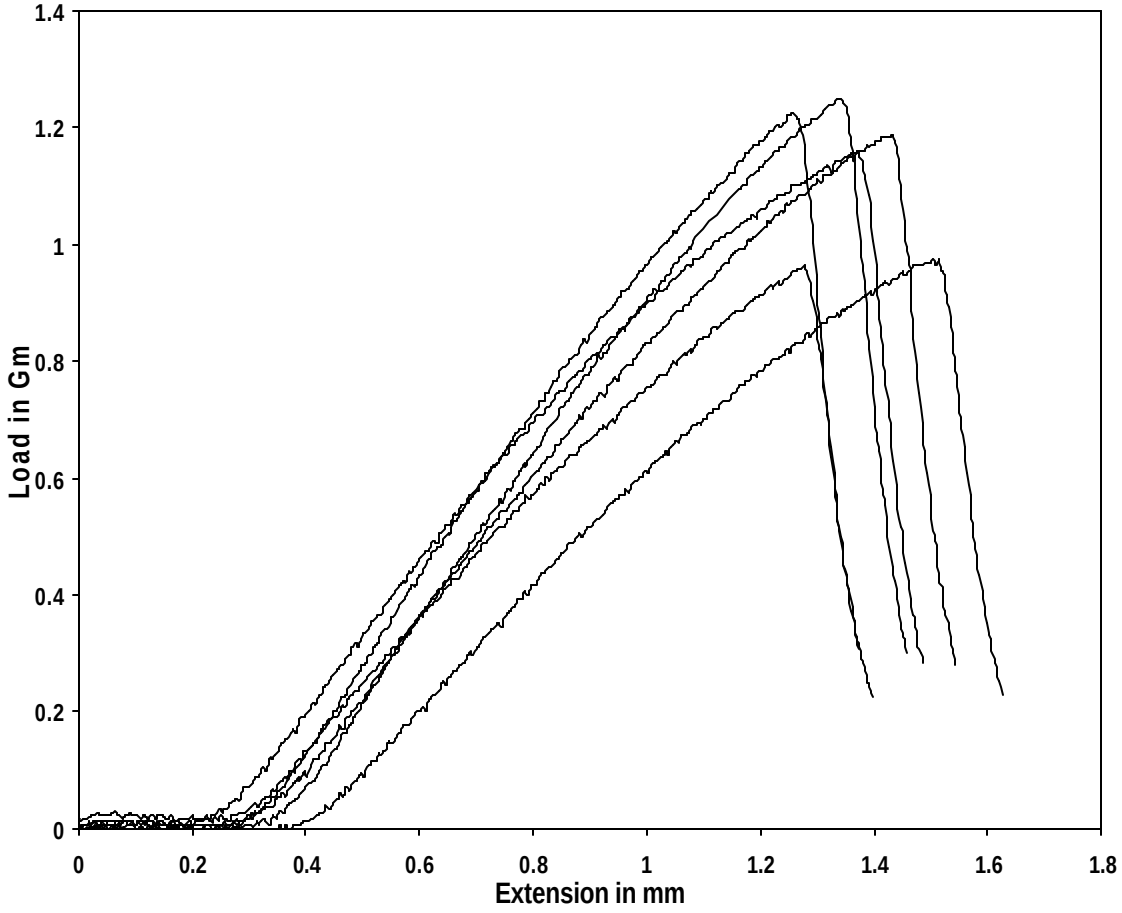

Figure 4.29. Load–Extension curves of ppt-PET fibers

4.11.4. Discussion of load-extension behavior of the two PETs

As clearly observed from Figures 4.28. and 4.29. the two fibers respond differently to load. The ar-PET fiber behaves in a ductile manner, whereas the ppt-PET fiber is brittle in nature. Ar-PET fibers show distinct yielding, while the ppt-PET fibers do not. This is because the properties of the ar-PET are predominantly dependent on its amorphous phase, whereas for ppt-PET fibers this is not the case, because of much higher crystallinity. This can be

explained by the two phase model, i.e., the coexistence of crystalline and amorphous/non-crystalline phases. Ar-PET fibers have the presence of two distinct phases (crystalline and amorphous) that are coupled in series and ppt-PET fibers have their two phases (crystalline and non-crystalline) distributed without distinct boundaries and without serial coupling, and this morphological difference may be contributing to the different behaviors of their fibers.

The yield point of the ppt-PET fiber is quite close to the fracture point. In the case of the ar-PET fibers, we can say that there exist two yield points – the first one can be taken to be in the small extension region and the other one close to the fracture point. This difference can also be attributed to differences in their arrangements of crystalline and amorphous/non-crystalline regions [58]. As stated above, in ar-PET the crystalline and the amorphous phases are quite distinct and may be stacked in series, whereas in ppt-PET sharp boundaries may not separate the crystalline from the non-crystalline samples regions. The load sharing hence is better in the case of ppt-PET fibers; and so when a load is applied, the material initially extends uniformly. Strain is getting uniformly distributed in the ppt-PET fibers and the crystalline phase also contributes to the resistance to deformation. Orientation in the non-crystalline regions of ppt-PET is also high and hence they offer resistance to further extension, and so result in the absence of the plateau region. As the yield point is reached, most of the tie molecules (shown in the AFM image Figure 4.21. (b)) snap leading to fibrillar slip and bending of the stress-strain curve toward the strain axis. PET is a glassy material so this deformation could take place only up to a limited extent, and the fiber finally fractures.

In the case of ar-PET fibers a different arrangement of the crystalline and amorphous phases exist together, and it does not show the presence of tie molecules (Figure 4.21.(a)). Due to the limited number of straight connecting molecules in the ar-PET crystals, load

cannot be withheld for a long period of time. Load concentration is high and this gives the initial yield points of the ar-PET fibers. Then, the molecules in the amorphous regions share the load and hence result in the plateau region and strain hardening. The second yield point for the ar-PET fibers is the result of the slip process as explained for the ppt-PET fibers.

Fiber tenacity of the ar-PET is slightly higher than that of the ppt-PET (0.08 Gm/Denier vs. 0.05 Gm/Denier). Tenacity is represented by the breaking load divided by the linear density of the fiber before deformation. In ar-PET fibers the deformation is large, and hence the linear density decreases by the time the fiber breaks and this increases the tenacity. According to Samuels [59] "When the rate of deformation is slow enough for the molecules to reach the highest orientation possible before the flow mechanism predominates, the force required for a given cross-sectional area of the sample is independent of the starting orientation of the sample". The reason for this is that molecules are equally oriented at the time of break, irrespective of the initial orientation state.

The toughness of the fiber also called the work of rupture is given by the area under the load-extension curve [60]. The ar-PET fiber possesses a higher work of rupture compared to the ppt-PET fibers. This is because of the ductile nature of the ar-PET fiber and the brittle solid nature of the ppt-PET fibers.

5. Conclusions

The structures, morphologies, and chain conformations of bulk PET samples formed using the precipitation method, have been demonstrated to be distinct from those of solution or melt processed samples. All the experimental techniques have given us evidence that the ppt-PET has all together different properties than that of the ar-PET and behaves similar in all respects to coalesced PET. There exists a molecular level difference between the two PET's. The non-crystalline portions of the ppt-PET sample differ from those of the ar-PET. Non-crystalline chains of the ar-PET appear completely disordered, so upon melting the entangled and randomly coiling PET chains are readily quenched into a completely amorphous sample. On the other hand PET chains in the non-crystalline portions of the ppt-PET sample appear to be more extended and less randomly coiled and entangled than in a typical PET melt. As a result, cooling rapidly immediately after melting results in a rapid recrystallization below T_m. Even if the sample is held in the melt ($T > T_m$) for a longer period of time, the ppt-PET does not revert to a completely disordered, entangled, randomly coiled melt, and so, upon subsequent rapid cooling, could not be quenched to a predominantly amorphous sample.

We have also observed that the ppt-PET and ar-PET can be blended in different proportions in order to obtain a blend that will behave more like ppt-PET. If a blend has more than 50 mole % of ppt-PET it found to crystallize rapidly on fast cooling.

In light of the conformational characteristics of both the randomly coiling and highly extended PET chains, of ar-PET and ppt-PET, respectively, the analysis of the FTIR spectra of the as-received and precipitated PET has led us to interpret the conformationally sensitive vibrational bands. The 973 and 1340 cm^{-1} bands that correspond to the trans conformer are found in the ppt-PET, because it is more crystalline than the ar-PET.

The non-crystalline portions of the ppt-PET are denser than the amorphous regions of the ar-PET, as confirmed by density measurements. Even the X-ray results confirm that ppt-PET is more oriented and is more crystalline. Strain-induced crystallization is also not prominently observed in the ppt-PET films. It is more evident in ar-PET, where the film is found to shrink abruptly at around T_g. This indicates that the two materials are microscopically different. Ppt-PET film response to the application of a load differs from the ar-PET film. Ppt-PET is rigid in its behavior and ar-PET shows high extensibility upon application of load. To further characterize the materials macroscopically, rheological properties of the two materials were observed, with the outcome that the two materials are macroscopically different. Sorption studies on PET films have leaded us to conclude that the two PET's differ in their diffusivity and solubility towards CO_2.

The general conclusion that can be drawn from all these observations is that ppt-PET has all together different organization and differs microscopically and macroscopically from ar-PET. Its thermal behavior is the same as coalesced PET. It can be characterized to be more crystalline and also with non-crystalline regions that are distinct from ar-PET.

6. Future Work

Precipitated PET will prove to be very useful because of its unique properties. As-received PET is a slow crystallizing material while precipitated PET crystallizes rapidly. After the complete characterization of precipitated PET, the next step would be to scale up the production of precipitated PET.

Also, non-woven web samples can be blown from the precipitated PET, as this material crystallizes fast enough. Mechanical properties of the films and the fibers need to be analyzed in more detail. Blending of precipitated and as-received PET had been carried out mechanically (mixing by hand in different proportions) and studied by DSC. Alternatively, intimate blending of the two PET's can be carried out in a Minimelter and then the blend behavior can be studied. Density calculations for all the three samples of PET can be carried out in a column designed for particularly for PET density measurements. Also, permeability to gases other than carbon dioxide, such as oxygen, nitrogen etc needs to be studied. Permeability studies and the behavior of the ppt-PET and the annealed ar-PET will be compared and studied in detail.

Overall, the unique properties of precipitated PET can be utilized to produce novel products that will be commercially viable, because PET is already the most widely used commercially produced polymer.

7. References

1. K. J. Saunders. Organic Chemistry of Polymers. *Chapman & Hall,* New York.
2. A. E. Tonelli. Polymers from Inside Out. *Wiley Interscience*, New York.
3. Report on Packaging Materials: 1.Polyethylene Terephthalate (PET for Food Packaging Applications. ILSI Europe Packaging Material Task Force, 83 Avenue E. Mounier, Box 6, B-1200 Brussels, Belgium
4. DuPont Teijin Films "Introduction to Mylar® polyester film"
5. A. E. Tonelli. Pet v. PEN: What difference can a ring make?. *Polymer*, 43: 637– 642, 2002.
6. P. M. Morse. Chemical Engineering News, 10: 8-14, 1997.
7. Leonard E. Ambroski and Donald W. Flierl. Physical properties of poly(ethylene terephthalate) films. *Industrial & Engineering Chemistry,* 45: 2290-2295, 1953.
8. Y. Kong and J. N. Hay. The enthalpy of fusion and degree of crystallinity of polymers as measured by DSC. *European Polymer Journal,* 43: 1721-1727, 2003.
9. R. C. Roberts. Poly(ethylene terephthalate) I-Heat of fusion. *Polymer*, 10: 113-116, 1969
10. Denis Gerard, Marie-Rose Garda and Jean-Marc Saiter. Experimental protocol to determine the ability of PET to crystallize. *Journal of Thermal Analysis,* 7: 155-160, 2003.
11. A. Wasiak, P. Sajkiewicz and A. Wozniak. Effect of cooling rate on crystallinity of i-Polypropylene and Polyethylene Terephthalate Crystallized in nonisothermal Conditions. *Journal of Polymer Science: Polymer Physics Edition*, 37: 2821–2827, 1999.

12. Susheng Tan, Alhua Su, Weihua Li and Enle Zhou. New insight into melting and crystallization behavior in semicrystalline polyethylene Terephthalate. *Journal of Polymer Science: Polymer Physics Edition*, 38: 53–60, 2000.
13. A. Booth and J. N. Hay. The use of differential scanning Calorimetry to study polymer crystallization kinetics. *Polymer*, 10: 95-104, 1968.
14. W. H. Cobbs and R. L. Burton. Crystallization of poly(ethylene terephthalate). *Journal of Polymer Science: Polymer Physics Edition*, 10: 275-290, 1953.
15. R. G. J. Miller and N. A. Willis. An independent measurement of amorphous content of polymers. *Journal of Polymer Science*, 19: 485-494, 1956.
16. Akihisa Miyake. The infrared spectrum of poly(ethylene terephthalate) I The effects of crystallization. *Journal of Polymer Science*, XXXVIII: 479-495, 1959.
17. Ying Zhang, Jianming Zhang, Yonglai Lu, Yongxin Duan, Shouke Yan and Deyan Shen. Glass transition temperature determination of polyethylene Terephthalate thin films using reflection-absorption FTIR *Macromolecules*, 37: 2532-2537, 2004.
18. James M. O'Reilly and R. A. Mosher. Conformational energies of steroregular poly(methyl methacrylate) by Fourier transform infrared spectroscopy. *Macromolecules*, 14: 602-608, 1981.
19. J. R. Atkinson, F. Biddlestone and J. N. Hay. An investigation of glass formation and physical ageing in poly(ethylene terephthalate) by FT-IR spectroscopy. *Polymer*,41: 6965-6968, 2000
20. J. Radhakrishnan and A. Kaito. Structure formation during the isothermal crystallization of oriented amorphous poly(ethylene terephthalate) films. *Polymer*, 42: 3859-3866, 2001

21. F. J. Balta Calleja, M. C. Garcia Gutierrez, D. R. Rueda and S. Piccarolo. Structure development in poly(ethylene terephthalate) quenched from the melt at high cooling rates: X-ray scattering and micro hardness study. *Polymer*, 41: 4143-4148, 2000.
22. S. N. Dhoot, B. D. Freeman, M. E. Stewart and A. J. Hill. Sorption and transport of linear alkane hydrocarbons in biaxially oriented poly(ethylene terephthalate). *Journal of Polymer Science: Polymer Physics Edition*, 39: 1160-1172, 2001.
23. D. J. Sekelik, E. V. Stepanov, S. Nazarenko, D. Schiraldi, A. Hiltner and E. Baer. Oxygen barrier properties of crystallized and talc-filled poly(ethylene terephthalate). *Journal of Polymer Science: Polymer Physics Edition*, 37: 847-857, 1999.
24. S. B. Lin and J. L. Koenig. Spectroscopic characterization of the rotational conformations in the disordered phase of poly(ethylene terephthalate). *Journal of Polymer Science: Polymer Physics Edition*, 20: 2277-2295, 1982.
25. Wen-Hao Lee, Hao Ouyang, Ming-Chih Shih and Ming-Huang Wu. Kinetics of solvent-induced crystallization of poly(ethylene terephthalate) at the final stage. *Journal of Polymer Science: Polymer Physics Edition*, 10: 133-137, 2003.
26. Christopher Freure, Guoliang Chen and J. Hugh Hortan. Examination of solvent interactions at the surface of poly(ethylene terephthalate) films using atomic force microscopy and infrared spectroscopy. *Surface Science*, 437, 231-238, 1999.
27. Hao Ouyang, Wen-Hao Lee, Wen Ouyang, Sham-Tsong Shuie and Tzong-Ming Wu. Solvent-Induced crystallization in poly(ethylene terephthalate) during Mass transport: Mechanism and boundary condition. *Macromolecules*, 37, 7719-7723, 2004.

28. Hao Ouyang, Wen-Hao Lee and Ming-Chih Shih. Three stages of crystallization in poly(ethylene terephthalate) during mass transport. *Macromolecules*, 35: 8428-8432, 2002.

29. J. M. Huang, P. P. Chu and F. C. Chang. Conformational changes and molecular motion of poly(ethylene terephthalate) annealed above glass transition temperature. *Polymer*, 41: 1741-1748, 2000

30. S. B. Lin and J. L. Koenig. Spectroscopic characterizing of solvent-induced crystallization. *Journal of Polymer Science: Polymer Physics Edition*, 21: 1539-1558, 1983.

31. Michael R. Hibbs, Jeremy Holtzclaw, David M. Collard, Richard Y. F. Liu, Eric Baer Hiltner and David A. Schiraldi. Poly(ethylene terephthalate) modified with aromatic bisester diamides: Thermal and oxygen barrier properties. *Journal of Polymer Science: Polymer Chemistry Edition*, 42: 1668-1681, 2004.

32. J. A. Slee, G. A. J. Orchard, D. I. Bower and I. M. Ward. The transport of oxygen through oriented poly(ethylene terephthalate). *Journal of Polymer Science: Polymer Physics Edition*, 27: 71-83, 1989

33. N. Qureshi, E. V. Stepanov, D. Schiraldi, A Hiltner and E. Baer. Oxygen-barrier properties of oriented and heat-set poly(ethylene terephthalate). *Journal of Polymer Science: Polymer Physics Edition*, 38: 1679-1686, 2000.

34. A. Polyakova, R. Y. F. Liu, D. A. Schiraldi, A. Hiltner and E. Baer. Oxygen-barrier properties of copolymers based on ethylene terephthalate. *Journal of Polymer Science: Polymer Physics Edition*, 39: 1889-1899, 2001.

35. A. Polyakova, D. M. Connor, D. M. Collard, D. A. Schiraldi, A. Hiltner and E. Baer. Oxygen-barrier properties of polyethylene terephthalate modified with a small amount of aromatic comonomer. *Journal of Polymer Science: Polymer Physics Edition*, 39: 1900-1910, 2001.

36. http://www.azom.com/details.asp?ArticleID=2047#_Key_Properties

37. E. L. V. Lewis, R. A. Duckett, I. M. Ward, J. P. A. Fairclough and A. J. Ryan. The barrier properties of polyethylene terephthalate to mixtures of oxygen, carbon dioxide and nitrogen. *Polymer*, 44: 1631-1640, 2003.

38. M. Wei, W. Davis, B. Urban, Y. Q. Song, F. E. Porbeni, X. Wang, J. L. White, C. M. Balik, C. C. Rusa, J. Fox and A. E. Tonelli. Manipulation of nylon-6 crystal structure with its α-cyclodextrin inclusion complex" *Macromolecules*, 35: 8039-8044, 2002.

39. X. T. Shuai, F. E. Porbeni, M. Wei, I. D. Shin and A. E. Tonelli. Formation of and coalescence from the inclusion complex of a biodegradable block copolymer and α-cyclodextrin: A novel means to modify the phase structure of biodegradable block copolymers. *Macromolecules*, 34: 7355-7361, 2001.

40. M. Wei and A. E. Tonelli. Compatiblization of polymers via coalescence from their common cyclodextrin inclusion compounds. *Macromolecules*, 34: 4061-4065, 2001.

41. T. A. Bullions, M. Wei, F. E. Porbeni, M. J. Gerber, J. Peet, M. Balik, J. L. White and A. E. Tonelli. Reorganization of the structures, morphologies, and conformations of bulk polymers via coalescence from polymer-cyclodextrin inclusion compounds. *Journal of Polymer Science: Polymer Physics Edition*, 40: 992-1012, 2002.

42. A. Harada, J. Li, S. Suzuki and M. Kamachi. Complex formation between polyisobutylene and cyclodextrins: inversion of chain-length selectivity between .beta.-cyclodextrin and .gamma.-cyclodextrin. *Macromolecules*, 26: 5267-5268, 1993.
43. L. Huang, E. Allen and A. E. Tonelli. Inclusion compound formed between cyclodextrins and nylon-6. *Polymer*, 40: 3211-3221, 1999.
44. A. E. Tonelli. Modeling the conformations and mobilities of aliphatic polyamides and polyesters confined to channels. *Macromolecules*, 24: 1275-1278, 1991.
45. J. Lu, I. D. Shin, S. Nojima and A. E. Tonelli. Formation and characterization of the inclusion compounds between poly(ε-caprolactone)-poly(ethylene oxide)-poly(ε-caprolactone) triblock copolymer and α-and γ-cyclodextrin. *Polymer*, 41, 5871-5883, 2000.
46. M. Wei, T. A. Bullions, C. C. Rusa, X. Wang and A. E. Tonelli. Unique morphological and thermal behaviors of reorganized poly(ethylene terephthalates). *Journal of Polymer Science: Polymer Physics Edition*, 42: 386-394, 2004.
47. C. C. McDowell, B. D. Freeman and G. W. McNeely. Acetone sorption and uptake kinetic in poly(ethylene terephthalate). *Polymer*, 40: 3487-3499, 1999.
48. N. S. Murthy, S. T. Correale and H. Minor. Structure of the amorphous phase in crystallizable polymers: poly(ethylene terephthalate). *Macromolecules*, 24: 1185-1189, 1991.
49. Prashant Chandran and Saleh Jabarin. Biaxial orientation of poly(ethylene terephthalate). Part I: Nature of the stress-strain curves. *Advances in Polymer Technology*, 12: 119-132, 1993.

50. Ulrich Goschel. Thermally stimulated structural changes in highly oriented glassy poly(ethylene terephthalate). *Polymer*, 37: 4049-4059, 1996.

51. R. R. Light and R. W. Seymour. Effects of sub-Tg relaxations on the gas transport properties of polyesters. *Polymer Engineering & Science*, 22: 857-864, 1982.

52. K. Toi, K. Oba, Y. Maeda, T. Ito, T. Shirakawa, I. Ikemoto and T. Tokuda. Determination of Dual-mode sorption and mobility parameters from permeation experiments. *Journal of Polymer Science: Polymer Physics Edition*, 24: 121-131, 1986.

53. W. J. Koros and D. R. Paul. CO_2 sorption in poly(ethylene terephthalate) above and below the glass transition. *Journal of Polymer Science: Polymer Physics Edition*, 16: 1947-1963, 1978.

54. A. S. Michaels, W. J. Vieth and J. A. Barrie. Diffusion of gases in polyethylene terephthalate. *Journal of Applied Physics*, 34: 13-20, 1963.

55. Ken-Tchi Okamoto, Kazuhiro Tanaka, Osamu Yokoshi and Hidetoshi Kita. The effect of morphology on sorption and transport of carbon dioxide in poly(4,4'-oxydiphenylene pyromellitimide). *Journal of Polymer Science: Polymer Physics Edition*, 27: 643-654, 1989.

56. C. D. Bechav and J. T. Mishinev. Structural changes in draw-textured poly(ethylene terephthalate) filaments during heat setting. *Journal of Applied Polymer Science*, 45: 29-35, 1992.

57. A. Donneally, T. Ohara and C. Birkinshaw. Characterization of the physical and molecular structure of thermally elongating poly(ethylene terephthalate) fibers. *Journal of Applied Polymer Science*, 66: 989-995, 1997.

58. V. B. Gupta and Satish Kumar. The effect of heat setting on the structure and mechanical properties of poly(ethylene terephthalate) fiber. III. Anelastic properties and their dependence on structure. *Journal of Applied Polymer Science*, 26: 1885-1895, 1981.

59. R. J. Samuels. *Structured Polymer Properties*, 1974, Wiley, New York.

60. V. B. Gupta and Satish Kumar. The effect of heat setting on the structure and mechanical properties of poly(ethylene terephthalate) fiber. IV. Tensile properties other than modulus and their dependence on structure. *Journal of Applied Polymer Science*, 26: 1897-1905, 1981.